Master's Thesis

Transfer of spectral purity to strontium and mercury optical lattice clocks

University of Copenhagen

l'Observatoire de Paris | SYRTE

Systèmes de Référence Temps-Espace

Christian Ørtoft Bærentsen

Transfer of spectral purity to strontium and mercury optical lattice clocks

Author	Christian Ørtoft Bærentsen
Internal advisor	Jan Westenkær Thomsen
External advisor	Rodolphe Le Targat

Quantum Metrology Group | Métrologie des fréquences optiques
The Niels Bohr Institute | LNE-SYRTE, l'Observatoire de Paris

Submitted to the University of Copenhagen
September 3, 2019
Corrected - May 7, 2020

Acknowledgements

I want to thank my supervisor in Paris, Rodolphe Le Targat for giving me the opportunity to work at SYRTE under his guidance. Rodolphe has been a very committed supervisor, always finding time to discuss the experiments and the theories with me - even with a baby at home. It has been a tremendous experience and honor to work in the laboratories of SYRTE. It is an experience that I would not have been without, and that I will never forget.

Additionally I would like to thank:

Jan Westenkær Thomsen and Eugene Simon Polzik for recommending me to Rodolphe Le Targat, and making my work at SYRTE possible. You gave me the opportunity, for which I am forever grateful.

Héctor Álvarez Martínez - my co-worker and friend. Thank you for the time spend at SYRTE and for the many discussions. We have really spend a lot time together in the laboratory while during experiments, which I will miss.

Jérôme Lodewyck - with whom I have been sharing office space. Jérôme has always taking the time to explain complex problems, and making it comprehensible. He has always been helpful whenever needed.

Sébastien Bize - the head of the optical frequency group. It has really motivated me that you have showed so much interest in my work, all the times asking; "If I was ready to do dual transfer of spectral purity", to which I felt that my work was really appropriated.

The whole strontium, mercury and spectral hole burning team - I would like to thank all of you for investing a lot of time in the laboratories, making sure that everything was running while we were doing measurements.

Mads Bebe Krog Tønnes and Mikkel Ibsen - my friends. Thank you for the many walks from City Universitaire to SYRTE, for the many laughs, and for your great support in this journey to Paris. It would not have been the same without you.

Finally, I want to thank my fiancée Camilla Folkersen for being part of my life and supporting me throughout my 12 month stay in Paris, particularly for waiting patiently for me to come home.

Abstract

In an optical lattice clock, neutral atoms are trapped in an optical lattice while an ultra stable laser repeatedly probes a narrow (<1 Hz) transition. Nowadays the optical lattice clocks can average down to a fractional stability in the 10^{-16} range at 1 s, with a possibility of reaching the 10^{-18} range for longer integration times. The main effect limiting the stability is the sampling of the residual frequency noise of the laser probing the narrow metrological transition. This sampling, known as the Dick effect, arises from the cyclic operation of the clock. I will present my work at LNE-SYRTE, going towards ultra stable lasers through transferring the stability from a 1542 nm ultra stable laser to target metrology frequencies at 698 nm (strontium) and 1062 nm (mercury) used to probe the atoms of the clocks. This involves rethinking the construction of the frequency chain, and the establishment of the setups for transfer of spectral purity to strontium and mercury optical lattice clocks.

Contents

Glossary

AM Amplitude Modulation.

AOM Acousto-Optic Modulator.

comb optical frequency comb.

CSO Cryogenic Sapphire Oscillator.

CUS Cavity Ultra Stable.

DC Direct-Current.

DDS Direct Digital Synthesis.

EDFA Erbium-Doped Fiber Amplifer.

H-maser hydrogen maser.

Hg mercury.

HNLF High Non-Linear Fiber.

IR Infra-Red.

MOT Magnetic Optical Trap.

NLPR NonLinear Polarization Rotation.

OADM Optical Add-Drop Multiplexer.

PBS Polarization Beam Splitter.

PLL Phase-Locked Loop.

PM Phase Modulation.

RF Radio-Frequency.

SHB Spectral Hole-Burning.

SHG Second Harmonic Generation.

SNR Signal to Noise Ratio.

Sr strontium.

VCO Voltage-Controlled Oscillator.

Chapter 1

Introduction

1.1 Context

What is the limit to the uncertainty of a measurement? The question of units is a central point of Physics, as they must be universal and based on unchanging references, if it is for time, length, mass, temperature, etc. A meter of platinum was made in 1792 [1] that should define the length, it was meant for calibration of tools, so that everyone had the same length for one meter. However, this method of measuring the meter was neither stable nor repeatable. When defining an universal unit, the ability to duplicate a measurement in another place and time with equal outcome is one of the pillars science is built upon. Nowadays the meter is redefined, so it is the distance light travels in vacuum for an interval of $\frac{1}{299{,}792{,}458}$ seconds [2], the length will then be interlinked with the measurement of time and the definition of the speed of light.

The energy between two electronic states is universal, the frequency of the source necessary to excite this transition is therefore fixed. This is the power of using the caesium atom to define time, so the measurement can be reproduced with equal outcome. Today time is defined using a hyperfine splitting in a caesium-133 atom, where the second is defined as 9,192,631,770 periods measured from the ground state hyperfine splitting [3]. The definition of the second is best realized by the microwave fountains, with a fractional accuracy that can reach $2 \cdot 10^{-16}$ [4]. The stability is the noise of the frequency for the measurement. The statistics must be accumulated in order to progressively refine the knowledge of the mean frequency. The uncertainty (called the accuracy in case of cesium) is the interval of confidence around this mean frequency after corrections of all the systematics (frequency shifts due to temperatures, dipole-shifts, magnetic-fields, etc).

The pursue of clocks with even better accuracies have pushed the uncertainty on the clocks to even lower levels, where new prospects are arising;

- Search for a possible drift of fundamental constants, to which atomic frequencies are connected (electron to proton mass ratio, fine structure constant, reduced mass of the light quark). Tracking the ratio Sr/Cs for instance was started 15 years at SYRTE, and has already allowed demonstrating that the change is anyway smaller than 10^{-16}/year.

- Test of Lorentz invariance: Using comparisons between multiple clocks on earth (connected via the European optical fiber network in charge of disseminating an ultra stable optical reference at 1542 nm) and/or in space (PHARAO-ACES mission, starting from 2020).

- Chronometric geodesy: Using optical clocks to determine the geoid and detect temporal variations of the gravitational potential.

- In a more prospective way: Search for dark matter[5] as proposed recently, by correlating events resulting in a brief and sudden change of frequencies of clocks spread on the surface of the Earth.

Strontium optical lattice clocks have shown a capability of reaching fractional accuracies in the 10^{-18} range, as the optical lattice clocks utilize the reduced light shifts and ultra cold atoms in order to achieve high accuracies. Strontium has a narrow optical transition (< 1 Hz) to be probed with a large lever arm due to its high frequency compared to the hyperfine microwave splitting of the caesium atoms. Optical frequencies are necessary for reaching ultra low levels of fractional stability, because the stability $\frac{\Delta\nu}{\nu_n}$ is renormalized by the nominal clock frequency $\frac{\Delta\nu}{\nu}$ to get the fractional stability. In perspective to the stability of the atomic clock; We could imagine placing a strontium optical lattice clock at the beginning of time - 14 billion years ago. If the clock ran to reach our present time from 14 billion years ago, the stability of the clock would reach an uncertainty of time that is less than 1 second, which is incredible to think about and it illustrates the amazing stability of the strontium optical lattice clock.

How to measure 429 Terahertz

There are no detectors that are fast enough to detect anything at 429 THz (the fastest existing detectors have a bandwidth of 100 GHz), so for a long time, the development of optical atomic clocks was hindered by the quasi impossibility to connect the optical frequencies to the definition of the second/hertz.

With the invention of the so-called frequency comb a new era started. An optical frequency comb is like a ruler for frequencies. The spectrum of an optical frequency comb is composed of frequencies displaced with equal spacing as peaks just like the lines on a ruler. The optical frequency comb can then be measured against different laser frequencies, and a relative frequency between between the laser and the frequency comb can be counted by the number of teeth separating the frequencies. The spacing between adjacent teeth in the Radio-Frequency (RF) domain are less than 1 GHz, where all the frequencies are small enough to be measured easily with conventional methods. An analogy to the optical frequency comb could be the measurement of the thickness of a piece of paper, where the measurement of a paper would be hard to do, due to it being so thin. But by measuring the thickness of a large pile of identical papers, the measurement of the paper's thickness suddenly becomes possible like the measurement of the optical frequencies with an optical frequency comb.

1.2 Taking full benefit of ultra narrow lasers

I have been working towards improving the stability of the optical lattice clocks at SYRTE[1] by improving the probing laser. The biggest limitation to the stability is the Dick effect (see section 2.3.4), an effect linked to the residual frequency noise of the probing laser. The Dick effect arises because of the limited probing time due to the decoherence induced by the clock laser, and also mainly because of the cyclic operation of the clock over a cycle time of T_c: The frequency noise at Fourier frequencies equal to harmonics of the clock cycle frequency $1/T_\mathrm{c}$ (with T_c typically 0.5 or 1 s) average much more slowly, because it is experienced by the atoms in a "stroboscopic" way.

Transfer of spectral purity between lasers has the goal of achieving ultra stable lasers at desired frequencies. One of the benefits of this method is that lasers can be built at target metrological frequencies, in order to match the needs of various atomic clocks. My predecessors built a master laser at 1542 nm, because it is a range that is convenient, where it matches the central frequency of an erbium comb. Any slave laser within reach of the comb's spectrum after broadening (from 1 μm to 2 μm) can be phase locked to the master laser via the transfer of spectral purity. Another advantage of linking the systems on an ultra stable master laser in the C band[2] is that it may be distributed by a network of propagation-stabilized optical fibers in Europe and used as a common mode reference by several "clock" laboratories.

We want to transfer the spectral purity to the clock lasers driving the strontium (Sr) and mercury (Hg) optical lattice clocks, in order to reach better stabilities for optical lattice clocks than our present fractional stability of 10^{-15} at 1 s with the target of 10^{-16} at 1 s, when going to more stable lasers. This would result in a gain of 100 in terms of integration time, since the atomic clocks are dominated by white frequency noise, where the stability averages down with the square root of the integration time ($\tau^{-1/2}$).

We want to transfer the most stable laser that we have available to target metrological frequencies. One of our best lasers is called Cavity Ultra Stable (CUS), which is an ultra stable laser at 1542 nm. The optical frequencies are too far separated for us to measure a beat note between any of our metrology lasers - Sr, Hg or CUS. We are able to measure the individual beat notes, when using an optical frequency comb (comb) as a comparison tool between the frequencies to transfer the spectral purity.

[1]SYRTE stands for Sytèmes de Référence Temps Espace, it is a department under Observatoire de Paris - Université PSL

[2]The C band has an interval of 1530-1560 nm in the Erbium window[6]

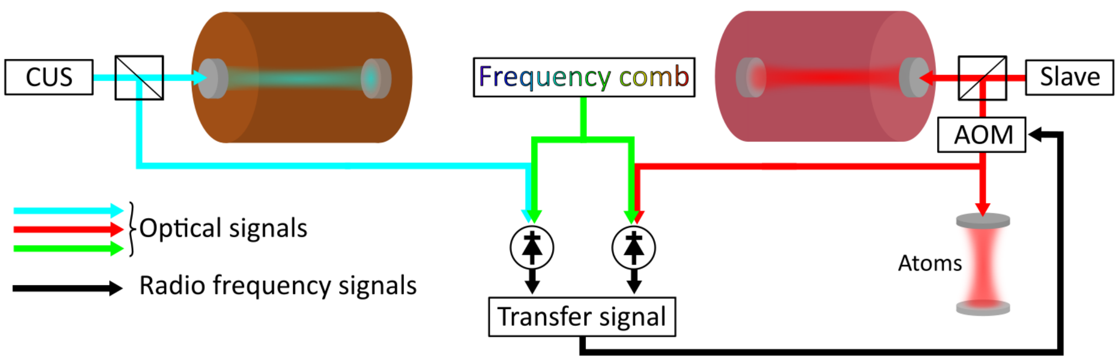

Figure 1.1: Measuring the beat notes with two lasers to an optical frequency comb on two photodiodes. The blue, green, red line is the path of the CUS, comb and the slave laser respectively. The Acousto-Optic Modulator (AOM) is used to make small frequency changes to the slave laser with a transfer signal created by the transfer of spectral purity.

On figure 1.1 the idea behind the transfer of spectral purity from an ultra stable laser to a clock laser is illustrated. The master laser called the CUS is stabilized to an ultra stable cavity, the light is afterwards combined with the comb on a photodiode. The slave laser is stabilized to a stable cavity, where it is measured with the comb on another photodiode. The comb will act like a "ruler" relating the two beat notes to each other, so the two frequencies can be compared. A frequency chain after the photodiodes will rescale the beat notes, so that the noise of the technical parameters of the comb are eliminated and the spectral purity can be transferred without degradation to the slave laser. The signal to stabilize the slave will be fed to the Acousto-Optic Modulator (AOM) placed after the slave laser, this will close the loop, phase locking the slave to the CUS. The light going to the atoms will then have the inherited spectral purity of the CUS (under the assumption that the comb, laser paths and frequency modulation are not contributing to the noise). This thesis will give a detailed explanation of the setups I have installed at SYRTE to transfer the spectral purity between our metrology lasers and my work involving the comparison of state of the art optical lattice clocks.

In chapter 2 (Framework of optical clocks), I will layout the fundamental knowledge behind optical lattice clocks with tool (like an optical frequency comb) that are needed to assess them. In chapter 3 (Metrological connections between atomic clocks), I will describe the operational setups that connects the lasers and atomic clocks, the improvements on the frequency chain to reach even better stabilities, and a new methods to detect the offset of the optical frequency comb. In chapter 4 (Transfer of spectral purity), I will layout my main results for the transfer of spectral purity, and the results for the elimination of the Dick effect with the help of the transfer of spectral purity. Finally, I will conclude in chapter 5 and give an outlook on how we can further improve the setups, as well as the ideas we would like to implement.

Chapter 2

Framework of optical clocks

This chapter will give a description of the theory and components needed to understand the following chapters. This chapter will go into the basics behind a Fabry-Pérot interferometer, the physics of an optical frequency comb and the fundamental knowledge of atomic clocks. This is necessary in order to understand the reasoning behind going to more stable lasers with the help of transfer of spectral purity.

2.1 Fabry–Pérot interferometer

There are many areas in optics where a Fabry–Pérot interferometer are being used, but two essential areas that will be presented in this thesis are to create an ultra stable laser and to create an optical lattice for an atomic clock.

Imagine having two plane mirrors separated at a distance L with the mirrors parallel to each other. If we had some light bunching between the two mirrors, and if we were to assume perfect mirrors with no losses in the system. The light would accumulate a phase on each round trip bouncing between the mirrors, this phase can be expressed as; $\varphi = k2L$. If the wavenumber k does not fulfill φ being equal to an integer number of 2π, the phase on each round trip would be accumulated, resulting in constructive and destructive interference between the light fields creating zero intensity between the two mirrors for wavelengths not fulfilling $k = \frac{\pi}{L}m$, where m is an positive integer. The only solution to this problem would be a standing wave between the two mirrors. The separation between the allowed frequencies (the free spectral range) would then be $\nu_{FSR} = \frac{c}{2L}$. The allowed frequencies would then be;

$$\nu_m = m\nu_{FSR} \quad + \nu_0, \tag{2.1}$$

where m is a positive integer, and the equation illustrates a "perfect" Fabry–Pérot interferometer (when discarding ν_0). The beams are gaussian shaped, and the mirrors need to adapt to the phase front of the beams, the most commonly used configuration are plane-concave or concave-concave mirrors. The light could otherwise not be confine between the mirrors. The gaussian modes gives rise to an offset on the interferometer's resonance; ν_0, which can be calculated from the geometry of the cavity (see appendix C).

We can describe the cavity a bit more explicit, because the mirrors are in practice not perfect reflectors without loses. The transmission through the cavity can be expressed as;

$$\frac{I_T}{I_0} = \frac{1}{1 + (2\mathcal{F}/\pi)^2 \sin^2(\varphi/2)}, \tag{2.2}$$

where $\mathcal{F}$ is the finesse and r is the amplitude reflection coefficient. The explanation/derivation of equation 2.2 is shown in appendix A.

The finesse is defined for the linewidth of the resonator modes to follow;

$$\delta\nu = \frac{\nu_{FSR}}{\mathcal{F}}. \tag{2.3}$$

This is fulfilled when having the following relation for a symmetric cavity;

$$\mathcal{F} = \frac{\pi\sqrt{r}}{1 - r}. \tag{2.4}$$

The finesse is a very important parameter of a cavity. A high finesse means that the cavity has a narrow linewidth, this is greatly used to stabilize oscillators to the sharp modes of the cavity. There are also other purposes for high finesse cavity like multiple interactions with atoms.

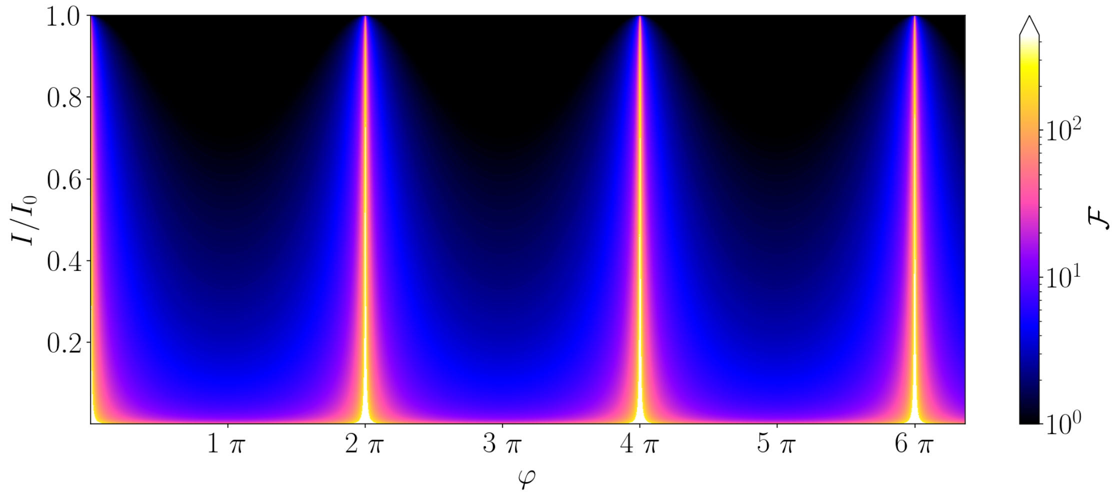

Figure 2.1: The transmission of a cavity following equation 2.2 for different values of the finesse ($\mathcal{F}$).

Figure 2.1 shows the transmission through the cavity following equation 2.2. We can see that for higher value of $\mathcal{F}$, the narrower is the linewidth of the resonator modes, the center of the resonance is at φ equal to a multiple of 2π (In non gaussian mode). The phase can be described from the frequency and the free spectral range;

$\varphi = 2\pi\frac{\nu}{\nu_{FSR}}$. The free spectral range is defined, so it is the amount of times that the phase is equal to $m2\pi$ (m is an integer) at a round trip in the resonator. We can now write the complete equation for the transmission by rewriting equation 2.2;

$$\frac{I_T}{I_0} = \frac{1}{1 + (2\mathcal{F}/\pi)^2 \sin^2(\pi\nu/\nu_{FSR})}. \tag{2.5}$$

It physically makes sense that this ratio is at most 1 due to the energy conservation. The equation assumes that all the light is mode-matched to the cavity, which is a bit more tricky in the case of a gaussian beam. It is also assumed that both mirrors have the same reflexion coefficients, which is not always the case. It is now clear the power of the Fabry-Pérot interferometer with its ability to create stable signals. This is especially true when having a high finesse, where an ultra stable signal can be created from narrow modes that are allowed within the interferometer [7, 8].

2.2 Optical frequency comb

An optical frequency comb is a light source containing a lot of different frequencies as narrow peaks with all the peaks equally separated. An illustration of an optical comb is shown on figure 2.2, which illustrates a comb within the visible domain. The comb can only generate its teeth within the gain medium that the comb is using to generate its light.

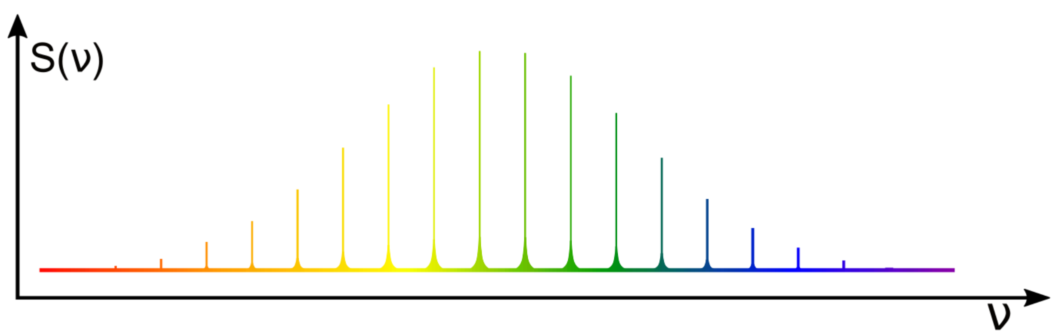

Figure 2.2: Illustration: Spectrum of an optical frequency comb in the visible domain.

We are using NonLinear Polarization Rotation (NLPR) combs that create a mode lock in a pulsed laser, many modes are lasing simultaneously, and the NLPR leads to a phase locking between all the modes: this is the base of a frequency comb [9]. When having a mode lock between the modes in a resonator, a constructive interference occurs every T, where T is the time for the light to make one trip in the cavity. These pulses will then go through an optical fiber inducing NLPR so the polarization changes. The polarization of the pulses will be filtered away by a Polarization Beam Splitter (PBS), so the output of the comb only will take place having a mode lock. If the modes are not mode locked the NLPR will not take place, because the intensity will not be high enough (not having the pulses), this means the light will be transmitted through the PBS, going around the system again until a mode lock occurs [10].

The comb has very short pulses with a separation in the low nanoseconds range between each pulse. The Fourier transform of the envelope containing the pulses are the frequencies emitted by the comb. The time between each pulse (T) decides the separation between each tooth in the frequency range. This is seen as the separation between each tooth on figure 2.2. We call this separation between the frequencies the repetition rate, which can be calculated from; $f_{\mathrm{rep}} = \frac{1}{T}$. There is a small phase shift of the pulse with respect to the envelope ($\Delta\varphi_{\mathrm{ev}}$), it corresponds to having a small offset in the frequency domain (f_0), it is equal to $f_0 = \frac{\Delta\varphi_{\mathrm{ev}}}{2\pi} f_{\mathrm{rep}}$. Taking all this into account, the frequency offset (f_0) and the repetition rate (f_{rep}), an equation for the frequency spectrum can be expressed as;

$$f_N = N f_{\mathrm{rep}} + f_0, \tag{2.6}$$

where N is an integer expressing the number of the tooth.

The width of the comb's spectrum is only a few tenths of nanometers after creating the comb, so a broadening of the comb is necessary for the self-referencing of the comb (the derivation of f_0). The light of the comb is being sent through a Erbium-Doped Fiber Amplifer (EDFA) to amplify the light before it is sent through a High Non-Linear Fiber (HNLF). A nonlinear effect is going to broaden the comb called the four-wave mixing [11];

$$f_i jk = f_i + f_j - f_k. \tag{2.7}$$

The comb has a separation between the teeth of $N f_{\mathrm{rep}}$, this means the four-wave mixing generates new frequencies that has the same repetition rate, but now in the gain of the medium. This process of creating new frequencies is called stimulated Raman scattering [9]. The EDFA gives us the possibility to have a frequency comb going from $\sim 1\ \mu m$ to $\sim 2\ \mu m$.

The interference between a comb and a laser can be measured on a photodiode. We can use equation 2.6 for the frequency of the comb and ν_L as the laser frequency to express the beat note between them;

$$f_L = N f_{\mathrm{rep}} + f_0 - \nu_L. \tag{2.8}$$

The explanation to the above equation is done further in appendix B. The parameters of the comb can then be measured to calculate the frequency of the laser from the measured beat note of equation 2.8.

We can measure the repetition rate of the comb on a photodiode, where all the teeth will do self-interference with each other creating a signal at f_{rep}, $2f_{\mathrm{rep}}$, $3f_{\mathrm{rep}}$.... This can be seen as the beat note;

$$n f_{\mathrm{rep}} = f_N - f_{N-n}, \tag{2.9}$$

where the N and n is only restricted by the spectrum of the comb.

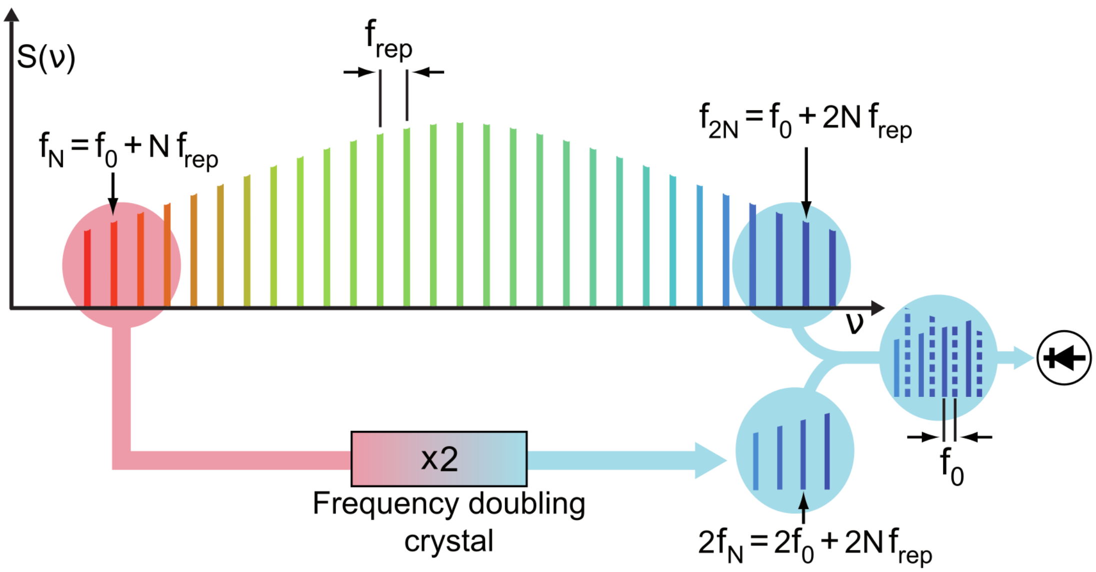

Figure 2.3: Illustration: How to measure f_0 in an optical frequency comb with the $f-2f$ method.

Measuring f_0 is more complicated than measuring f_{rep}. It is crucial for the detection of f_0 that the comb is octave spanning (having a gain spanning from tooth N to $2N$). Frequency doubling of the tooth N will create a signal at $2f_N$ corresponding to; $2f_N = 2Nf_{\text{rep}} + 2f_0$. This is illustrated as the red tooth going through the Second Harmonic Generation (SHG) medium on figure 2.3. The light then does interfering with the the already existing tooth at $f_{2N} = 2Nf_{\text{rep}} + f_0$;

$$f_0 = 2f_N - f_{2N} = 2(Nf_{\text{rep}} + f_0) - (2Nf_{\text{rep}} + f_0). \tag{2.10}$$

This is called the $f-2f$ method, because the comb does self interference with twice the frequency, and it is important to add that many "couples" of teeth contribute to the strength of the signal. It is a bit different in practice than I have shown on figure 2.3, since the whole comb is being sent through the SHG medium. The SHG is only optimized for the 2 μm of the comb, so the rest of the transmitted light goes unchanged through the SHG medium having both $2f_N$ and f_{2N} in the spectrum of the light.

To measure the tooth number of a beat note with the comb, a controlled modulation of the repetition rate needs to occur. We can use equation 2.8 to describe the change in a beat note, when changing the repetition rate of the comb with Δf_{rep};

$$f_L + \Delta f_L = N(f_{\text{rep}} + \Delta f_{\text{rep}}) + f_0 - \nu_L. \tag{2.11}$$

The beat note will change with $\Delta f_L = N\Delta f_{\text{rep}}$ as seen on equation 2.11, when changing the value of the repetition rate. The N value can then be calculated from the relation; $\Delta f_L/\Delta f_{\text{rep}}$. We just need to have a low enough uncertainty to distinguish the integer numbers that N can take. How the comb is operated in practice will be explained further in section 3.1, where the experimental operations are described.

2.3 Atomic clocks

The sections to atomic clocks will give a better idea of how to measure the stability of an atomic clock, and analyzing the data with the method called the Allan variance. The sections will also give a general description of the different types of optical lattice clocks we have at SYRTE, the interrogation method used for atomic clocks and an explanation of the Dick effect. The Dick effect is the big limiting factor when it comes to the stability, and it is therefore why the project described in this manuscript explores new methods to increase the laser's stability in order to decrease the impact of the Dick effect.

2.3.1 Allan variance

We need a tool to calculate the stability of atomic clocks, where we can distinguish the different types of noises in our system. This tool is called the Allan variance which is widely used for analyzing sources of noise.

The stability of a frequency can be characterized by the two correlated variables $x(t)$ and $y(t)$, the time error function and the fractional frequency respectively. The error time function is related to the phase fluctuation by $\varphi(t) = x(t) \cdot 2\pi\nu_n$, where ν_n is the nominal frequency. The fractional frequency is $y(t) = \frac{\nu(t)-\nu_n}{\nu_n}$. To explain the concept of the time error and the fractional frequency, we could imagine an oscillator with the signal;

$$V(t) = V_0 \cdot \sin(2\pi\nu_n t + \varphi(t)), \tag{2.12}$$

where V_0 is the amplitude of the oscillation, and $\varphi(t)$ is the phase fluctuation. The relation between the phase fluctuations and the frequency of equation 2.12 is;

$$\nu(t) = \nu_n + \frac{1}{2\pi}\frac{\mathrm{d}\varphi}{\mathrm{d}t}. \tag{2.13}$$

Inserting this into the equation for the fractional frequency;

$$y(t) = \frac{1}{2\pi\nu_n}\frac{\mathrm{d}\varphi}{\mathrm{d}t} = \frac{\mathrm{d}x}{\mathrm{d}t}. \tag{2.14}$$

The time error function appears, when we integrate over the fractional frequency, so we can calculate the error in time from the frequency stability. This relates the fractional stability of our measurement to the time error of the clocks.

The Allan variance is taking the variance between adjacent sample averages as a function of sample sizes. it is using M samples and taking the variance between the samples by the following;

$$\sigma_y^2(\tau) = \frac{1}{2(M-1)}\sum_{i=1}^{M-1}(\overline{y}_{i+1} - \overline{y}_i)^2. \tag{2.15}$$

The Allan variance looks at the Shot to shot fluctuations at 1 second, and for the next points it makes sub- averages under the form of sets, and then compare the shot to shot fluctuations between the adjacent sets. While a moving average would erase progressively any type of time structure, the Allan variance tells you exactly on which time scale you have frequency fluctuations.

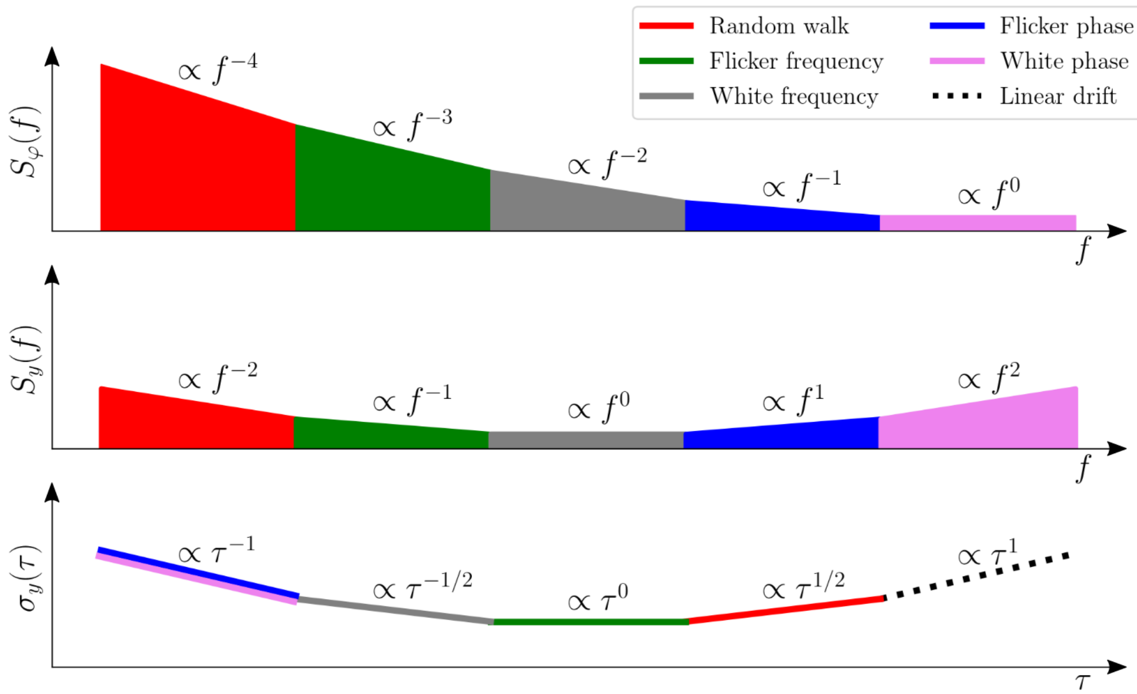

Figure 2.4: Power laws for the one-sided power spectral density of the phase fluctuations, the normalized frequency fluctuations and the Allan deviation. The two quantities, $S_\varphi(f)$ and $S_y(f)$, are the one-sided power spectral density of the phase fluctuations and the normalized frequency fluctuations, corresponding to a Fourier analysis of the samples.

In general, we can encounter 5 main types of noise, white phase, flicker phase, white frequency, flicker frequency and random walk noise [12]. Even if we would build a system insensitive to any kind of external perturbation, we would always have a floor that we can not exceed, due to this white phase noise. This is the reason why the Signal to Noise Ratio (SNR) sets a limit to the best result you can achieve.

If we were to imagine that we only had white frequency noise, the stability measured by the Allan variation would go down as $\sigma_y^2(\tau) \propto 1/\tau$, where τ is the averaging time (the time span of the average over the samples). This is because of the variance of an average goes down as $1/N$ for white frequency noise. Figure 2.4 shows the power density spectrum for the various noises, where we can see that the white frequency noise has a slope of f^0 in the power density spectrum of the frequency noise. A white noise is random noise, which means you have all the Fourier components in the spectrum of the noise. The power laws for the other frequencies can be seen as well on figure 2.4.

To distinguish the flicker phase noise from the white phase noise the modified Allan variation can be used, where the slope of the white phase noise decline with $\tau^{-3/2}$ instead of τ^{-1}, so the phase noises can be distinguished.

The experiments done in our laboratory are using two kinds of averaging for the frequency counting with dead free time counters. The counters are collecting data every millisecond, but storing this amount of data for all the experiments would be an extensive challenge of data storing. The counter does internal averaging of the data, so we have a data point for every second. The two methods commonly used for averaging are the Π-counters or Λ-counters. The Π-counters determines the data point at 1 s from an average, which resembles the method that the Allan deviation is taking the averages. The Λ-counters determines the data point at 1 s from a Λ-weighted average, which resembles the method that the modified Allan deviation is taking the averages, which differs for the two methods when averaging white phase noise [13]. This means that it is advantageous to use Allan deviation when using the Π-counters, and the modified Allan deviation when using the Λ-counters, so all the data is averaged with the same method.

2.3.2 Optical lattice clocks

SYRTE has built 3 operational optical lattice clocks, two based on ^{87}Sr and one based on ^{199}Hg. A keystone of optical lattice clocks is the confinement of neutral atoms in a so-called magic optical lattice. This ensures a tight confinement and therefore makes the frequency measurement immune to atom motional effects. The magic features ensure that the light shift induced on both clock states is identical, and therefore the frequency measurement is immune, to first order, to power fluctuations of the laser providing light for the lattice. An optical lattice uses the interaction potential of the dipole moment (p) in the field (E) of the light. The interaction potential can be written as;

$$U_{\text{dip}} = -\frac{1}{2}\langle pE \rangle = -\frac{1}{2\epsilon_0 c}\text{Re}\{\alpha(\omega)\}I(x,y,z), \tag{2.16}$$

where ϵ_0 is the vacuum permittivity, c is the speed of light and α is the complex polarizability [14]. The potential is negative for a red detuned wavelength ($\omega_{\text{laser}} < \omega_{\text{atom}}$), the atom will then always go towards the lower potential - towards the higher laser power. The optical lattice uses the potential to catch the atoms by creating a standing wave in a cavity. The lattice and the atoms confinement can be seen on figure 2.5. The standing wave is slicing the atoms spacial displacement into discs with a separation of half the wavelength of lattice light along the longitudinal direction ($\lambda_l/2$). In the transverse direction, atoms are confined by the gaussian profile of the beam (x and y on figure 2.5). The confinement is more "loose", but it hardly matters, it is the confinement in the direction along which the clock laser is probing that matters (z on figure 2.5).

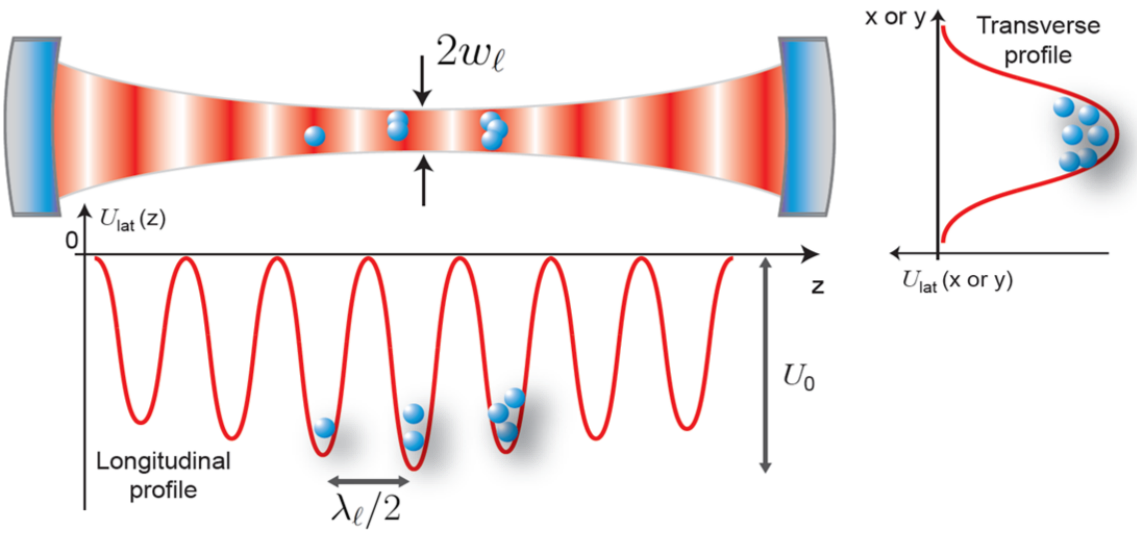

Figure 2.5: An illustration of the intensity profile for an optical lattice, and the atoms' confinement in the intensity peaks of the lattice. λ_l is the wavelength of the laser, and U_0 is trap depth of the lattice. The figure was taken from [15].

The advantages of having such a lattice is the high number of atoms ($\sim 10^4$) that is obtainable, and the motional suppression that is achievable. The regime for the motional suppression is called the Lamb-Dicke regime, where the average quantum motional number in the direction of strong confinement is smaller than $n = 1$ (most of the atoms in the fundamental motional state $n = 0$), which means that the Doppler effects becomes negligible [16].

The atoms need to be cooled before they can be caught in an optical lattice, since the band of the optical lattice is too narrow to catch the hot atoms. The optical levels to cool Sr and Hg are shown on figure 2.6. Even if Hg is an ideal metrological candidate for a clock (very heavy = very immune to residual motional effects, very low sensitivity to the black-body radiation shift and spin 1/2 making the tensor correction of the differential polarizability zero, etc.), it is an atomic species cumbersome to manipulate: indeed the large energy differences between the levels must be addressed by lasers in the UV domain, which are always difficult to operate and to maintain [17]. The Hg laser is stabilized to 4 times the wavelength of the clock transition at 1062 nm, which makes the comparison and stabilization of the clock laser much easier. This is achieve by frequency doubling the 1062 nm clock laser twice in two frequency doubling crystal to from the necessary wavelength at 266 nm for the clock transition of Hg.

The first cooling stage of Sr is to catch the atoms in a Magnetic Optical Trap (MOT). The MOT is a 3-dimensional trap based on the combination of a magnetic field gradient (with a 0 at the center), and 6 pairs of contra propagating beams red-detuned from a strong internal transition. If an atom moves away from the 0 of the magnetic field, the frequency of the transition is changed by the Zeeman effect so that the atom eventually absorbs a photon (radiation pressure), which kicks it back towards the center. The process is confining along all the direction of space, creating a cloud of cold atoms around the 0 of the B-field.

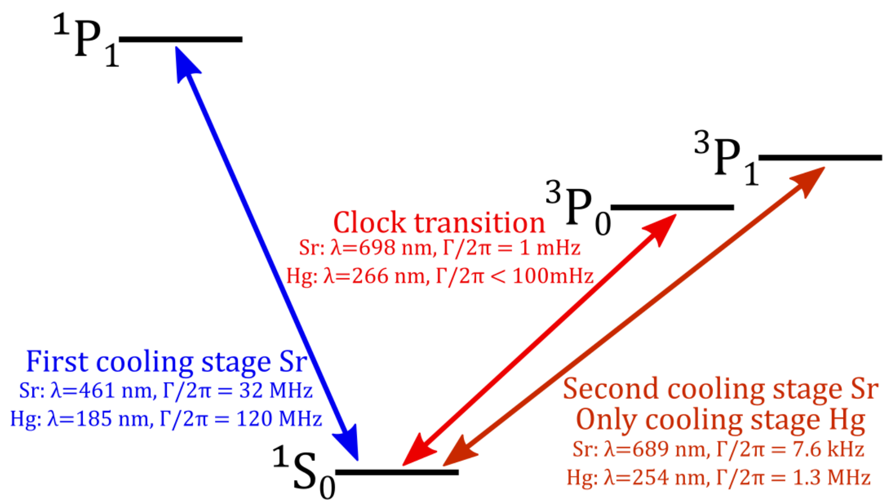

Figure 2.6: Diagram to show the most important transitions for the Sr and Hg optical lattice clocks. The atoms, Hg and Sr, are based on two electron atoms which gives the possibility to have broad and strong cooling transitions (BLUE) and narrow clock transitions (RED) for further cooling and clock interrogation. Data and inspiration was taken from [16].

The cooling transition for Sr is $|^1S_0\rangle \rightarrow |^1P_1\rangle$, which captures the atoms in the mK range. Atoms are captured directly from the blue 461 nm MOT, thanks to a technique called atomic drain: Two additional lasers overlapped with the center of the lattice "shelve" the atoms in the metastable state, where the Sr atoms do not experience the blue MOT light any more in this case, therefore they accumulate. They are this way captured in the lattice, where they are repumped back to the ground state, and then there is some further cooling taking place with the $|^1S_0\rangle \rightarrow |^3P_1\rangle$ transition to accumulate as much as possible in the fundamental motional state in the z direction.

The scheme is a bit modified for Hg. The only cooling stage for Hg is to catch the atoms in a MOT with the transition $|^1S_0\rangle \rightarrow |^3P_1\rangle$. This can still work for Hg, because of the broader linewidth for the transition. The temperature of the captured atoms are of the order of 30 μK for a Hg MOT, which is sufficient for catching the atoms in a lattice [16].

Sr and Hg both comes from the same species - alkaline earth like atoms (two valence electrons). This is critical for optical lattice clocks since there exist a magic wavelength, where the polarizability is the same for both the $|^1S_0\rangle$ state and the $|^3P_0\rangle$ state. The light shift is then rejected to first order due to the polarizability, when capturing the atoms at the magic wavelength. This can be seen for strontium on figure 2.7, where the magic wavelength is at 813 nm for the lattice light to first order [18]. The clock transition is $|^1S_0\rangle \rightarrow |^3P_0\rangle$ for both Sr and Hg due to the existence of the magic wavelength. The clock transition also has the needed sub Hz linewidth - the clock transition is in principle forbidden since there is no change in the electron's angular momentum $J = 0 \rightarrow J' = 0$, and because it is a singlet to a triplet transition. The transition towards $|^3P_0\rangle$ is only allowed due to a hyperfine mixing of the pure states $|^3P_0^0\rangle$, $|^3P_1^0\rangle$, $|^3P_2^0\rangle$ and $|^1P_1^0\rangle$ [19] (the raised 0 denotes a pure state).

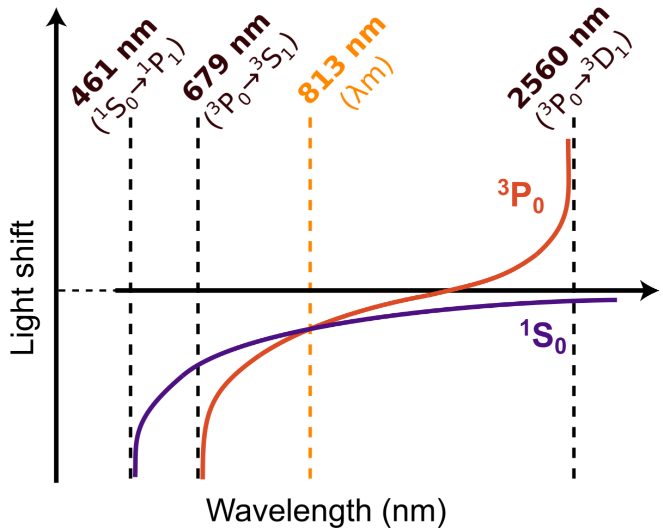

Figure 2.7: The light shift of the $^1S_0$ and the $^3P_0$ states for Sr. Showing the the magic wavelength of ^{87}Sr at the crossing of the blue curve ($^1S_0$) and the red curve ($^3P_0$), where the first order polarizability of the two states matches at 813 nm for the magic wavelength [18].

If it was not for the magic wavelength, the differential light shift would depend on the intensity of the lattice light. If there was a coupling of the frequency to the trapping intensity, the stability would degrade a lot, but thanks to the existence of this magic wavelength for alkaline-earth like atoms, the effect can be decreased by many orders of magnitude. The magic wavelength still depends on the intensity for higher order dipole moments, but the higher order terms are weaker, so the frequency are less affected.

2.3.3 Clock interrogation

There are two common methods to interrogate the atoms of an atomic clock, the Rabi interrogation, the Ramsey interrogation and the Dick effect (see 2.3.4), which is directly linked to the interrogation method.

Rabi interrogation

Rabi interrogation of an atomic clock uses the transition probability to see, if we are on resonance with the atoms. The transition probability between two atomic states without any decoherence effects can be expressed as;

$$P_2 = \frac{\chi^2}{\Omega^2}\sin^2(\frac{\Omega}{2}t), \tag{2.17}$$

where χ is a frequency also known as the resonant Rabi frequency, and Ω is the Rabi frequency. The Rabi frequency can be written as; $\Omega = \sqrt{\chi^2 + \Delta^2}$, where Δ is the detuning from the resonance ($\Delta = \omega - \omega_0$). The Rabi frequency is proportional to the experienced E-field, and the transition dipole moment; $\langle 1|\, x\, |2\rangle$ [20]. The transition probability as function of probing time can be seen on figure 2.8. The blue curve represents the transition probability with no detuning, where the probability oscillates between 0% and 100% excitation. we are able to excite all the atoms by having a pulse of light at a duration of $\chi t = \pi$, this model is of course theoretical assuming no decoherence effects. The orange curve ($\Delta = \frac{1}{2}\chi$) and green curve ($\Delta = 10\chi$) show the Rabi model with some detuning, where the Rabi frequency and the amplitude of the transition probability changes accordantly. We can express the excitation of atoms to the maximum for a given detuning as; $\Omega t = \pi$, such an operation is called a π-pulse.

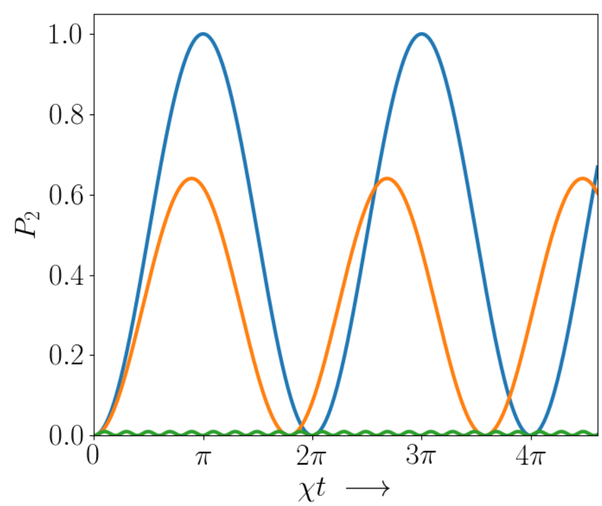

Figure 2.8: The figure shows excitation probability as a function of interrogation time for the the Rabi model, calculated from equation 2.17. The blue curve is with no detuning, the orange curve is with a detuning of $\Delta = \frac{1}{2}\chi$ and the green curve is with a detuning of $\Delta = 10\chi$.

The Rabi interrogation uses a π-pulse to excite the atoms and by changing the detuning of the laser, so the atoms' resonance can be calculated.

Ramsey interrogation

Ramsey interrogation is a bit different from the Rabi interrogation, but they are using the same principles to measure the laser detuning to the resonant of the atomic transition.

The first step of the Ramsey interrogation is to excite the system with a $\frac{\pi}{2}$-pulse of duration τ. The $\frac{\pi}{2}$-pulse excites the atoms to a superposition of the ground state and the excited state; $\frac{|\mathrm{g}\rangle + i|\mathrm{e}\rangle}{\sqrt{2}}$. This excitation can be seen on figure 2.9 as the red points. There will be a free evolution time after the first excitation, during which the phase of the oscillator and the phase of the atomic coherence are evolving independently. This evolution in this time window (T) will accumulate the phase; $\mathrm{e}^{-iT\Delta}\,|\mathrm{e}\rangle$ as an evolution around the Bloch sphere's equator, which can be seen on figure 2.9 as the green points. To see the effect, I chose a big detuning of $T\Delta = \pi/6$ to give a visual example, to show what happens on the Bloch sphere. At the time $\tau + T$ a second $\frac{\pi}{2}$-

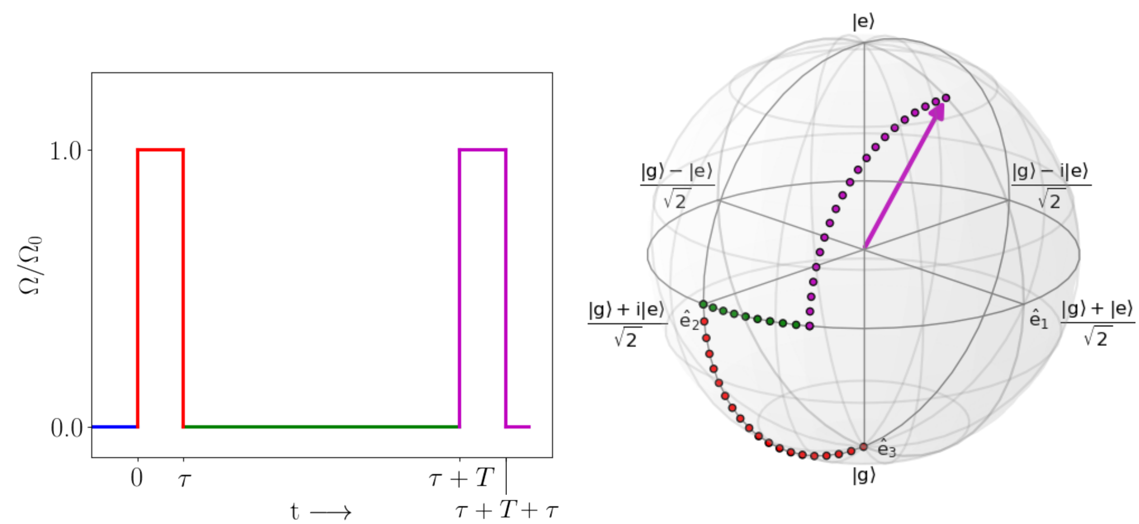

(a) (b)

Figure 2.9: Illustration of Ramsey spectroscopy: In (a) the Rabi frequency (the laser intensity) is shown as a function of time for Ramsey spectroscopy, where the colors correspond to the atom states shown on figure b. In (b) Ramsey spectroscopy on a Bloch sphere with an evolution time and detuning equal to $T\Delta = \pi/6$.

pulse will rotate the pseudo spin around $\hat{e}_1$ again, so that the effect of the detuning is turned into a population difference, which can be easily detected. This is illustrated on figure 2.9 as the pink points.

We can describe excitation percentage of the entire Ramsey interrogation by the approximating formula;

$$P_2 = 4\frac{|\chi|^2}{\Delta^2}\sin^2(\frac{1}{2}\Delta\tau)\cos^2(\frac{1}{2}\Delta[T+\tau])\ [8]. \tag{2.18}$$

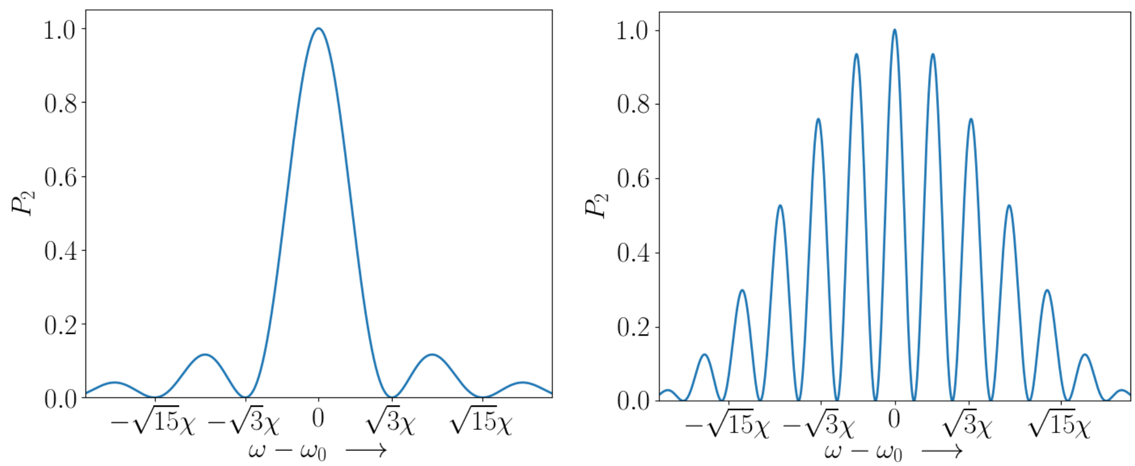

(a) (b)

Figure 2.10: Comparison of Rabi and Ramsey spectroscopy on a two level atom: In (a) the Rabi model is plotted as a function of the detuning from equation 2.17 with a π-pulse ($t = \pi/\chi$). In (b) the Ramsey interrogation is plotted as function of detuning for equation 2.18 with $T = 6\tau$.

The equation shows that by extending the evolution time T, the system becomes more sensitive to detuning. The behavior of the equation for the Ramsey model can be seen on figure 2.10b as a function of detuning. The system is very similar to the Rabi interrogation shown on figure 2.10a, but the system is even more sensitive to detuning for the Ramsey model; which makes the frequency discrimination even better. The fast oscillating term seen on figure 2.10b comes from the waiting time T between the two $\frac{\pi}{2}$-pulses, which becomes faster for larger values of T.

2.3.4 The Dick effect

The stroboscopic measurement due to dead time and cyclic probing in the atoms interrogation loses a part of the information about noise of the probing laser. The effect of sampling of the residual noise due to the stroboscopic measurement is known as the Dick effect. It is the biggest limitation to the stability of optical lattice clocks, limiting them at best to a stability of 10^{-16} at 1 s (with the best laser), while the quasi-fundamental limit due to quantum projection noise allows in principle for stabilities in the 10^{-18} range at 1 s (10^4 atoms), where the quantum projection noise would set the limitation to the stability.

The large dead time is due to the fact that the detection of the excitation of the clock transition is a fluorescence detection. The fluorescence detection is probing the ground state by lasing on a strong transition [21], where a ratio between the ground state and the excited clock transition can be established. The advantage of this method is that it gives a strong signal. The disadvantage with the fluorescence detection is that it kicks the atoms out of the optical lattice, which means the trapping procedure has to start over again. The decoherence of the laser is the limitation to the interrogation time, since the atoms have to be interrogated before the information of the excitation is lost due to the residual noise of the probing laser. The Sr optical lattice clocks have an interrogation of approximating 150 ms with a cycle time of 700 ms. This gives a duty cycle ($\eta = T_{\text{int}}/T_c$) of around 20%. We want to have as little dead time as possible, because the residual noise of the laser is lost within this window. The Dick effect can therefore also be reduced by increasing the duty cycle.

There will be a change in the excitation probability (δP) of the atoms when having frequency fluctuations ($\delta\omega$) of the probing laser. The change in excitation probability during the interrogation can be expressed as;

$$\delta P = \frac{1}{2}\int g(t)\delta\omega(t)dt, \tag{2.19}$$

where $g(t)$ is the sensitivity function, which is defined from this formula [22]. The sensitivity functions is the sensitivity to the frequency fluctuation, it will be 0 during the dead time, since the atoms will be insensitive to the residual noise of the probing laser during this period. The sensitive will then vary depending on the type on the interrogation which is used, and on the duty cycle of the clocks.

The change in the stability due to the Dick effect then takes the form of;

$$\sigma_y^2 = \frac{1}{\tau g_0^2}\sum_{m=1}^{\infty}|g_m|^2 S_{LO}(m/T_c), \tag{2.20}$$

where S_{LO} is the one-sided power spectral density of probing laser's frequency noise, T_c is the cycle time, and g_m is the complex Fourier components of the sensitivity function;

$$g_m = \frac{1}{T_c}\int_0^{T_c} g(t)\mathrm{e}^{-2\pi imt/T_c}dt \text{ [16]}. \tag{2.21}$$

The fractional uncertainty due to the Dick effect is only affected by the Fourier frequencies equal to m/T_c, because the residual noise of the probing laser repeats itself with the Fourier components matching the cycle time of the atomic clocks.

The stability of the probing laser is the biggest technical limitation to the Dick effect (S_{LO}). The need for an improvement of the probing laser's stability is therefore vital for the advancement of the optical lattice clocks.

A thorough explanation of the Dick effect can be read in the PhD thesis of Pierre Lemonde [23](in French), else a pure theoretical impact of the Dick effect can be read from the article [22].

Chapter 3

Metrological connections between atomic clocks

A chain is as strong as its weakest link. The phrase is very true when dealing with high stability lasers, where it is the component with the worst stability that will set the limit of the system. This chapter will go through the setups around our cavities and optical setups for measuring metrological frequencies. This involves the dedrifting of cavities, a new dispatching of our ultra stable lasers, a new method to measure the offset of the comb and the automation of the experimental setups (feedback loops in particular).

3.1 Frequency chain

The frequency chain is the ensemble of oscillators and connections that is necessary to form the frequency ratio between the two references (e.g clocks and lasers) that must be compared. This involves how our stable μ-wave reference is generated and how it is referencing our equipment in order to achieve better stabilities. SYRTE is using two sources to generate the μ-wave reference - a Cryogenic Sapphire Oscillator (CSO) and a hydrogen maser (H-maser). The CSO has a fractional stability of $2 \cdot 10^{-15}$ at 1 second, but drifts for longer integration times. The H-maser is locked to the 21-cm line of the spin transition in a hydrogen atom, which is far more stable for long periods of time than the CSO. The H-maser's short term stability is a lot worse than the CSO, but the fractional stability of the H-maser is a few 10^{-16} within a day. In order to benefit both from the short term stability of the CSO and from the long term stability of the H-maser, the ultra stable reference is generated by phase locking with a large time constant (1000 s) the CSO frequency to the H-maser frequency. This way, after showing a stability at (1-2) 10^{-15} up to 1000 s, where the stability starts dropping and hits the 10^{-16} range for longer periods. It is vital to have an external reference on synthesizers, Direct Digital Synthesis (DDS), counters, etc, so all the equipment share the same ultra stable source in common mode. The μ-wave reference is therefore rescaled to a RF signal at 10 MHz or 1 GHz to drive the equipment.

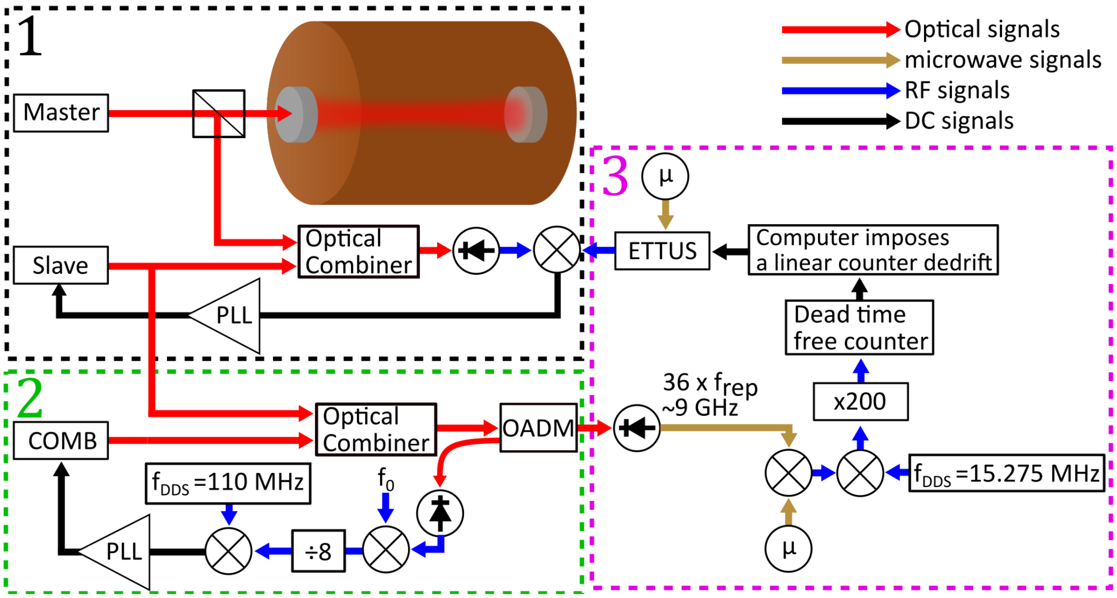

Figure 3.1: The frequency chain used for generating a stable frequency source, and locking of the comb. OADM is an optical add-drop multiplexer, PLL is a phase lock loop and μ is the μ-wave reference. All the synthesizers and counters are being referenced to the μ-wave reference as well. The ETTUS is a special DDS to generate RF signals.

Figure 3.1 shows the setup for stabilization of our ultra stable cavity (the CUS) as well as the locking of the comb to the CUS. The setup stabilizes the CUS to the μ-wave reference for long term stabilities, since cavities have poor long term stabilities, because of frequency drifts due to temperature fluctuations. The drift is a problem because:

- When the beat note crosses an RF filter, it explores the phase of the gradient, therefore a frequency drift turns into a phase gradient, and therefore a frequency bias.
- There is a problem with the atoms also: if the laser is drifting too hard, it leads to a bias called "servo error", which simply means that you are always running after the resonance.
- Finally a residual drift makes the synchronization of the measurement in Paris, Strasbourg, PTB[1], NPL[2], much more stringent: if it drifts, it must be measured exactly at the same time to avoid a bias. At the contrary, if the quantities to measure are stationary, the constraint on the synchronization is relaxed a lot. This will be mentioned further in section 3.2.

[1]PTB (Physikalisch Technische Bundesanstalt) is the German's national metrology institute
[2]NPL (National Physical Labratory) is the UK's national metrology institute

The challenge of the stabilization of the CUS to the μ-wave reference is the difference in frequency between the two. The μ-wave reference has a frequency of $\sim$ 8.985 GHz, and the CUS has a frequency of $\sim$ 194 THz (1542 nm). To overcome this challenge we use a frequency comb to compare the two frequencies. I will split the explanation of the dedrift of the CUS into 3 segments, which can be followed on figure 3.1 where each segment is numbered to ease the understanding:

1. **Locking of the slave laser to the CUS**. The master laser has a wavelength of 1542.14 nm, and it is locked to the CUS. The master laser will then have the stability of the CUS. The cavity is free running and can have large excursion (several MHz in a week), the drift must therefore be compensated, which can be done with an offset lock to a slave laser: We form a beat note between The CUS and the slave laser on a photodiode, where an offset Phase-Locked Loop (PLL) acts back on the current of the slave laser to stabilize it to the CUS. The PLL will act on the slave laser the following way; $\nu_s = \nu_{\text{CUS}} + f_{\text{ETTUS}}$. The frequency of the ETTUS is explained in the 3rd segment.

2. **Locking of the comb to the slave laser**. We want to transfer the spectral purity of the CUS to the comb, so that all the optical beat notes will be narrow. The approach for f_0 is: We mix it out everywhere. The approach for f_{rep} is: We lock it to an ultra stable laser.

   The slave laser is being combined with the comb, where it goes to an Optical Add-Drop Multiplexer (OADM)[3]. The beat slave vs comb is reflected in a narrow band, while all the rest (rest of the spectrum of the comb) is transmitted. The reflection sees the signal in a narrow band and does not suffer from the shot noise that all the other teeth of the comb would bring, while the many teeth transmitted will yield a strong signal at the harmonics of f_{rep}. The reflected light of the OADM that contains the beat note is then detected on a photodiode. f_0, detected elsewhere, is mixed out of the beat note, yielding a f_0-free beat; $f_S = Nf_{\text{rep}} - \nu_S$. The f_0-free beat note is then being rescaled to decrease the amplitude of the phase excursion, so the repetition rate of the comb can be locked to the frequency of the slave laser. The PLL locking the repetition to the frequency of the slave laser is expressed as; $\frac{Nf_{\text{rep}}-\nu_s}{8} = 110$ MHz.

3. **Dedrifting of the slave laser by the μ-wave reference**. The transmitted light through the OADM is detected on a photodiode. It only detects the light of the comb, which has the interference between the teeth creating a signal of f_{rep}, $2f_{\text{rep}}$, $3f_{\text{rep}}$... The signal we are interested in is $36f_{\text{rep}}$ which gives a signal of $\sim$ 9 GHz, since the repetition rate is $\sim$ 250 MHz. The μ-wave reference at 8.985 GHz is then mixed with the signal at $36f_{\text{rep}}$. There is a problem with this signal: The noise to detect is smaller than the resolution of the counter. The solution: A DDS signal close to 15.275 MHz is subtracted, which gives a result around

[3] An Optical add-drop multiplexer is the fibered equivalent of an interference filter

275 kHz that is multiplied by 200 (giving a frequency at 55 MHz) in order to get a signal whose noise can be resolved by the counter. This can also be seen from the following equation; $\mathrm{Ch1} = -200 \cdot (36 f_{\mathrm{rep}} - \mu_{\mathrm{reference}} - 15.275\ \mathrm{MHz}) \simeq 55\ \mathrm{MHz}$.

The repetition rate is locked to the frequency of the slave laser, which means the signal detected on the dead time free counter is the drift between the slave laser and the μ-wave reference. In order to counteract this drift, a counter drift ("dedrift") is applied to the offset of the lock between the master and the slave, which updates the slope of the dedrift every 30 s, where the stability of the μ-wave reference exceeds the stability of the slave laser. The dedrift is imposed on the ETTUS, which is a special DDS programmed by a FPGA, which is a very fast microcontroller (it is made by the company ETTUS).

The optical scheme explained above has two purposes; the first is to create an ultra stable laser that we can use for measurements and distributions to other laboratories. This ultra stable laser is now the slave laser, which has the short term stability of the CUS and the long term stability of the μ-wave reference. I will refer to this signal as the CUS in the rest of the thesis, since it has the stability of the CUS. The second purpose is to create an ultra stable comb that has a stable repetition rate. All of our other ultra stable lasers like the clock lasers for Hg and Sr are also dedrifted. They are dedrifted by measuring the frequency difference between the laser and the atoms. This means the lasers are not drifting in respect to each other, which makes measurements over long periods of time a lot easier, as we do not have to change any frequencies or filters due to drifts.

3.1.1 Noise compensation

Fiber noise

A few centimeter of optical fiber can easily be the limiting factor when it comes to the noise floor of a system operating below a fractional stability of 10^{-17} at 1 s. It is therefore essential to do fiber noise compensation whenever using optical fibers for ultra stable lasers.

An illustration of how fiber compensation works is shown on figure 3.2. A laser is injected into a fiber, where it is split up by a beam splitter into the two paths B and D. Path B is going to a mirror that retro-reflects the light back to path C, where it hits a photodiode. Path D is going to an AOM that shifts the frequency with a few MHz. The light then proceeds to a new beam splitter E and F. Path E goes to the desired location (the optical setup). Path F is going to another mirror that retro-reflects the light back through the same path it came from - it first goes through the AOM again shifting the frequency of the light again, where it goes to path C and hits the same photodiode.

The light will accumulate a phase shift along the fiber in the form of phase noise. We can write the phase of the light reflected on the first mirror in path B,

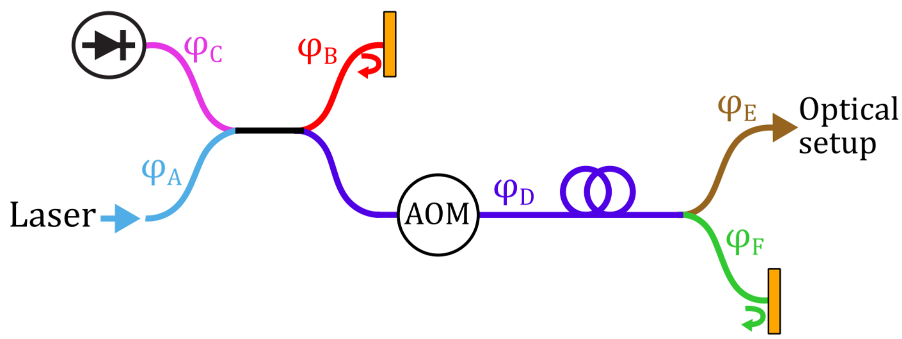

Figure 3.2: The optical setup needed for fiber compensation, with the the phase φ shown as the phase change over the given distance.

and hitting the photodiode as; $\varphi_1 = \varphi_{\text{laser}} + \varphi_A + 2\varphi_B + \varphi_C$. The light goes two times through path B, which gives the factor 2 of the phase φ_B. We can write the light going to the second mirror, and reflected back to the photodiode as; $\varphi_2 = \varphi_{\text{laser}} + \varphi_A + 2\varphi_{\text{AOM}} + 2\varphi_D + 2\varphi_F + \varphi_C$. The signal from the interference between φ_1 and φ_2 on the photodiode can be written as;

$$\varphi_{\text{PD}} = \varphi_2 - \varphi_1 = 2\varphi_{\text{AOM}} + 2\varphi_D + 2\varphi_F - 2\varphi_B. \tag{3.1}$$

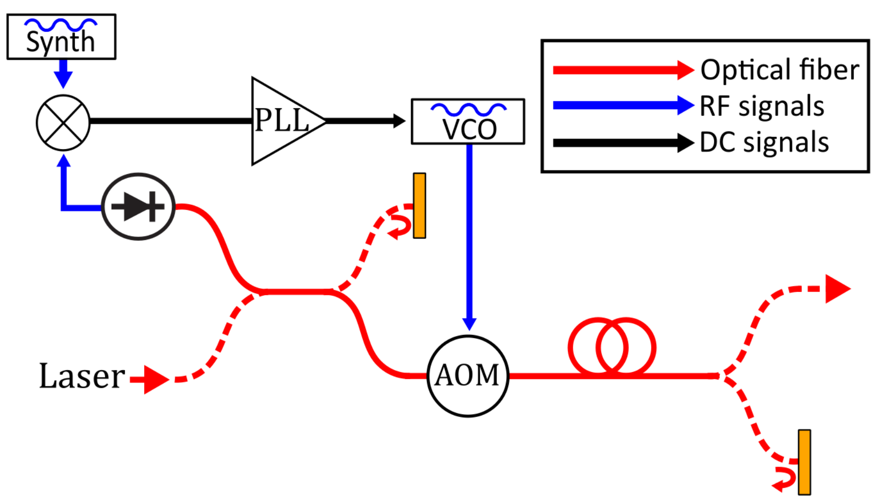

Figure 3.3: The setup needed for fiber noise compensation. The dashed optical paths are the uncompensated paths that will affect the noise of the propagation of light. The error signal detected on the photodiode goes to a RF chain, which sends the correction through a PLL to the AOM for the fiber noise compensation.

The RF chain of the fiber compensation can be seen on figure 3.3. The beat note detected by the photodiode (φ_{PD}) is going to a mixer whose other input is fed by an ultra stable source (e.g DDS, synthesizer), close to the central value of $2\varphi_{\text{AOM}}$. The signal then goes through a PLL yielding a feedback to a Voltage-Controlled

Oscillator (VCO) that drives the AOM. The PLL will lock the mixed signal between φ_{PD} and φ_{synth} to a Direct-Current (DC) signal creating the PLL;

$$2\varphi_{\text{AOM}} + 2\varphi_D + 2\varphi_F - 2\varphi_B = \varphi_{\text{synth}}. \tag{3.2}$$

φ_{synth} is stabilized to the μ-wave reference which has a fractional stability of $2 \cdot 10^{-15}$. The synthesizer is working in frequencies of $\sim$ 100 MHz which gives a stability in the sub-μHz level, so we can discard the noise of the synthesizer. The noise of the paths that will be corrected in equation 3.2 are the paths D, F and B. The light we want to correct is taking the path A→D→E. The output phase (φ_{out}) going to the optical setup when exchanging the phase φ_{AOM} with the phase of the PLL shown on equation 3.2;

$$\begin{aligned}
\varphi_{\text{out}} &= \varphi_{\text{laser}} + \varphi_A + \varphi_{\text{AOM}} + \varphi_D + \varphi_E \\
&= \varphi_{\text{laser}} + \varphi_A + \left[\frac{1}{2}\varphi_{\text{synth}} - \varphi_D - \varphi_F + \varphi_B\right] + \varphi_D + \varphi_E \\
&= \varphi_{\text{laser}} + \varphi_A + \frac{1}{2}\varphi_{\text{synth}} - \varphi_F + \varphi_B + \varphi_E.
\end{aligned} \tag{3.3}$$

There will be an over correction to the paths F and B, which will add noise to the compensation. The length of paths B and F are in practice a few centimeters, and the fiber compensated path D is usually in the orders of meters or more, which is the power of the fiber compensation making it very favorable. The uncompensated paths on figure 3.3 are all the paths marked with dashed lines. The principles for the fiber noise are general, and they can all be applied for free-space noise, some refinements to fiber noise compensation will be explained in the next sections.

Using this setup for ultra stable lasers would not be optimal, since there would be too much fiber noise added along the fiber. I will in the next sections explain a better way of designing the setup.

We have made some measurements of the consequence of the fiber noise. The optical setup we used to measure the fiber noise is shown on figure 3.4. The setup is similar to the setup shown on figure 3.3, but another branch is added with the objective of making an out-of-loop measurement. The setup is constructed so we have interference between path A and B on the photodiode to the right on figure 3.4.

The first measurement we did was to do fiber noise compensation on both path A and B, so we had a control/reference measurement, where we tried to make the compensation as perfect as possible, and we see where we are at in this case. All the paths that usually would be considered uncompensated (like the red paths on figure 3.3) would not be in this case. The uncompensated paths are in common mode for this measurement, since they share the same uncompensated paths for the fiber compensation. The only paths that are not in common mode are the paths A and B, and they are compensated. The result can be seen on figure 3.5 as the green data with a fractional stability of $9 \cdot 10^{-18}$ at 1 s. This measurement is a control measurement of how it would look with fiber noise, but there is a limit to the noise compensation. The reason why the stability is limited to $9 \cdot 10^{-18}$ at 1 s could be due

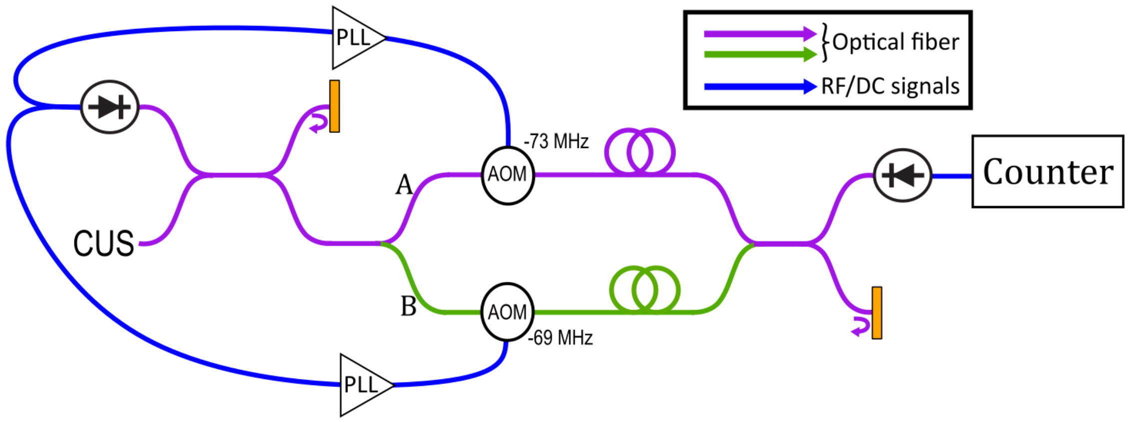

Figure 3.4: Experimental setup for measuring the fiber noise: Path A is always fiber compensated. Path B has the option to be fiber compensated, and a changeable length for the fiber.

to small retro-reflection after the AOMs along the fiber of path A and B due to light reflection after the AOM. This will for instance have the same frequency as the light reflected by the last Faraday mirror, therefore there can be an interference, aka: you do not compensate exactly the right thing because there is a contamination in your error signal by something you do not want to compensate. This is a known problem, and I will explain how to go around it later in this section.

We stopped the noise compensation of path B in the next measurement. We did this by powering the AOM in path B with a synthesizer, without having a PLL acting on the fiber compensation, because we want to measure the fiber noise in a given length of optical fiber. We will have the sum of noise from the fiber AOM and the uncompensated fiber with the total length of path B being 10 m. We got a stability of $7 \cdot 10^{16}$ at 1 s, which is shown as the red data on figure 3.5. We can clearly see that the system becomes a lot less stable without any fiber compensation, where the stability is almost two orders of magnitude worse than with path B compensated.

We also did this measurement where we removed the AOM to see the contributions from the thermal fluctuations of the AOM. The black data shows the setup without the AOM in path B, but the stability does not look affect by the AOM's thermal fluctuations. We also extended the fiber to 30 m which is seen as the pink data. The data was a bit noisy due to activity in the laboratory, probably due to polarization changes, which can cause fluctuations in the SNR. Therefore I only took the stretch of data corresponding to no activity in the laboratory. The data removed for the black and the pink data have been marked on the time trace graphs.

Theoretical speaking, the standard deviation decreases with $\sqrt{L}$ for uncorrelated noise, where L is the length of the fiber [24]. The stability of the pink data for a 30 m fiber would be expected to have a $\sqrt{3}$ worse stability than for the black data with a 10 m fiber. This is also the case when having a stability of $2 \cdot 10^{-15}$ at 1 s for a 30 m uncompensated fiber. The same logic can be used to imagine shorter fiber

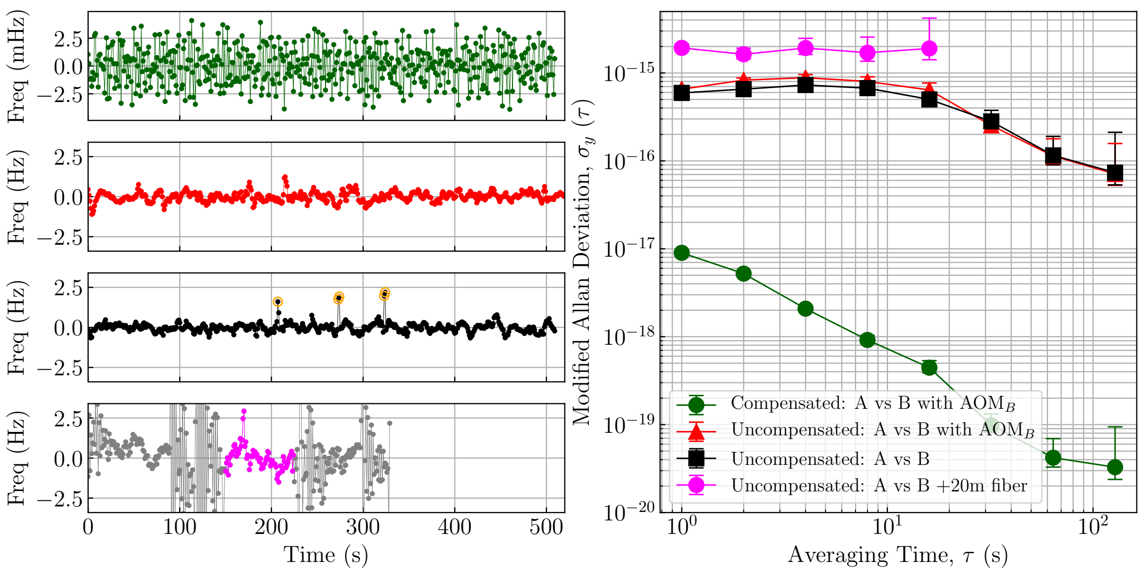

Figure 3.5: Measurement of the degradation in stability due to fiber uncompensated paths. The experiment is measured from the setup shown on figure 3.4. The removed data is shown on the time trace data to the left. The measurements have been measured with a frequency counter in Λ-mode (see section 2.3.1).

lengths, where 1 cm of uncompensated fiber would add an instability contribution of $\frac{7\cdot 10^{-16}}{\sqrt{1000}} = 2 \cdot 10^{-17}$ at 1 s. This is of course a very rough estimate, but it illustrates that just 1 cm of uncompensated fiber is enough to limit the stability of a high level stability setup like the transfer of spectral purity.

Free-space noise

I have measured the free-space noise to know the limitation of our setups when changing the setups from fiber to free-space optics. The setup needed for noise compensation in free-space is shown on figure 3.6. The setup shows noise compensation in free-space when a beat note with the comb is acquired. The setup for free-space compensation is very similar to the fiber compensation explained above. The light we want to compensate in this example is the clock laser from one of the atomic clocks to create a beat note with the comb. The idea of a free-space noise compensation setup is to have the uncompensated path in free-space, where the amount of added noise is lower. This is because of the index of refraction is smaller in air than fiber, where the fluctuations of the index will be much smaller, which will cause much less phase noise for the propagating light.

On figure 3.6, the phase front of the light after AOM_2 is gaussian shaped as shown by the black curves on the red beam. The whole phase front would not be reflected identical to itself, if we were to retro-reflect the light at this point when the phase front is not flat. A cat's eye is used for the reflection of the phase front, so we achieve a flat phase front on reflection. A cat's eye is composed of two lenses displaced by the sum of the two focal lengths of the lenses. The waist of the light will be at the focal length away from the lenses, where a retro-reflecting plate is placed to reflect the flat phase front. The retro-reflecting plate in the cat's eye does not need to reflect a lot, as it reflects in the order of 10% of the light ($\sim 50\mu$W). The transmitted light will be collimated after the cat's eye, because it works as a telescope. The light after the cat's eye will be combined with the comb to form a beat note. The reflected light of the retro-reflection plate will go back through the AOMs to the photodiode, where a beat note with the local oscillator is detected to do the noise compensation between the two interferometer arms.

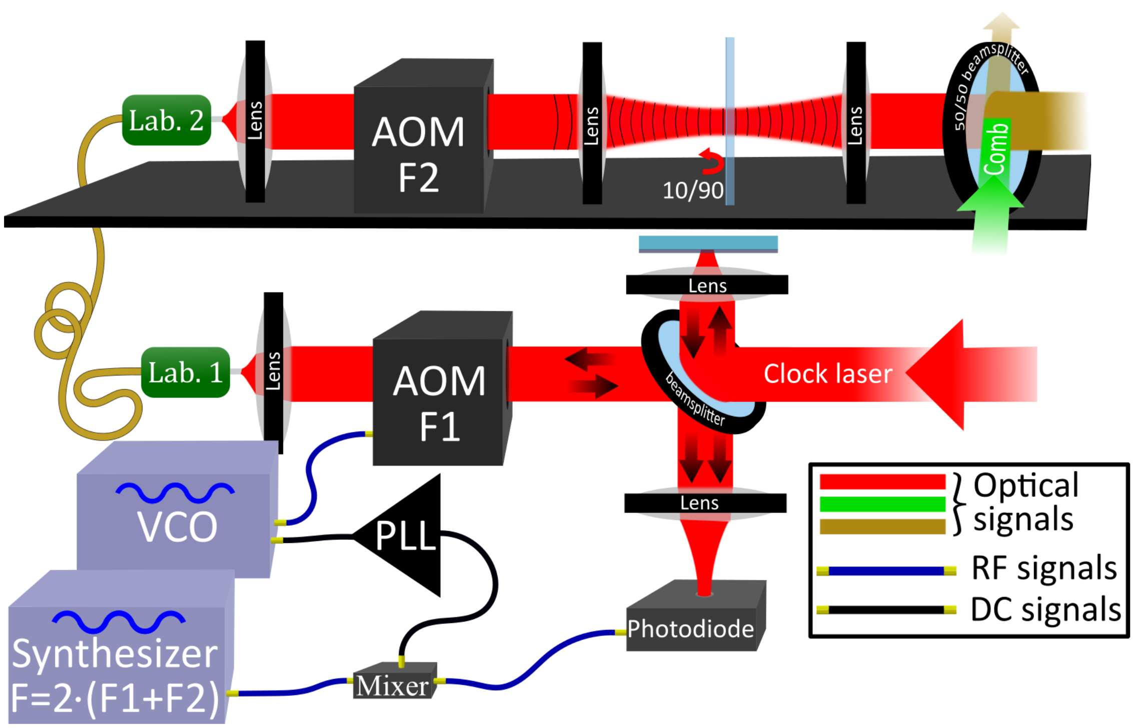

Figure 3.6: RF and optical system needed for a compensation of the fiber and free-space noise when acquiring a beat note with the comb. The setup starts in the bottom right corner, where the clock laser first goes to a beam splitter to reflect the light for the local oscillator of the noise compensation. The transmitted light goes to AOM_1, which will be responsible for the noise compensation. The setup is illustrating a transport of the clock laser between two laboratories (or between two optical setups within the same laboratory). The light after AOM_1 will go to an optical fiber that delivers the light between the two independent laboratories, lab. 1 to lab. 2. The light to be compensated is done on the retro-reflecting plate, where the transmitted light is combined with the comb.

The detected beat note on the photodiode will be at a frequency of $2(F1 + F2)$, since we are double passing the light through both AOMs. The signal will be mixed with a synthesizer at a fixed frequency, so a PLL can act on a VCO to correct the frequency of AOM_1.

The stray reflection in the fibers and the reflection on the cat's eye would be at the same frequency, so there would be no way to distinguish them and it create a delusion to the error signal that would be used for locking. In order to fight that, AOM_2 creates a frequency shift between the stray reflection in the fibers and the reflection on the cat's eye. The stray reflection in the fibers would create a beat note on the photodiode at $2 \cdot F1$. This would not be seen on the compensation, since the reflection on the cat's eye will be at a frequency of $2(F1+F2)$. The frequency would be the same of both reflection, if AOM_2 was not placed. This would add some noise in the system, which makes AOM_2 critical to have installed.

The setup shown on figure 3.6 can still be modified a bit, if the noise compensation of the fiber is taking place within the same laboratory. The fiber compensation can act on AOM_2 instead of AOM_1, where you can remove AOM_1. This will only require one AOM, and you will still overcome the reflection problem, since the reflections in the fiber would not have any frequency shift, and the frequency lock would be at $2 \cdot F2$. This would not work with a transport of the frequency over a long distances, because the RF signal to correct the AOM also has to be transported to AOM_2, where the RF signal could accumulate noise over the long distance.

There are two types of noise sources: The first type of noise is the interferometric noise which is added to the low frequencies that comes from the free-space interferometer. The noise we see here comes from optical length fluctuations induced by the sensitivity of the refraction index to vibrations, pressure change, temperature change and so on. In my effort to limit this kind of noise in our setup, I have made a distribution chain, which will be discussed in section 3.4. The second type of noise is for the higher frequencies, which comes from the small time delay of the reflected light traveling back and forth. This reflection noise would not be compensated beyond frequencies of $\frac{c}{n2L}$, where c_n is the speed of light in the medium of propagation and L is the length of the compensated path [25]. The compensation will not work at those frequencies since the time constant for the compensation is slower than the frequencies. When we are transporting a fiber between laboratories, the length is a maximum of 30 meters long. This would cause a delay bump in the compensation at 3 MHz, which is beyond the tracking bandwidth of the compensation. The tracking usually has a bandwidth of 100 kHz, so these fast processes occurring at a few MHz are not compensated, which will not affect the compensation. The limit to the band of compensation would most likely come from the propagation of sound in the AOM. We would not expect any noises to be added by the propagation, since most common noise sources will be in the low kHz range. The noises we will see in the fiber compensation are thermal and mechanical sources. The thermal noise will be in a band of 100 Hz, which we easily can remove, and the mechanical noises are acoustic noise and vibrational noise, which have band of approximating 50 kHz.

The atomic transition also works as a perfect low-pass filter, because the atoms only catch the low Fourier frequencies around the resonance frequency, which is important when considering the noise to compensate for the transfer of spectral purity. We can write the excitation probability in the Rabi model from the following equation; $P_2 = \frac{\chi^2}{\chi^2+\Delta^2}\sin^2(\frac{\Omega}{2}t)$ (see equation 2.17). The amplitude of the excitation at a detuning Δ is therefore: $\frac{\chi^2}{\chi^2+\Delta^2} \simeq \frac{\chi^2}{\Delta^2}$ for $\chi \ll \Delta$. This is the case when we have frequency noise larger much larger than the Rabi frequency of close to 1 Hz. The atoms will therefore see the 1 kHz noise with an excitation attenuated by; $\frac{1\ \mathrm{Hz}^2}{10^6\ \mathrm{Hz}^2} = 10^{-6}$, which is negligible for an atomic ensemble of around 10^4 atoms.
The band of tracking is more critical for comparing atomic clocks from distant laboratories through fiber links. The travel distance can be several hundreds of kilometers, where the delay bump will affect the tracking, which gives a band at a few 100 Hz. The fiber links will be discussed briefly in section 3.2, when discussing the comparisons with PTB and NPL.

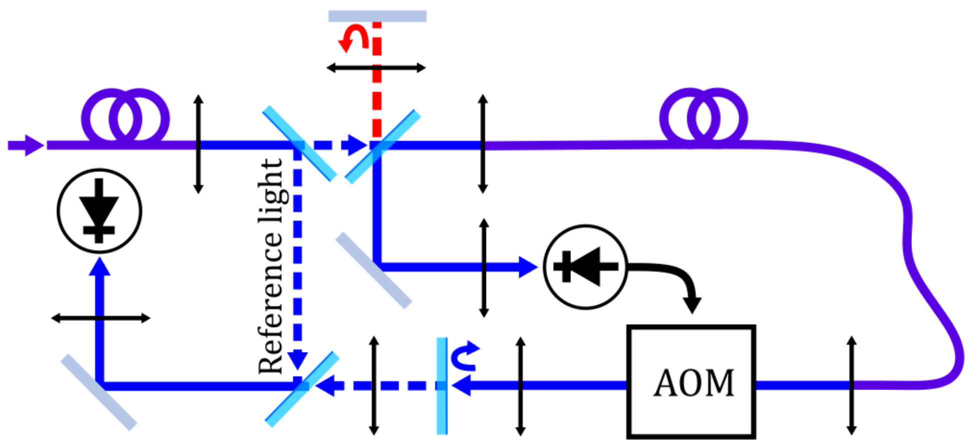

Figure 3.7: Setup for measuring the free-space noise with the option of changing the length of the uncompensated interferometer arm (marked as a red line). The setup starts in the upper left corner where the light at 1542 nm is sent to a beam splitter. The Reflected light is our reference light that is being sent directly to another beam splitter, where the two light paths later will be combined again to measure the noise of the uncompensated paths. All the uncompensated paths are marked by a dashed line. The black arrow is a RF signal imposing the correction on the AOM for the fiber compensation.

I have designed a test setup to measure the free-space noise when doing noise compensation with a fiber and a free-space local oscillator arm (the red path). The setup is shown on figure 3.7. The transmitted light through the first beam splitter is going to our noise compensation setup which is the same setup as shown figure 3.6, where the light is being split up to do the local oscillator for the compensation, and the transmitted light is going through to a fiber. After the fiber an AOM is placed to act on the noise compensation. The cat's eye is placed shortly after with the retro-reflecting plate placed at the waist in the cat's eye. The two light sources are now combined again on a photodiode. The frequency of the beat note $f_{\text{synth}}/2$ is decided by the synthesizer mixed with the compensation error signal for the PLL controlling the fiber compensation.

The noise of the optical setup shown on figure 3.7 will have the noise of all the uncompensated paths drawn as dashed lines. When the small local oscillator arm marked as red for the noise compensation is made as small as possible, the total uncompensated length reaches 13 cm, where the blue uncompensated paths correspond to the 9 cm out of the 13 cm of uncompensated paths. The reference light and the fiber path are combined just before the photodiode. The noise will be negligible after recombination as the lasers will be in common mode.

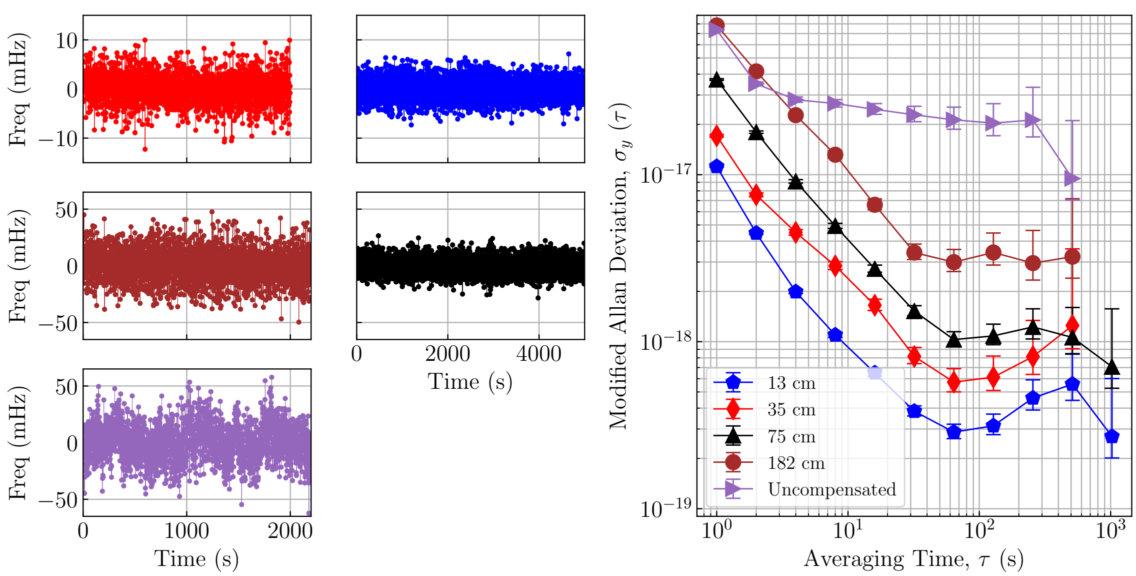

Figure 3.8: Measurement of the degradation in stability due to free-space uncompensated paths. The setup for the measurements is shown on figure 3.7. The legend states the total length for the uncompensated path. The optical setup was placed in a room with air-conditioning. The measurements have been measured with a frequency counter in Λ-mode.

Results for the effect on the stability due to the amount of free-space uncompensated paths are shown on figure 3.8. All the results show that the uncompensated paths are dominated by flicker phase noise for the first 20-30 seconds of integration time. The bumps are then caused by temperature fluctuations, because the temperature is changing the path lengths of the uncompensated paths. The influence of vibrations is set to a minimum (placed on a anti-vibration table), and is expected to hardly contribute in a free-space setup any way. The setup is close to the worse case scenario since there is an air-condition hood placed a few meters from the optical setup. This is not really how the optical setups are installed, since the uncompensated paths are installed in plastic or metallic boxes to limit the air and temperature fluctuations.

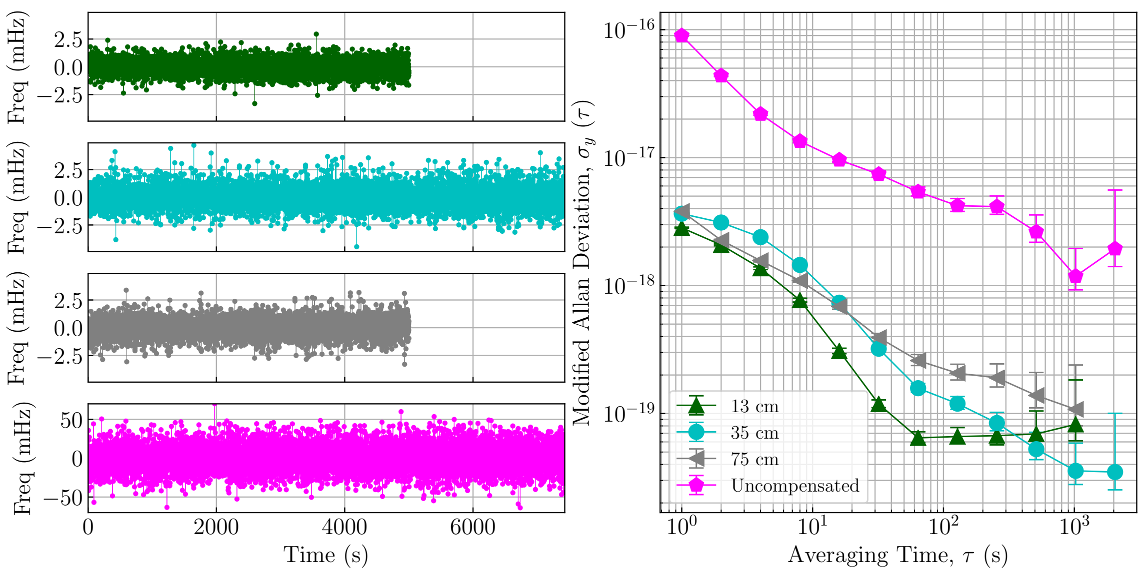

Figure 3.9: Protected setup: Measurement of the degradation in stability due to free-space uncompensated paths. The setup for the measurements is shown on figure 3.7. The legend states the total length for the uncompensated path. The optical was setup protected with a blanket. The measurements have been measured with a frequency counter in Λ-mode.

The experiment was repeated where a thermal blanket made from metallic polyester was placed over the experiment. The measurement was rather sensitive to placement of the blanket, because it was difficult to shield equally all the parts of the optical setup. The results for the protected setup measuring the stability of the free-space uncompensated paths are shown on figure 3.9. The stability got a lot lower, with at least a factor of 3 for the stability at 1 s; e.g going from a fractional stability above 10^{-17} to below $3 \cdot 10^{-18}$ at 1 s for 13 cm of uncompensated paths. The blanket also isolated the thermal fluctuations of the optical paths, which can be seen by the much lower stabilities, where the bump kicks in due to the thermal fluctuations. The stability changed a lot depending on the time a day for the protected measurement, because the behavior of the temperature depends on the time a day the measurement has been done. The long term stability changed the most, which can be seen on the 35 cm of uncompensated path, which had a better long term stability, because it was taken through the night, where the temperature fluctuations are smaller.

The measurement of the free-space uncompensated paths shows that the amount of uncompensated path hardly depends on the length for a stability at 1 s when the paths are well protected, and the thermal fluctuation are also suppressed a lot from the protection. This shows the importance of protecting the optical setup, not having air floating through the setups. We were able to reach a fractional stability of $4 \cdot 10^{-18}$ at 1 s with 75 cm of free-space uncompensated paths. This gives an upper bound on the stability for 75 cm of uncompensated paths in our optical setups due to air fluctuations, since the uncompensated paths of the optical setups are protected in more isolated environments like 1-3 cm of plastic/metal instead of a thin blanket.

3.2 Clock comparison

One of the fundamental pillars of science is that you should be able to repeat an experiment at any given time and place, and to obtain the same result within the theoretical frame work's description of the experiment. The atomic clocks are built exactly with this as the reason for their existence, and it is therefore important to compare the atomic clocks around the world.

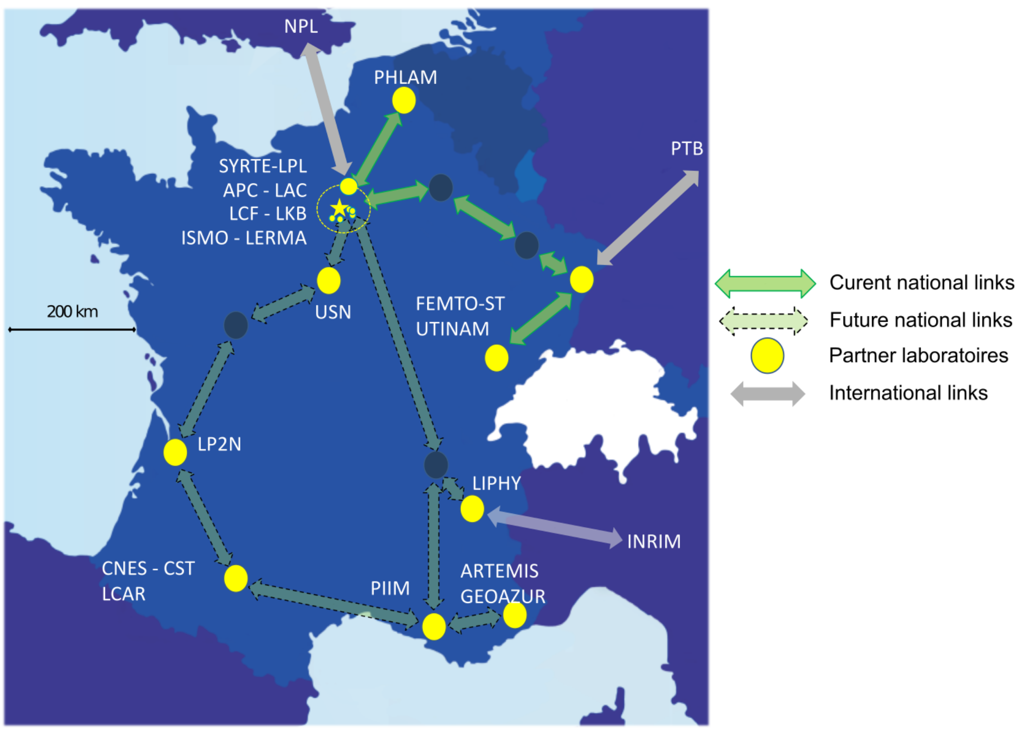

Figure 3.10: Optical fiber links of the French network for frequency comparisons within Europe. The map of fiber link network was taken from [26, 27].

We are comparing our optical lattice clocks with NPL and PTB via an international network of optical fibers distributed to the European laboratories a common mode ultra stable reference at 1542 nm (see figure 3.10). The comparison between the clocks allows measurements of the residual biases as well as assessing of the operational limits of the clocks.

We could e.g have a bias from the fact that we have two Sr optical lattice clocks. They are both operated by the same clock laser, and the most of the electronics, temperature, etc. We could have a bias originating from the spectrum of the clock laser, e.g a sideband that would pull the resonance systematically on one side on both clocks. We could also have a mistake on the estimation of the gravitational redshift, which would cause a systematical frequency shift on all the optical lattice clocks. There could be many similar cases, which need to be investigated through comparisons of clocks in different locations with different designs.

The light from clock lasers can not be sent directly through the optical fiber links. The optical fiber links transmit best in the C-band, with attenuation as low as 0.2 dB/km around 1550 nm. We need to translate the frequency of the clock laser into a frequency in the C band in order to compare the clocks. We use the CUS at 1542 nm (in the C band) to compare the frequencies. Figure 3.11 shows the comparison between SYRTE's and PTB's atomic clocks via the optical fiber link, described below:

1. The clock laser is first compared with the atoms to measure the resonance frequency of the clock transition.

2. The clock laser is then measured against the frequency comb, where it is possible to compare it to the CUS. The ratio in frequency between the clock laser and the CUS can then be calculated.

3. The CUS light is sent towards Strasbourg, where a beat note with the equivalent laser on the German side is counted. We compensate all the noise in the Fourier band of interest (up to 100 Hz), there are repeater laser stations or amplifiers along the fiber links. The 1542 nm laser is a common mode reference for the different laboratories, its therefore possible to compare all the clocks to this common mode reference.

The frequency ratio between the compared atomic clocks are derived in post-processing by combining the measurements atom vs laser and lasers vs lasers. The measurement of lasers vs lasers involving the comb are measured with the "transfer oscillator" method, which removes the parameters of the comb from the comparison of frequencies, so it is a "all-optical" measurement (the "transfer oscillator" method is explained in section 4.1).

3.2.1 Automation

In our efforts to prepare for the implementation of a continuously running system for the optical lattice clocks, an automation of the electronics has been a lengthy process when being in the process of making a completely continuous running laboratory. This is especially important because SYRTE will be one of the key laboratory involved in the PHARAO-ACES mission, projected to start in 2020. A large fraction of the data acquisition and processing will be performed by the laboratory, therefore

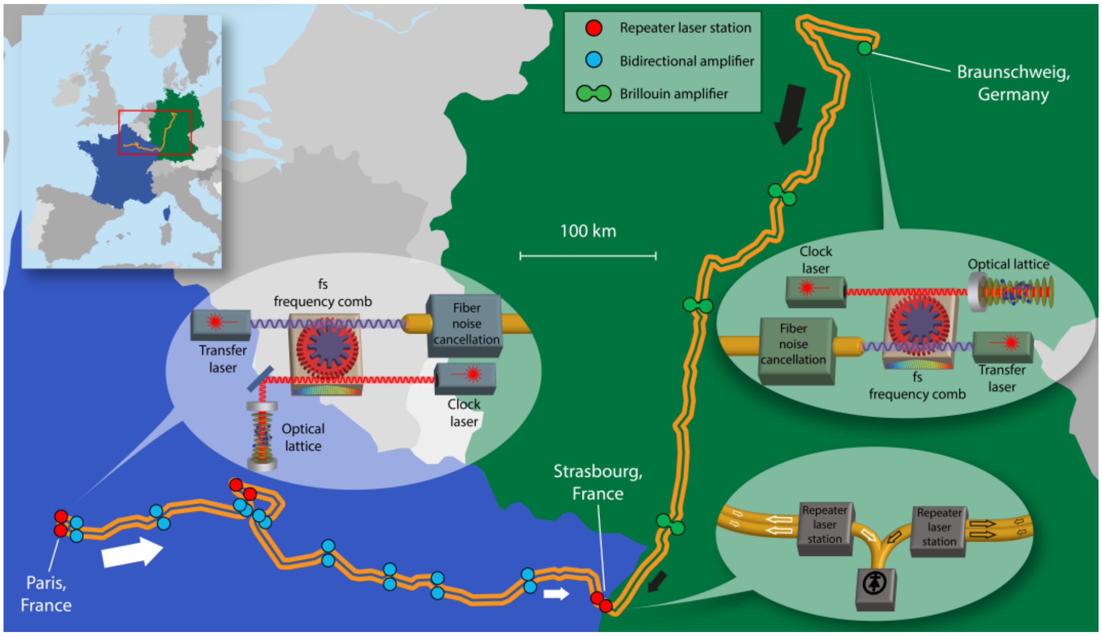

Figure 3.11: The comparison between SYRTE (Paris, France) and PTB (Braunschweig, Germany). The comparison between the clock lasers and the frequency combs can be seen in both Paris and Braunschweig, where the final comparison between the 1542 nm lasers of SYRTE and PTB are measured in Strasbourg (France). The figure was taken from [28].

justifying the need for a high degree of automation. The PHARAO is the first ever cold-atom clock to orbit earth, which is going to be used for clock comparison and metrology experiments. The clock comparison between the caesium clock on board the PHARAO has to be compared multiple times a day when it passes over Paris. The laboratories need to run automatically for the clocks to be measured on each round trip. Continuity is in general important when we are talking about atomic clocks, and it is also one of the things requested if we are going to have a redefinition of the second based on the optical lattice clocks.

It has been my responsibility to automate frequency controls of DDSs called "AD9912" and a beat note monitoring system, which can be used to control and correct other devices in the laboratory. We have also made a software that re-lock phase lock loops, which we are using to re-lock our frequency combs.

To ease the redevelopment of software, we are now programming everything in the programming language python. This ensures that everyone uses the same programming language, which makes it easier for others to make changes in old softwares. My softwares are made into executable files, which makes them easier to distribute due to the need for different python packages will harm the flexibility, as well as the need for a python console to be open.

Controlling the DDSs: AD9912

It is vital for a fully automated laboratory to control synthesizers over the Internet, so we can re-center the beat notes, send new lock frequencies, etc. This can be controlled automatically by a monitoring software or be done manually without any presence in the laboratory. One of the DDSs we have been using is called AD9912 (datasheet AD9912). It is a DDS with 48 bits and it calculates the frequency from the formula:

$$f_{\text{out}} = \frac{f_{\text{in}}}{2^k} n, \tag{3.4}$$

where k is the number of bits, f_{in} is the input frequency, and n is the tuning word. The tuning word is an integer that can be between $[0, 2^{k-1}]$. The DDS can take any given input, and create a rescaling of the signal. We are mostly using the DDS for generating stable RF signals by having the input signal derived from the μ-wave reference. We have also used the DDSs for the transfer of spectral purity, where we rescale beat notes with the DDSs, which is described in section 4.1. The user interface of the AD9912-software can be seen on figure 3.12. The user interface of

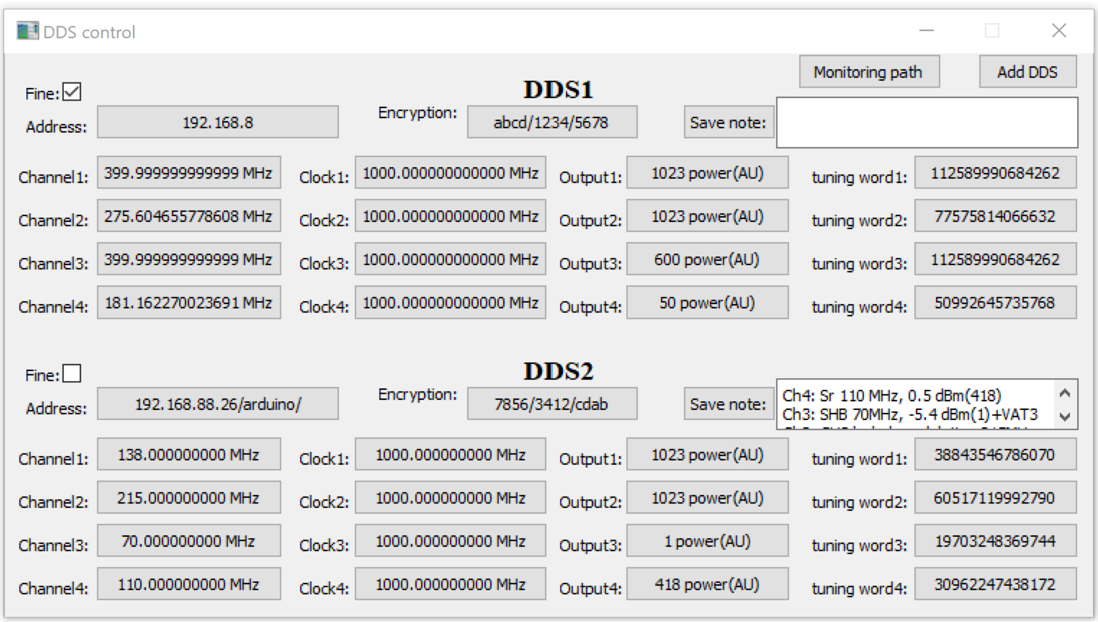

Figure 3.12: Graphical interface for the software controlling the AD9912s.

the program is to ease the usage of the software. Any monitoring software can then talk to the program, if a new frequency or rescaling is needed like a new frequency for an AOM, re-centering of a frequency, etc.

The commands for the DDS are sent as the tuning word in hex-decimals. There is just the concern, that the order of the hex-decimals are changing depending on the AD9912 for an unidentified reason. I have therefore made an encryption function to customize the encryption of the hex-decimals to the DDS.

There is a flaw with the AD9912: That it can not take any uneven numbers for the tuning word. We have therefore decided that we always want a frequency "below or equal to" the requested frequency for an even tuning word.

We have rescaled our μ-wave reference to 1000 MHz, as it is the maximum input frequency. An example of how the program makes decisions on the frequency could be following: If we want a tuning word that matches a frequency of 200 MHz, and we were to calculate the tuning word; $\frac{200}{1000}2^{48} = 562\ 949\ 953\ 421\ 31.2$. We would then get the closest tuning word to be an uneven number instead of an even. The desired tuning word would be at $n = 562\ 949\ 953\ 421\ 30$, because it would give us the closest frequency below the requested frequency of 200 MHz. I have gone with this code line to reach the requested tuning word;

$$\left[\mathrm{int}\left(\frac{f_{\mathrm{out}}}{f_{\mathrm{in}}}2^{47}\right)\right] \cdot 2, \tag{3.5}$$

where int is taking the closest integer below or equal to. I then multiply by 2^{47} instead of 2^{48}, so I can multiply by 2 after I have calculated the integer, since an integer number multiplied by 2 always gives an even number. The int-function always rounds down, so we get the desired tuning word. Putting a frequency of 200 MHz into equation 3.5 a tuning word of $n = 562\ 949\ 953\ 421\ 30$ is achieved, which was the desired tuning word. The achieved frequency would be 199 999 999.999 996 Hz, with a hexadecimal of "333333333332".

Beat note monitoring

Another important feature is to monitor the beat note between the comb locked to the CUS and the clock lasers on the one hand, as well as the lattice lasers on the other hand. I have made a software that talks to a RF switch and a spectrum analyzer to monitor the beat notes. The RF switch has 6 input ports and 1 output port, and an Internet control to change the input port. The output port is then connected to the spectrum analyzer to analyze the spectrum of the signal. This gives the option to change individual beat notes to check their frequencies. The user interface of the program is shown on figure 3.13.

The program is streaming the data and the controls on the servers of SYRTE. This allows the user to control the program anywhere. This program is vital when it comes to continuous measuring the optical beat notes, because it grants the possibility for problem shooting without being present in the laboratory. It also gives the possibility for an automatic re-centering of the optical beat notes to the counters, since the program can measure the frequency of the beat notes.

Re-locking of phase lock loops

We have also made a software for automatic re-locking of PLLs, because some PLLs have tendencies to unlock. The software is used for re-locking the phase lock loop

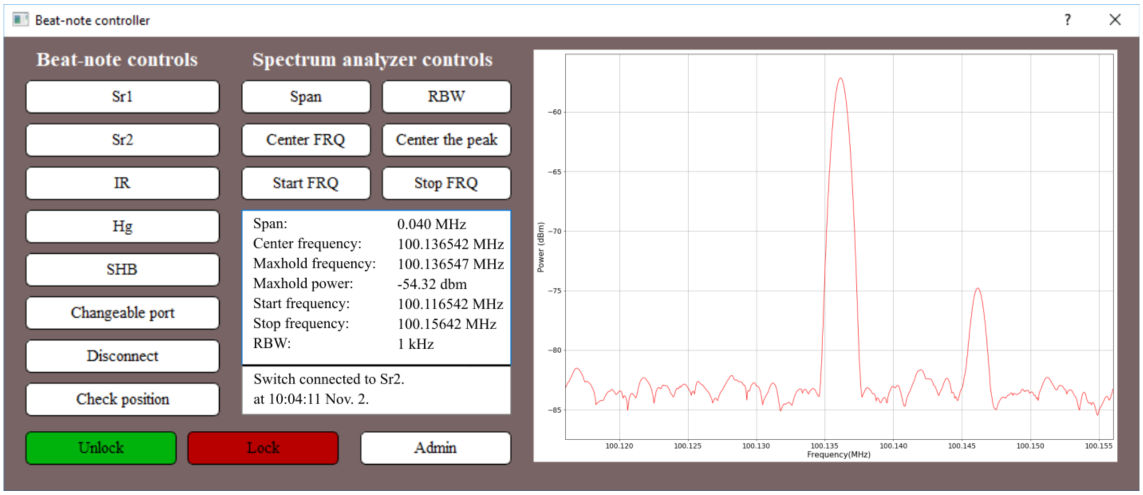

Figure 3.13: Graphical interface for the software controlling and monitoring beat notes.

between the frequency combs and the CUS. Whenever the phase lock loop unlocks, the software starts to scan over the error signal until it finds the lock point, where it locks. It then checks if the repetition rate is the right one, by checking the frequencies of the beat notes that are known. It will then start the search all over again, if it is turns out to be the wrong lock point. The offset of the comb also drifts out of the filters used for filtering of the signal. The software also acts on the current for the offset of the comb, so the offset is re-centered to the central frequency of 70 MHz for filter, that is filtering any additional peak away from the signal.

3.3 A new method to detect the offset of the comb

The frequency peaks of an optical frequency comb are not ultra stable, as a beat note between an ultra stable laser and a comb would have a broad linewidth around 1 MHz, because it still contains the carrier-envelope offset frequency in the beat note. The offset is left free running, and it is therefore not ultra stable. This means the beat note has the same linewidth of the offset of the comb (f_0), but the stability becomes ultra stable when f_0 is mixed out with the beat note (if the measured laser is ultra stable as well as the repetition rate). The detection of the offset is crucial, since we want to remove exactly the same offset as in the beat note of the comb.

The setup for the detection of f_0 in the usual way is seen on figure 3.14. The setup starts by having the whole octave spanning spectrum after the EDFA, which goes to the SHG medium (the theory behind the detection of f_0 has been explained earlier in section 2.2). After the SHG the signals to detect f_0 are within the spectrum of the light, which will be at the highest frequencies of the spectrum. f_0 comes from the interference between the spectrum at 1050 nm and the frequency doubled spectrum at $\frac{2100}{2}$ nm. The spectrum is then split up with a PBS, where it reflects some of the

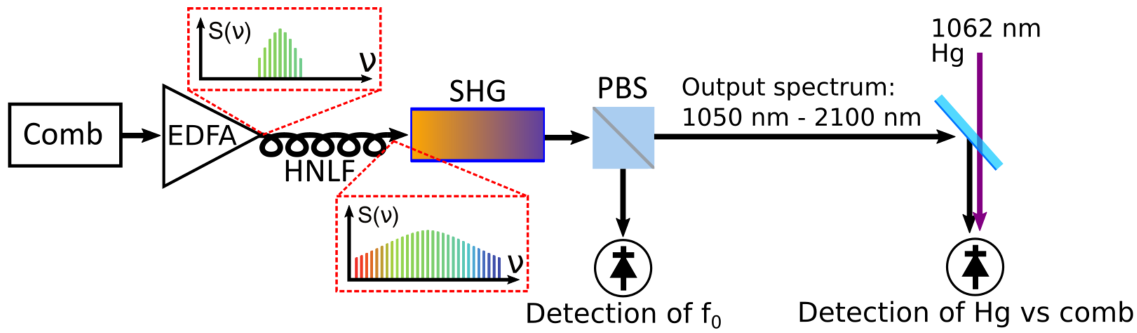

Figure 3.14: The optical components in the comb for the detection of f_0, and the detection of the optical beat note between the comb and the Hg laser. HNLF is a highly non-linear fiber, The SHG medium is optimized to frequency double around 2100 nm. The mirrors, lenses and lambda plates are not shown. The spectrum shown before/after the HNLF is to illustration the broadening of the spectrum.

spectrum for the detection of f_0, and it transmits the rest for the detection of the beat note between the comb and the Hg laser.

We detect f_0 in a dedicated RF output of the comb, coming from the photodiode named "Detection of f_0" on figure 3.14. On top of that we discovered, by chance, that a spectral peak corresponding to f_0 was also present in the detection of the optical beat notes formed with the same EDFA as the one used to detect f_0. The presence of f_0 there makes sense, because the same spectrum to detect the offset of the comb is also transmitted through the beam splitter cube, propagating with the comb's full spectrum for the detection of the beat note with the Hg laser. We realized we could use it at our benefit, and we started an investigation of the what we started calling "magic-f_0".

We have tried different self-modulating RF chains for the demodulation of the beat notes with magic-f_0. This involves multipliers, mixers, amplifiers which all are non-linear components. The best solution we found for the most clean signal in the RF chains was a splitter and a mixer, where the signal first is split up and mixed with itself again. The two big question then arise; "can we trust the accuracy of this approach? And do we achieve a better stability by the self-modulation scheme than the usual way of demodulating with f_0?"

The two methods for the demodulation of f_0 are shown on figure 3.15. The signal is filtered and amplified after the detection of the beat note between the comb and the Hg laser. The frequency for the beat note is; $f_{\text{beat}} = Nf_{\text{rep}} + f_0 - \nu_{\text{Hg}}$. The beat note is then split up into f_{beat1} and f_{beat2}, where they are propagating for the two different demodulation chains. f_{beat1} is mixed with $f_{0,\text{EDFA}}$, which is the f_0 detected just after the EDFA shown on figure 3.14. We will then obtain the signal;

$$f_{\text{beat1}} = Nf_{\text{rep}} - \nu_{\text{Hg}} + f_0 - f_{0,\text{EDFA}}. \tag{3.6}$$

The signal is finally demodulated by a DDS in order to produce a beat close to 10 kHz, filtered by a narrow (1 kHz band) filter box centered at 10 kHz. The filter box

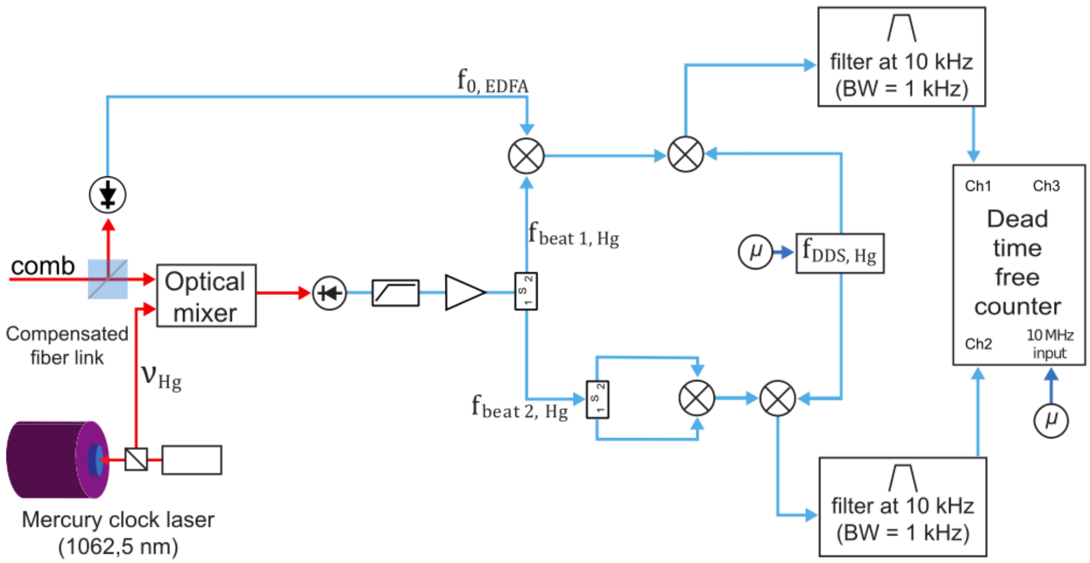

Figure 3.15: The setup for measuring a beat note the usual method with $f_{0,\mathrm{EDFA}}$ seen on the RF chain; $\mathrm{f_{beat\ 1,\ Hg}}$, and measuring the beat note with the magic-f_0 method (self-demodulating) seen on the RF chain; $\mathrm{f_{beat\ 2,\ Hg}}$ ($f_{0,\mathrm{magic}}$). After the photodiode the RF signal first goes to a high-pass filter then an amplifier before being split up into $\mathrm{f_{beat\ 1,\ Hg}}$ and $\mathrm{f_{beat\ 2,\ Hg}}$.

creates a square signal of the sinusoid to help the counting, because it makes sharp 0 crossings. The signal is at last counted by a dead time free counter.

We have two signals in f_{beat}. We got both a signal at the frequency of $f_{0,\mathrm{magic}}$ and $Nf_{\mathrm{rep}} + f_0 - \nu_{\mathrm{Hg}}$. We can have the two signal mixed by splitting up f_{beat2} and mixing it again with itself. We will then obtain the signal;

$$f_{\mathrm{beat2}} = Nf_{\mathrm{rep}} - \nu_{\mathrm{Hg}} + f_0 - f_{0,\mathrm{magic}}. \tag{3.7}$$

The signal is centered to the filter box and counted as well.

The intention is to eliminate f_0, but which value is the smallest $f_0 - f_{0,\mathrm{EDFA}}$ or $f_0 - f_{0,\mathrm{magic}}$. The measurements of f_{beat1} (red data) and f_{beat2} (green data) are shown on figure 3.16. The two datasets are limited by the stability of the comb against the Hg laser, since it is the stability of the comb against the Hg laser we are seeing. We can instead compare the difference between the two methods; $f_{\mathrm{beat2}} - f_{\mathrm{beat1}}$, where the parameters of the comb will cancel each other. This is shown as the pink data on figure 3.16, which are has an fractional stability of $8 \cdot 10^{-19}$ at 1 s. The measurement averages down dominated by the white frequency noise for the first 100 s. The accuracy is within the uncertainty of the stability with a mean offset of the frequency to be 21.44 μHz. The statistical uncertainty of the mean value would approximating be 15 μHz, which is comparable with the mean offset within 1.4σ.

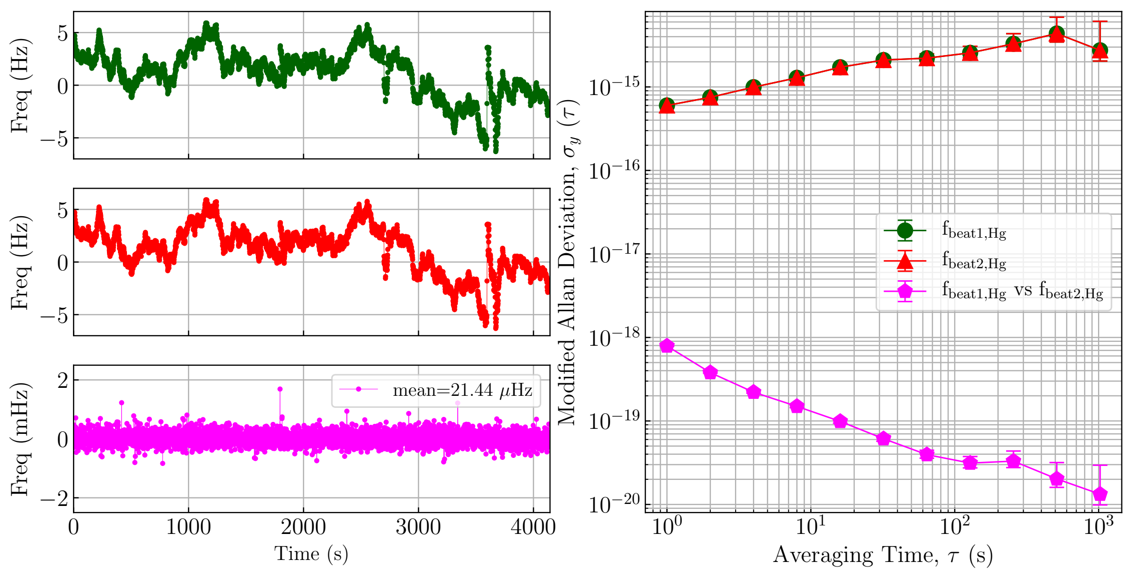

Figure 3.16: Measurement of the differential noise between the two methods for detecting the offset of the comb (f_{beat1} and f_{beat2}). The measurement is done using the RF setup shown on figure 3.15. Two data point of the pink data have been removed due to cycle slips (8 and 16 mHz away from the central frequency). The measurements have been measured with a frequency counter in Λ-mode.

3.3.1 The effect of the pointing instability

The pointing instability is introducing Amplitude Modulation (AM) noise for the detected beat notes, because the laser beam can fluctuate over the active area of the photodiode. The detection of $f_{0,\text{magic}}$ is done on the same photodiode as the Hg beat note, where the noise due to the pointing instability could be common for both beat notes, reducing the noise of the detection of f_0. The detection of $f_{0,\text{EDFA}}$ is detected on a different photodiode, which could add an uncorrelated noise source to the demodulation chain.

The setup to measure the pointing instability is shown on figure 3.17. The setup is combining the Hg laser and the comb on a 50/50 beam splitter, where the combined lasers proceed to two photodiodes. The advantage of this measurement is that the two photodiodes will have separate pointing instabilities, but the Hg laser and the comb will be in common mode on both photodiodes, because they are in common mode when they are split up. There are created two signals on each photodiode, which are f_{EDFA} and f_{magic} that are the equivalent of f_{beat1} and f_{beat2} respectively.

We see the results of the measurement on figure 3.18. The measurement has been done in Π-mode, which explains that the stability is a bit worse than shown on figure 3.16, where the pink data is the equivalent of the black and pink data on

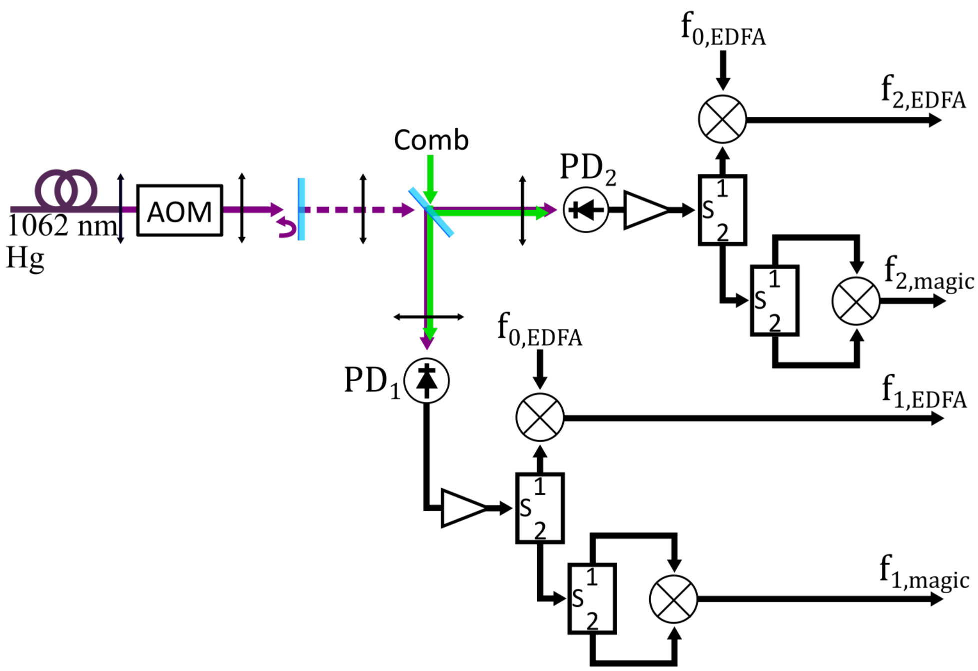

Figure 3.17: Setup to measure the difference in noise between two photodiodes due to the pointing instability. Both photodiodes have two different demodulation chains to demodulate with $f_{0,\text{EDFA}}$ and $f_{0,\text{magic}}$. The violet and green lines are optical signals, and the black is the RF signals.

figure 3.18. It can be seen that the result for all the configurations are fairly close in stability. The brown data is showing another measurement, where two identical RF chains fed by the same photodiode are being demodulated by $f_{0,\text{EDFA}}$ and compared on two counters. This measurement is a test of the limit to the setup, since we would expect the two branches to have the same noise. the measurement shows a small improvement in the stability, but we would expect a complete correlated dataset, which means the limit of the setup comes from the the end of the RF chain in the detection (either the filter boxes or the counters).

We have tested the signals after the filter boxes, and it shows that the filter boxes are treating the noise a bit differently, where the sensitivity to the noise varies for the filter boxes. This could very well be the limit to the chain, but the limitation can be overcome by feeding more stable signals to the filter boxes, because the sensitivity depends on the noise of the compared beat notes.

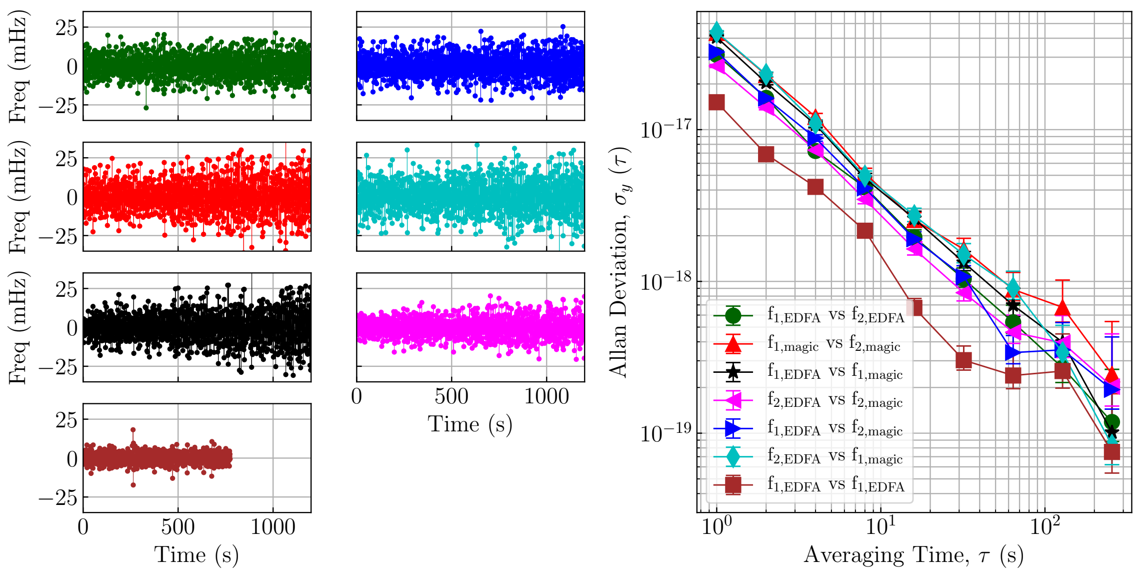

Figure 3.18: Measurement of the pointing instability affecting the offset of the comb: Measurements show all the combination of signals seen on figure 3.17. The brown data is showing a new combination, where two identical RF chains with $f_{1,\mathrm{EDFA}}$ are made and compared. The measurements have been measured with a frequency counter in Π-mode (see section 2.3.1).

3.3.2 Direct measurement of differential effects of the offsets

f_0 can not be measured directly by the counters, because the width of the signal is too broad to send it through the filter boxes. The different f_0 signals can instead be mixed together to create an ultra stable signal, but the problem is that it would create a DC signal, so we have designed the RF chain shown on figure 3.19. The RF chain mixes $f_{0,\mathrm{EDFA}}$ with DDS1 too put an offset on $f_{0,\mathrm{EDFA}}$ before it is mixed with $f_{0,\mathrm{magic}}$. The RF signal is then mixed with DDS2, which centers the RF signal to the filter box at 10 kHz to be counted.

There are several advantages of using this method to count our signals. The first is that we can measure the values for f_0 directly without involving the Hg laser, where its SNR could set the limit of the measurement. The statistical noise depends a lot on the SNR of a measurement, which easily can be the limitation to the counted signals. The SNR will in the end set the limit to the stability of a measurement due to the white phase noise, which sets the noise floor of the measurement, which sets the limit depending on how easily the measured carrier frequency can be distinguished from it. The second is that the signal we are feeding the filter box has extremely low noise, where the filter boxes have shown to be less sensitive to the low noise signals. The measurement of the frequency chain on figure 3.19 shows not to be limited by

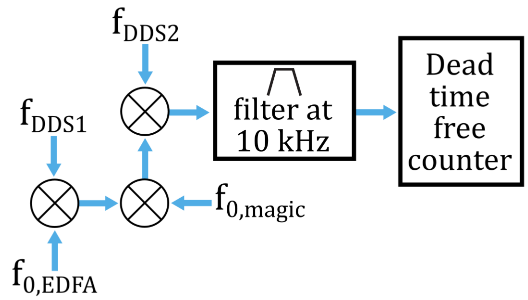

Figure 3.19: Setup used for comparing two signals that have the same mean frequency, where they are ultra stable when compared, which is the case for $f_{0,\mathrm{EDFA}}$ and $f_{0,\mathrm{magic}}$.

the filter boxes, because we are hitting the noise floor of the counters. This can be seen on figure 3.20, where the gray data shows the noise of the counter, because a quantization of the measured frequency starts to show. The noise are common among the channels of the counter, which can be seen on the black data, where the differential noise between two channels are measured.

The measurements on figure 3.20 show that when comparing $f_{0,\mathrm{EDFA}}$ with itself (the blue data) and $f_{0,\mathrm{magic}}$ with itself (the green data) the noise of the counter (the gray data) sets the limit to the measure for short term stabilities, which is what we would expect when comparing identical signals. There is some flicker for longer integration periods for $f_{0,\mathrm{magic}} - f_{0,\mathrm{magic}}$, which could come from the SNR, since the SNR sets the noise/stability floor of the measurement. This would explain the result for $f_{0,\mathrm{magic}} - f_{0,\mathrm{magic}}$ measurement, since we had some problems improving the SNR of the measurement.

We can therefore conclude that the limit to the difference in stability between $f_{0,\mathrm{EDFA}}$ and $f_{0,\mathrm{magic}}$ are at $3 \cdot 10^{-19}$ at 1 s seen as the red data on figure 3.20, because the RF chain is not the limit to the measurements. The comparison between $f_{0,\mathrm{EDFA}}$ and $f_{0,\mathrm{magic}}$ has an offset of the mean value by -1.11 μHz. This is within the statistical uncertainty of 2.8 μHz. The result shows that the accuracy is not affected by the two methods of demodulating with f_0, since the statistical uncertainty and the offset are comparable. An offset at the μHz level is very small compared to the best published uncertainty budgets, which are at the mHz level. Therefore this possible very small offset between $f_{0,\mathrm{EDFA}}$ and $f_{0,\mathrm{magic}}$ are orders of magnitudes away from affecting this budgets.

The advantage of detecting $f_{0,\mathrm{magic}}$ is that we can have more power for the detection of optical beat notes. The beam splitter for splitting the light for detection of $f_{0,\mathrm{EDFA}}$ (see figure 3.14) can be removed, since we do not have to detect f_0 the usual way anymore. This gives us the option to send all of the spectrum's power towards the optical setups giving us greater SNRs for the optical beat notes.

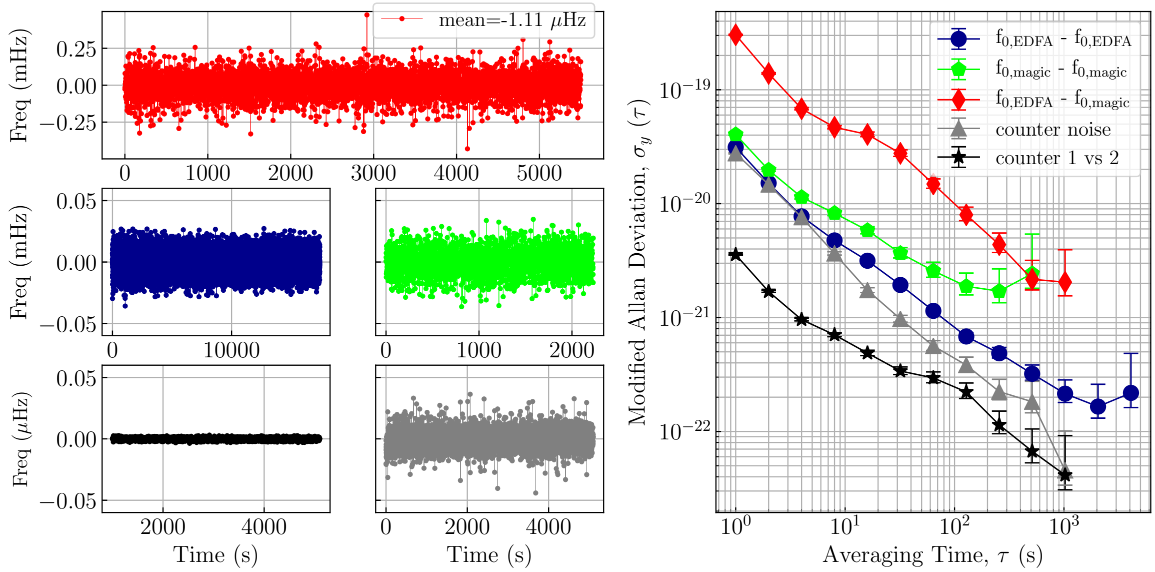

Figure 3.20: Measurements of the limitation to the frequency chain and to the offset of the comb. The red, blue and green data are measured using the setup shown on figure 3.19. The gray data is the noise introduced by the counter, which has been measured by feeding an ultra stable RF source to the counter, where the quantization of the output starts showing. The black data is the noise when identical signals are compared on two channels of a counter. All the fractional stabilities are measured against the Hg frequency, since the stabilities in the end will affect the stability of Hg when demodulated with f_0 in the RF chain. The measurements have been measured with a frequency counter in Λ-mode.

3.4 The dispatching of an ultra stable laser

The dispatching of the CUS has been done in fiber optics, so the CUS could be delivered to the optical setups at SYRTE. The optical setup for the dispatching can be seen on figure 3.21. The uncompensated paths are marked as dashed lines. The additional noise is from the fiber bringing the ultra stable laser to the dispatching setup and the small local oscillator arm for the reflection. The uncompensated paths will add noise to system, and the noise added needs to made as small as possible, so we can achieve the best oscillator for us to transfer the spectral purity to the Sr and Hg optical lattice clocks.

Some details can be improved further to the optical setup shown on figure 3.21:

1. All the branches are compensated on the same photodiode, which may result in a saturated photodiode. It will also be hard to amplify the beat notes for the fiber compensation, because the spectrum will be like a forest of beat notes that has to be filtered out, since the spectrum features many peaks, nonlinear

effects (in amplifiers,, mixers) may result in the apparition of unwanted peaks.

2. The local oscillator arm is an uncompensated fiber, which could be made in free-space to reduce the noise due to uncompensated paths.

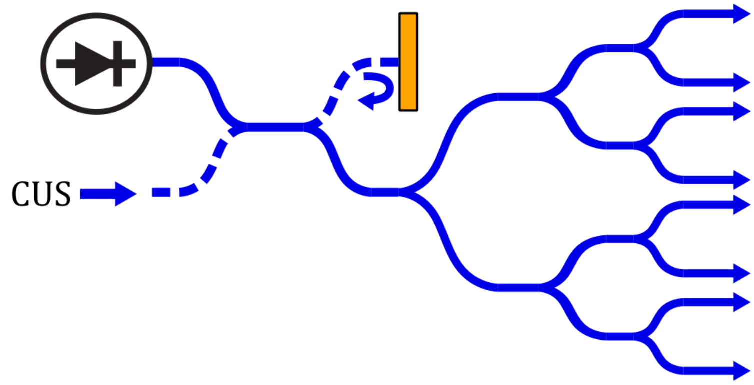

Figure 3.21: The optical setup used for distributing the frequency of the CUS. The uncompensated paths are marked as dashed lines. All the outputs (to the right) go to optical setups with retro-reflecting plates, so the light can be retro-reflected for the fiber compensation.

In order to minimize the impact of these issues, we decided to design a setup with uncompensated paths in free space, and multi-photodiodes. The optical setup of the free-space dispatching setup is shown on figure 3.22. In order to have more power and an average frequency that can be steered easily, a slave laser is locked to the master laser, with an adjustable offset. The lock is based on a beat note slave-master formed by the photodiode referred to as "Master lock" on figure 3.22. The compensation will then have an offset PLL acting back on the current of the slave laser. There will be three branches to be compensated on three separate photodiodes for each slave laser, instead of using one single branch with one photodiode to compensate all paths for one slave laser. This allows us to avoid saturation of the photodiodes. All the dashed lines are the uncompensated paths of this setup. The ultra stable points of the slave lock is at the beam splitters combining the master and Slave 1, and beam splitters combining the master and Slave 2. This means that the stability will be the best at Output 3 for Slave 1, and the best at Output 1 for Slave 2, because they have the shortest uncompensated path to the stable point.

We have also improve the locking of the master laser to the cavity, where we have almost no uncompensated paths involved. This means that the ultra stable point of locking to the cavity is noise compensated from the point of fiber compensating the light going to the "Cavity (output)". The noise compensation of the master laser uses the first local oscillator arm after the input of the master, where the error signal for the noise compensation is measured on the photodiode named "Cavity".

The setup is not only limited to 6 outputs (3 for each slave laser), because we can split up each output with a fiber beam splitter. This will create two fiber

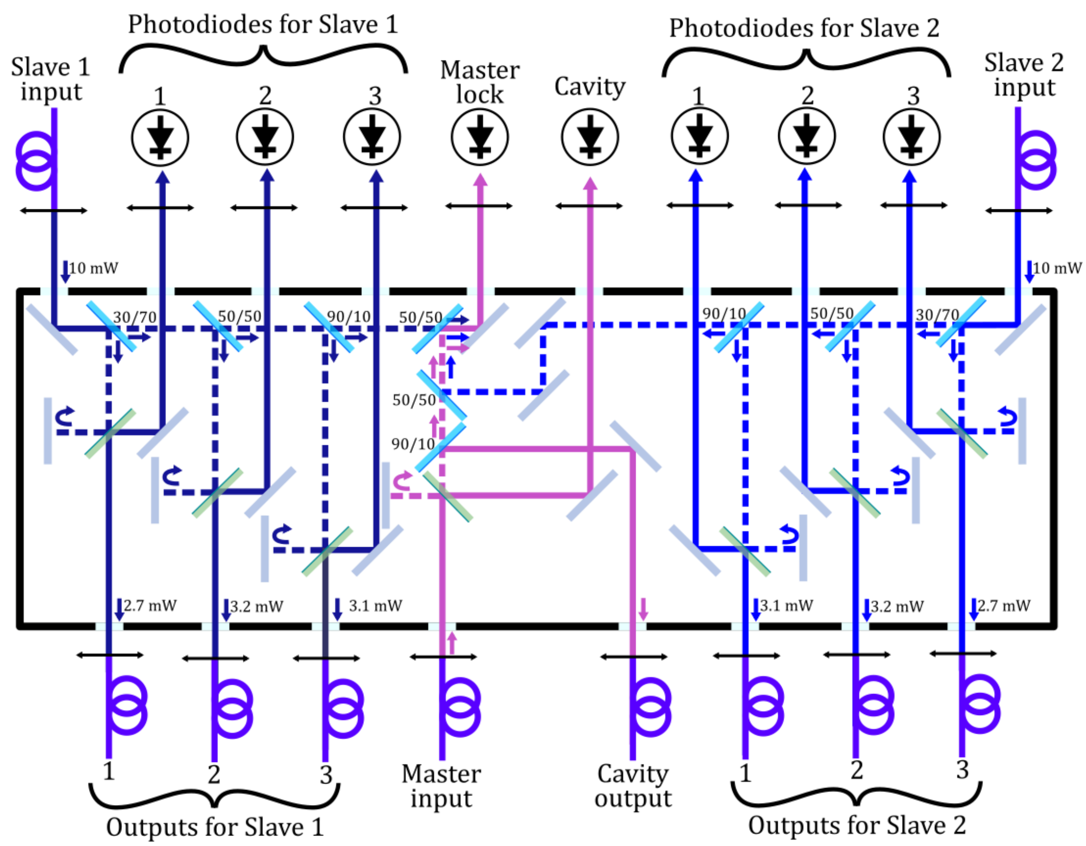

Figure 3.22: The frequency dispatching made to distribute the light of the slave lasers that are locked to the master laser, to distribute the light to the optical setups at SYRTE. The dashed lines are the uncompensated paths, Master lock is the photodiode for the locking of Slave 1 and Slave 2 to the master laser. The color of Slave 1 is Navy-blue, Slave 2 is light-blue, and the master laser is pink. "Cavity output" is the fiber bringing the master laser to the cavity setup. The beam splitters used for the local oscillator arm (for noise compensation) are green instead of blue (beam splitter for splitting the power of the slave lasers). The black box around the optical setup is the walls of the vacuum chamber surrounding the uncompensated paths.

compensations for each output, but it will not affect the stability of the setup or saturate any photodiode, since we only have two beat notes on each photodiode with low powers ($\sim 300\ \mu$W).

We still have some short distances, between light splitting and the splitters where the interferometric detection of the propagation noise is performed, which can not be compensated by definition. To address this issue, we have made a vacuum chamber around all the uncompensated paths of the setup. This will remove some of the air fluctuations that would normally be in an optical free-space setup. We need to take all the precautions that we can, as we are striving to reach a flicker floor in the 10^{-17} level for the future cavities. We reached a stability below $4 \cdot 10^{-18}$ at 1 s for

75 cm of uncompensated path (see on figure 3.9). The amount of uncompensated paths within this optical setup will be much less than 75 cm, and the uncompensated paths will be more protected from air-fluctuations and temperature fluctuations (in vacuum). Therefore the residual noise due to the uncompensated path will be lower than $4 \cdot 10^{-18}$ at 1 s. I have designed the vacuum chamber in the software "Solid Works", a 3d drawing of the vacuum chamber is shown in appendix D.

Chapter 4

Transfer of spectral purity

The field of transfer of spectral purity is a key technique within metrology physics, which has been pushed forwards by the new near-infrared that has shown to produce new even more ultra stable cavities. This chapter will go through the transfer oscillator technique, which is the method used to transfer the stability between the optical signals. There will also be presented the optical setups needed to create ultra stable beat notes, and the results we have gotten from the transfer.

4.1 The transfer oscillator technique

The transfer oscillator technique is used to phase link two oscillators together. The transfer is made via an optical frequency comb, but the technical parameters of the comb (f_{rep}, f_0) are eliminated. The technique is very favorable, if you have one super good cavity, its stability can be transfered to metrological target lasers (slave lasers), for instance at the wavelengths necessary to probe atoms in optical lattice clocks. This arguments is made stronger by the fact that cavities are better in the infra-red domain (waists are larger on the cavity mirrors, which means better averaging of the thermal noise), while clock frequencies are rather in the visible domain. Even if one cavity is not better than the other, the technique can be used to phase link two oscillators, and therefore the Dick effect is rejected when two clocks are probed synchronously, where the noise is averaged faster down for the comparison (see section 4.3).

The transfer oscillator technique consists of 6 steps that can be followed on figure 4.1. The 6 steps are the following:

1. The first step is to detect the beat notes between the comb and each of the two oscillators at play: the master laser (source of stability) on the one hand and the slave laser (in need of stability) on the other hand. The detections can be done on the same photodiode, or two different photodiodes. The detection of the two beat notes after detection will have the frequencies; $f_M = \nu_M - N_M f_{\text{rep}} - f_0$ and $f_S = \nu_S - N_S f_{\text{rep}} - f_0$.

2. We want to remove the parameters of the comb, so the first thing is to remove f_0 from the beat notes. This is done by mixing out f_0. The detection of f_0 is preformed with the f-2f method (see section 2.2). The f_0-free beat notes after mixing are denoted as; $\widetilde{f}_M = \nu_M - N_M f_{\text{rep}}$ and $\widetilde{f}_S = \nu_S - N_S f_{\text{rep}}$, both signals are shown on figure 4.1.

3. We want to rescale both beat notes with the intention of removing f_{rep}, but first we need to clean up the signals in a tracking oscillator, because a DDS with several inputs would not be able to distinguish the clocking frequency. A tracking oscillator consists of a VCO that is phase locked to the signal being tracked, and the locking bandwidth is adjusted to be as small as possible while satisfying the requirements of the experiment. This way, the signal and the low frequency Fourier noise are "copy and pasted" while the rest of the spectrum, often populated with multiple peaks, is disregarded. This is a simple and adjustable way of "cleaning" a RF signal. To this end, the signal from the VCO is mixed with the beat note and the resulting error signal is used to phase lock the VCO to the beat, with a bandwidth of a few kHz.

4. We can now rescale the beat notes. The rescaling is done with a DDS, and it uses the formula to compute the output signal: $f_{\text{out}} = \frac{f_{\text{in}}}{2^k} n = \frac{f_{\text{in}}}{M}$, where n is an integer in the range $[0, 2^{k-1}]$, and the number of bits (k) is 48. The master and the slave signals will be rescaled with the factors M_M and M_S. We want to do a rescaling, so the following is fulfilled; $\frac{N_M}{M_M} = \frac{N_S}{M_S}$.

5. The beat notes are now rescaled in such a way that f_{rep} will be rejected, when the signals are mixed with each other. We get the transfer signal to be;

$$f_t = \frac{\widetilde{f}_S}{M_S} - \frac{\widetilde{f}_M}{M_M} = \frac{\nu_S}{M_S} - \frac{\nu_M}{M_M}. \tag{4.1}$$

6. All the technical parameters of the comb have been eliminated in equation 4.1, therefore the comb was used only as an intermediate oscillator, or "transfer oscillator".

   The final step of the transfer is to correct the frequency of the slave laser, so it has the spectral purity of the master. The transfer signal is being mixed with a synthesizer that is fixed to a frequency close to the frequency of the transfer signal. The signal is then going through a PLL to a VCO that is correcting the frequency of the slave laser with an AOM (But it could also be done in e.g an offset lock instead of an AOM). The transfer of spectral purity scheme is now giving the slave laser the spectral purity of the master laser, when we disregards the noise in transfer scheme.

The transfer oscillator technique is locking the transfer signal to the synthesizer, so we need to make sure that the synthesizer is not adding any noise to the transfer.

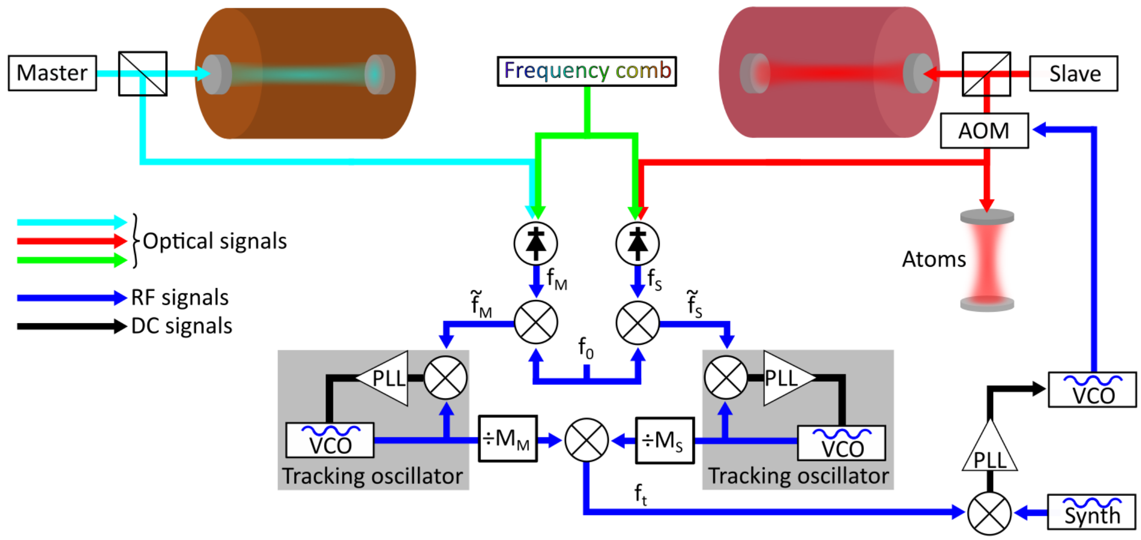

Figure 4.1: The transfer oscillator technique used for transfer of spectral purity. The transfer signal (f_t) formed after the rescaling of the beat notes is sent to the AOM to close the PLL to transfer the spectral purity to the slave laser from the master laser.

Once the PLL is closed, we have the following relation:

$$\frac{\nu_S}{M_S} - \frac{\nu_M}{M_M} = f_{\text{synth}}. \tag{4.2}$$

Note that this approach connects directly the master laser and the slave laser. The transfer oscillator approach is also used in post-processing of data to derive frequency ratios when clocks are compared, locally or in international campaigns, to neglect the parameters of the comb.

The frequency ν_M is typical in the order of a few 10^{14} Hz, where the frequency of f_{synth} is in the order of 10^7 Hz. We have 7 orders of magnitude difference between the two quantities. The synthesizers of our laboratory are referenced to the μ-wave reference, which has a fractional stability of $2 \cdot 10^{-15}$ at 1 s, which is sufficient to discard the noise of the synthesizer. The noise of the slave laser after the transfer can be calculated from equation 4.2, which is the following;

$$\sigma(\nu_S) = M_S\sqrt{\frac{\sigma^2(\nu_M)}{M_M^2} + \sigma^2(f_{\text{synth}})} \simeq \frac{M_S}{M_M}\sigma(\nu_M) \simeq \frac{\nu_S}{\nu_M}\sigma(\nu_M). \tag{4.3}$$

The number $N_S f_{\text{rep}}$ is very close to ν_S usually within 125 MHz, and the rescaling is trying to fulfill the quantity; $\frac{N_M}{N_S} = \frac{M_M}{M_S}$, which justifies the approximation $\frac{M_S}{M_M} \simeq \frac{\nu_S}{\nu_M}$ done in equation 4.3. The equation shows rescaling of the noise with $\frac{\nu_S}{\nu_M}$, which means the slave laser is copying the fractional noise of master.

The next thing to consider is how precise can we achieve the ratio $\frac{N_M}{N_S} = \frac{M_M}{M_S}$. We want to rescale our master laser, which is for the moment the CUS, so a rescaling of other beat notes can be rescaled to match the ratio; $\frac{N_M}{N_S} = \frac{M_M}{M_S}$. For practical reasons we have chosen the value $M_{\text{CUS}} = 2.5$, since $\nu_{\text{Hg}}/\nu_{\text{CUS}}$ is about 1.5, and the DDSs can be rescale by at least 2, it would not be sufficient to rescale only the Hg beat, it is necessary to rescale both beats. We want to choose the right tuning word of the DDS, so we have as little as possible of f_{rep} in our transfer signal. The amount of f_{rep} in our signal can be expressed by the ratio; $\varepsilon = \frac{N_M}{M_M} - \frac{N_S}{M_S}$. We can therefore rewrite the frequency of the slave laser from equation 4.2 including the repetition rate as;

$$\nu_S = M_S\Big(\frac{\nu_M}{M_M} + f_{\text{synth}} + \varepsilon f_{\text{rep}}\Big). \tag{4.4}$$

The number for the tooth of the comb (N) is in the order of 10^6, and for a DDS with $k = 48$ bits, ε can mostly vary with $N_S/2^{48}$, which is at most 10^{-8}. The fractional stability of f_{rep} is in order of 10^{-15} at 1 s, because it is referenced to the CUS. The noise contribution to the transfer signal from the repetition rate can then be calculated to be a fractional stability in the order of 10^{-29} at 1 s, where the repetition rate easily can be discarded as a noise source in the transfer oscillator technique.

4.1.1 Noise of the transfer

Every noise source has to be thought of when the goal is to reach fractional stabilities in the 10^{-18} level at 1 s for the transfer of spectral purity. We have two systems that we have to optimize, which are the RF setup and the optical setup. The RF setup starts at the detection of the beat notes on the photodiode, and to point where the frequency change has been imposed on the slave laser. To cover some of the noise components that should be thought of, when making a RF scheme for the transfer of spectral purity, the following elements have to be considered;

RF noise sources	
Non-linear components:	Mixers, multipliers, amplifiers and filter boxes
Tracking oscillator:	The band of the tracking, and the SNR of the beat notes
Ground loops:	Grounds connections between different laboratories, and many connections to same power source
AM to PM conversion:	Filter boxes, counters, photodiodes and mixers

Table 4.1: Noise components for the RF chain of a transfer scheme that can contribute to the noise floor.

One of the noise sources that has to be thought of is the band of the tracking. We want to track the noise of both the master laser and the slave laser, because we need to have instantaneous information on the differential noise between the master laser and the slave laser in order to induce a correction to servo this differential noise to the reference synthesizer. The band of tracking should not be to wide, because the tracking would pick up to much background noise. The band of the tracking also has to be the same for both lasers, since the noise would otherwise be tracked differently, and this would introduce a differential scaling of the noises, which would degrade the tracking. There are a lot of components like the filter boxes and counters that are involved in the assessment of the tracking, which are important to evaluate the level of the transfer. The AM to Phase Modulation (PM) conversion are often talked about due to the pointing instability, and we have not been able to understand the conversion in the filter boxes and counter in details.

The optical setup can easily be the limiting factor to a measurement (see section 3.1.1). The following table gives an overview of the noise components that should be thought of when making an optical scheme for the transfer of spectral purity;

Optical noise sources	
Pointing instability:	AM noise on the photodiode from mechanical fluctuations
Path length fluctuations:	Phase drift between the optical signals from temperature fluctuations, air fluctuations or mechanical vibrations
Back reflections:	Parasitic reflections at the same frequency as the peak carrying information about the path length fluctuations

Table 4.2: Noise components for the optical setup of a transfer scheme that can contribute to the noise floor.

Many of the noise sources mentioned above are of course mostly due to the fact that all the paths can not be compensated. The environment is very important when there are uncompensated path, so we want to minimize the temperature fluctuations, air fluctuations and mechanical vibrations of the optical setup. The measures we have been taking to prevent all of these things will be explained in the following sections.

4.1.2 Out-of-loop assessment

To assess the noise of the transfer, an out-of-loop measurement is necessary, because it is the only measurement that shows all the residual noise, while a measurement of the in-loop signal gives access to the noise of the locking signal within the bandwidth of the tracking, and the residual noise beyond the bandwidth of the tracking.

An out-of-loop measurement compares the locked quantity to the reference via an independent measurement device. The two measurements are then compared by the differential noise, which gives us an estimate of the noise of our system. The method used to evaluate the noise of the transfer is shown on figure 4.2. We have the transfer on the left hand side on the figure, where the transfer of spectral of purity from the master laser to the slave laser is completed. Another identical setup is prepared to assess the technical noise added by the transfer process. The setup uses the slave laser, the master laser and another comb to decouple the transfer from the assessment. It is important to use another comb to decouple the two systems from any bias noise added by the comb.

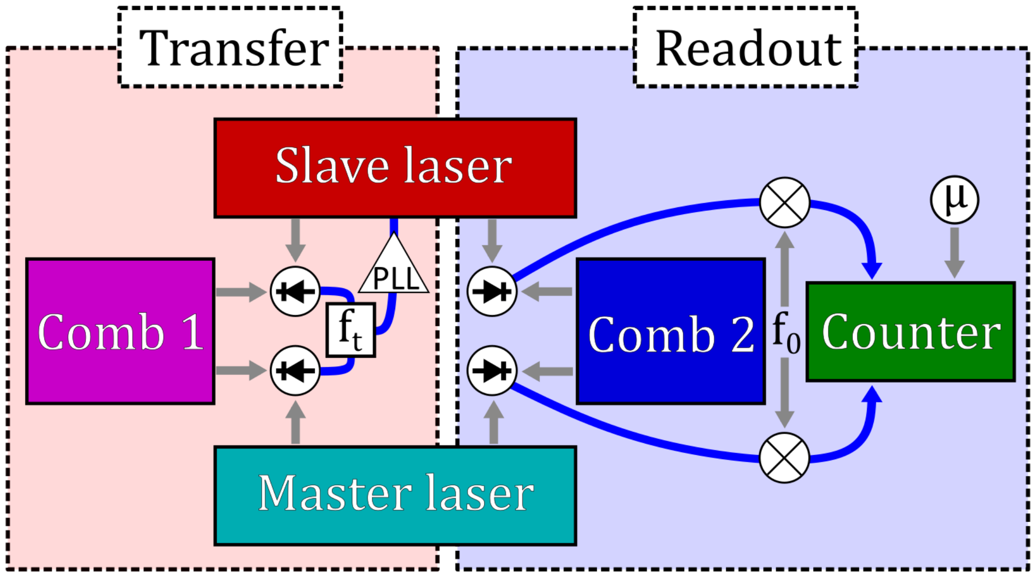

Figure 4.2: Out-of-loop measurement of transfer of spectral purity from the slave laser to the master laser. Comb 1 is transferring the spectral purity to the slave laser from the master laser, where Comb 2 is used for measuring the master laser and the slave laser to assess the noise of the transfer.

We can write the frequency of the slave laser after the transfer of spectral purity as;

$$\nu_S = M_S\Big(\frac{\nu_M}{M_M} + f_{\text{synth}} + \varepsilon_{\text{trans}}\Big), \tag{4.5}$$

where $\varepsilon_{\text{trans}}$ models the total noise added by the transfer. The readout setup will measure the two beat notes directly as f_0-free beat notes. We can do the same rescaling in the post-processing of the readout data, as we would do in the tracking oscillator technique. The noise of the transfer signal f_t' for the readout setup is;

$$f_t' = \frac{\nu_S}{M_S'} - \frac{\nu_M}{M_M'} + \varepsilon_{\text{detect}}, \tag{4.6}$$

where $\varepsilon_{\text{detect}}$ models the total noise added on the readout side. The readout setup will measure the frequency of the slave laser after the transfer as written in equation 4.5. The equation of the detections can be rewritten as;

$$f_t' = \Big(\frac{M_S}{M_S' M_M} - \frac{1}{M_M'}\Big)\nu_M + \frac{M_S}{M_S'}\Big(f_{\text{synth}} + \varepsilon_{\text{trans}}\Big) + \varepsilon_{\text{detect}}. \tag{4.7}$$

The noise of the synthesizer is negligible as discussed earlier. The coefficient in front of ν_M is small, because the ratios between the tooth numbers for the assessment and transfer comb are almost the same for both setups, since we are dealing with the same lasers and almost the same repetition rates. We can therefore do the approximation; $\frac{N_S}{N_M} \simeq \frac{N'_S}{N'_M} \rightarrow \frac{M_S}{M_M} \simeq \frac{M'_S}{M'_M}$. This makes the noise of ν_M negligible as well, because the pre-factor is insignificant. We can write the noise of the transfer signal that is detected at the readout as;

$$\sigma(f'_t) = \sqrt{\left(\frac{M_S}{M'_S}\right)^2 \sigma^2(\varepsilon_{\text{trans}}) + \sigma^2(\varepsilon_{\text{detect}})} \simeq \sqrt{\sigma^2(\varepsilon_{\text{trans}}) + \sigma^2(\varepsilon_{\text{detect}})}. \tag{4.8}$$

The total noise is the quadratic sum of transfer noise and the detection noise, because we see the two noise sources as uncorrelated systems. The transfer noise and the detection noise can be similar or completely different, depending on the part of the setup the noise comes from: The RF-chain of the two systems are not symmetric, because one deals with the transfer and the other with the detection. The noise could come from either the tracking oscillator, the filter boxes, etc. which are different components needed in the separate RF chains. The only thing we would be able to say in the scenario of being limited by the RF chain is that the noise of the transfer is below the total measured value, because of the asymmetry of the setup. Some of the asymmetry could be overcome by creating a new analog transfer beat, instead of doing it by post-processing, and measure the stability of the transfer signal directly.

The optical setup are made, so they are as similar as possible. If the measured noise would originate from the optical setup, we can assume the transfer noise and the detection noise equal to each other; $\varepsilon_{\text{trans}} = \varepsilon_{\text{detect}}$. The total noise of the transfer can then be seen as; $\sigma(\varepsilon_{\text{trans}}) = \sigma(f'_t)/\sqrt{2}$, so the noise is the square root of the detected stability. In fact $\sigma(f'_t)$ is the noise of transfer at the worst case scenario, where we would be in case of having; $\sigma(f'_t) = \sigma(\varepsilon_{\text{trans}})$.

4.2 Optical setup

The optical setup for the transfer scheme needs to be designed with the consideration of noise in every aspect of the design. The transfer of spectral purity can be designed in two methods called "single-branch" and "multi-branch" transfer of spectral purity, which are important to understand for the reduction of noise introduced by the EDFA. The single-branch transfer of spectral purity is straight forward, the two beats are formed with the same output of the comb, so the comb's noise is in common mode between the 2 signals. Reminding that the comb is an erbium comb, so the frequency span goes from approximating 1050 to 2100 nm after spectral broadening. The CUS (1542 nm) and the Hg laser (1062 nm) are both in the range of comb, so they can be measured and transferred directly by the comb. This is the single-branch transfer of spectral purity, because we are using the same output of the same EDFA to measure both frequencies.

In the multi-branch setup, the two beat notes are formed with independent outputs of the comb, therefore there is uncorrelated noise between the two f_{rep}, and it can not be removed completely. An illustration of a multi-branch setup is shown on figure 4.3, where the transfer of spectral purity is between Hg and Sr. The light of the comb needs to be frequency doubled to populate the spectral region around 698 nm, because the erbium comb does not reach the frequency of a Sr clock laser at 698 nm. EDFA 2 needs to be optimized at a frequency of 1396 nm, so we have more power for a SHG of the comb's light. The beat note between the Sr laser and the comb will be at $f_{\mathrm{Sr}} = 2mf_{\mathrm{rep}} + 2f_0 - \nu_{\mathrm{Sr}}$. The beat note will contain two times f_0 due to the frequency doubling of the comb's light. The beat note with the Hg laser is formed with the light of the comb coming from EDFA 1, where the transfer is directly done between Hg and Sr.

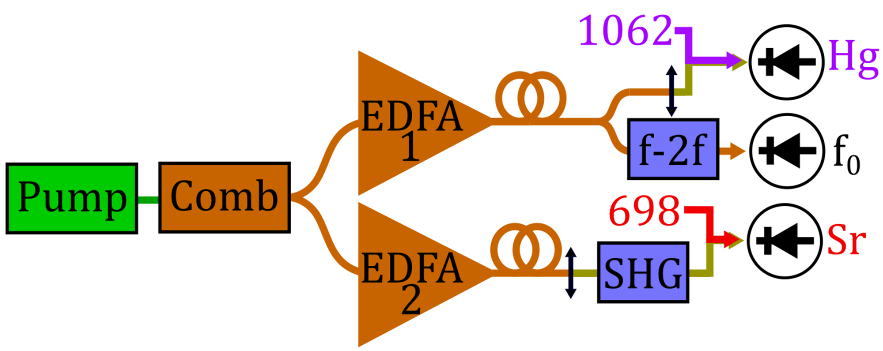

Figure 4.3: Illustration of an optical setup for multi-branch transfer of spectral purity between Hg (1062 nm) and Sr (698 nm). The transfer signal is form directly between the two EDFAs.

The results we got for the multi-branch transfer of spectral purity in free-space was a fractional stability of $3 \cdot 10^{-16}$ at 1 s. This result will be shown later on figure 4.10 as the pink data. The result is a lot worse than for the best lasers reaching stabilities of $4 \cdot 10^{-17}$ at 1 s [29]. The result for multi-branch is not sufficient for the transfer of spectral purity, and the only option is therefore to do single-branch transfer of spectral purity.

4.2.1 Single-branch transfer between 1062 nm and 1542 nm

The band of an InGaAs photodiode covers both 1062 nm and 1542 nm. The transfer of spectral purity will therefore be performed on the same photodiode for both beat notes. We have based the noise compensation setup on a technique developed by the PTB team "Working group unit of length". The setup we have designed is shown on figure 4.4, where it shows all the metrology lasers combined on the same long-pass 1400 dielectric before noise compensation. All the lasers then proceed to be combined with the comb to form the beat notes on the same photodiode. We have added an extra laser for the Spectral Hole-Burning (SHB). The purpose of the SHB project is to use rare-earth doped crystals to achieve better short term stabilities than possible with a cavity, because of the length fluctuations seen in a cavity (see reference [30]).

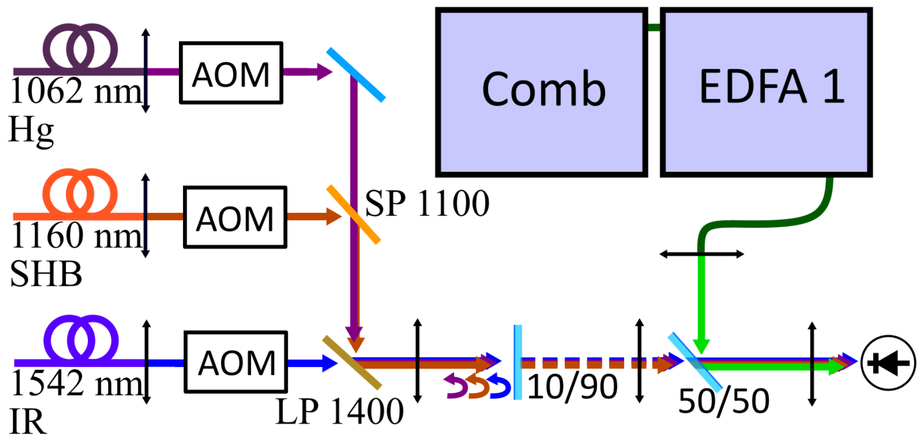

Figure 4.4: Optical setup for transfer of spectral purity from an Infra-Red (IR) laser (1542 nm) to the Hg laser (1062 nm), and with the option of using the SHB laser (1160 nm) for transfer of spectral purity. All the lasers are fiber compensated on the same retro-reflecting plate, where they are combined with the comb on the same 50/50 beam splitter before detection on a photodiode.

All the branches for the lasers on figure 4.4 starts by going through an AOM. This AOM will be used for propagation noise stabilization (see section 3.1.1). The AOM makes the retro-reflection for the fiber compensation distinguishable from any small reflection in the fiber, which makes a more robust fiber compensation. The Hg laser is combined with the SHB laser on a short-pass filter at 1100 nm, where they are met by a long-pass filter at 1400 nm to combine all the lasers. The lasers then go through a cat's eye, where 10% of the light is retro-reflected for the noise compensation. The light transmitted through the retro-reflecting plate is being combined with comb's light on a 50/50 beam splitter, where the beams follow each other to the photodiode.

The only uncompensated path in the optical setup will be right after the retro-reflecting plate until the lasers hit the photodiode. The comb will be in common mode with the lasers, when they are combined on the 50/50 beam splitter. The tooth of the comb and the lasers will be separated by frequencies less than 250 MHz, and it implies that differential dispersion effects can be neglected when the comb and the lasers are in common mode. We can discount any noise when the beams are in common mode, because the noise added will be equal for both frequencies, and the obtained beat note will therefore be unchanged.

A better understanding of the system

The path that is marked as a dashed line on figure 4.4 has often been expressed as the path, where the noise will be added to the optical setup. After a lot of consideration when writing my thesis, I got to the conclusion that this path would not be the main contributor of noise in the optical setup. The reason is that the transfer of spectral purity will not see noise added in the dashed line, because the noise of the Fourier components will be added to all the lasers. The noise will then be mixed out when comparing the beat notes in the transfer scheme.

A counterargument to my reasoning could be that the index of refraction would differ due to dispersion of the different lasers frequencies. The small phase change due to a difference in index of refraction can be written as;

$$\delta\varphi = \int_0^L \Delta n(s)\frac{\omega}{c}ds = \frac{\omega}{c}\int_0^L \Delta n(s)ds \simeq \frac{\omega}{c}\Delta n L, \tag{4.9}$$

where Δn is the change in index of refraction for the given wavelengths, c is the speed of light and L is the length of the distance, where the light will have accumulated the phase shift.

The residual noise of the transfer between the Hg laser and the CUS due to phase changes $\delta\varphi$ can be written as;

$$\begin{aligned}&\frac{\varphi_{\mathrm{Hg}} + \delta\varphi_{\mathrm{Hg}} - N_{\mathrm{Hg}} f_{\mathrm{rep}}}{M_{\mathrm{Hg}}} - \frac{\varphi_{\mathrm{CUS}} + \delta\varphi_{\mathrm{CUS}} - N_{\mathrm{CUS}} f_{\mathrm{rep}}}{M_{\mathrm{CUS}}} \\ &= \left(\frac{\varphi_{\mathrm{Hg}}}{M_{\mathrm{Hg}}} - \frac{\varphi_{\mathrm{CUS}}}{M_{\mathrm{CUS}}}\right) + \left(\frac{\delta\varphi_{\mathrm{Hg}}}{M_{\mathrm{Hg}}} - \frac{\delta\varphi_{\mathrm{CUS}}}{M_{\mathrm{CUS}}}\right),\end{aligned} \tag{4.10}$$

The repetition rate will be rejected due to the rescaling of the signals. We get a constant term and a fluctuating term from equation 4.10, where we can evaluate the constant frequency change due to the uncompensated path to be;

$$\left(\frac{\varphi_{\mathrm{Hg}}}{M_{\mathrm{Hg}}} - \frac{\varphi_{\mathrm{CUS}}}{M_{\mathrm{CUS}}}\right) = \left(\frac{\omega_{\mathrm{Hg}}}{M_{\mathrm{Hg}}} n_{\mathrm{Hg}} - \frac{\omega_{\mathrm{CUS}}}{M_{\mathrm{CUS}}} n_{\mathrm{CUS}}\right)\frac{L}{c} \simeq \frac{\omega_{\mathrm{Hg}}}{M_{\mathrm{Hg}}}(n_{\mathrm{Hg}} - n_{\mathrm{CUS}})\frac{L}{c}. \tag{4.11}$$

We can do the approximation $\frac{\omega_{\mathrm{Hg}}}{M_{\mathrm{Hg}}} \simeq \frac{\omega_{\mathrm{CUS}}}{M_{\mathrm{CUS}}}$, because the M values are chosen to reject f_{rep}, where we have a the same relation with ω, since ω is close in frequency to f_{rep}. The index of refraction for air to the respective wavelength are $n_{1542} = 1.000\ 273$ and $n_{1062} = 1.000\ 274$ (for 15 C$^{\mathrm{o}}$ and 101325 Pa) [31]. Evaluating the constant phase shift of equation 4.11 gives a phase shift of 2 mHz for the 8 cm of uncompensated paths after the noise compensation. This is only the constant phase change, which would not change the stability of the transfer, since it is constant. It is only the phase fluctuations $\delta\varphi$ that we care about, but they would be several orders of magnitudes smaller, since the change of air pressure and temperature would give an even smaller differential change in the air's index of refraction for the two wavelength. The noise added in the dashed lines on figure 4.4 can therefore be discarded.

There is just one thing to keep in mind when making this reasoning; "the comb also has a huge span of frequencies, and the same kind of dispersion will affect it as well". The light of comb first goes through a 1 m optical fiber where it is collimated into free-space for 5-10 cm before it is combined with the lasers on the

50/50 beam splitter. An Optical fiber has a much larger sensitivity to temperature and pressure changes than air, which is also why light that is propagating in free-space will accumulate less noise than in a fiber. The comb's light would dependently accumulate a lot more noise going from EDFA 1 to the 50/50 beam splitter than the light would accumulate in the dashed path shown on figure 4.4.

We want a good mode-matching when the beams are combined, the same noise will else not be seen by both beam, and it will then not be rejected when the beat note is detected. But it seems unlikely that the limit would be due to mode-matching of the beams, because the intensity profiles have similar waists within 25% and the beams overlap is as good as the human eye can distinguish. The beams are also hitting the same mirrors and photodiode, so the beams would see the same noise due to vibrations.

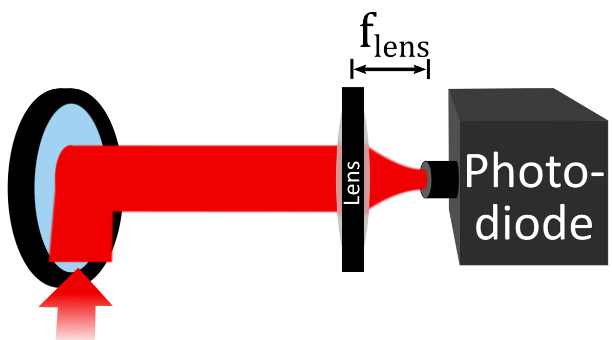

Figure 4.5: The optical setup for the transfer of spectral purity just after the lasers and comb are combined on the 50/50 beam splitter, where they are heading for detection on a photodiode. f_{lens} is the focal length of the lens.

To illustrate why a pointing instability would occur, the optical setup right before the beat notes are detected on the photodiode is shown on figure 4.5. There is one mirror between the photodiode and the point of combining the comb with the lasers, so the beams can be directed towards the photodiode. This mirror could be shaking a bit, where the beam would start to move across the photodiode. We want to overcome the problem of fluctuations of the detecting intensity due to a moving beam, which would be detected as AM noise. The first reason of placing a lens before the photodiode is to focus the beams down, so the waist is smaller than the radius of the active area of the photodiode. We want to place the lens at the focal length away from the photodiode, so the phase front is flat on detection. The beams also become very robust to mirror vibrations, when having a lens placed at the focal length away from the photodiode, since a beam coming far away to hit the lens will "almost" be seen as a plane wave, even for a moving beam with small angles. This means that the lens always will try to focus the beam into the focal point, which implies that we need to place the lens as close as possible to the focal length.

The transfer signal between the Hg laser and the CUS is locked to the following

PLL;

$$\frac{\nu_{\mathrm{Hg}}}{M_{\mathrm{Hg}}} - \frac{\nu_{\mathrm{CUS}}}{M_{\mathrm{CUS}}} = f_{\mathrm{DDS}}, \tag{4.12}$$

where the Hg laser and the CUS will be locked to the synthesizer.

Results

The results for the stability of the transfer of spectral purity from Hg to CUS is shown on figure 4.6. The fractional stability of Hg and the CUS are 10^{-15} at 1 s, when measured against the assessment comb, which are shown as the green and the red data respectively. The stability should be the same when having the transfer of spectral purity, which we are seeing. We use the following equation to assess the transfer beat;

$$f'_t/\nu_{\mathrm{Hg}} = (\widetilde{f}'_{\mathrm{CUS}}\frac{N'_{\mathrm{Hg}}}{N'_{\mathrm{CUS}}} - \widetilde{f}'_{\mathrm{Hg}})/\nu_{\mathrm{Hg}}, \tag{4.13}$$

where $\widetilde{f}'$ is the detected f_0-free beat notes, and N' is the tooth number for the assessment comb. The transfer beat (f'_t) is divided by ν_{Hg} to get the fractional stability.

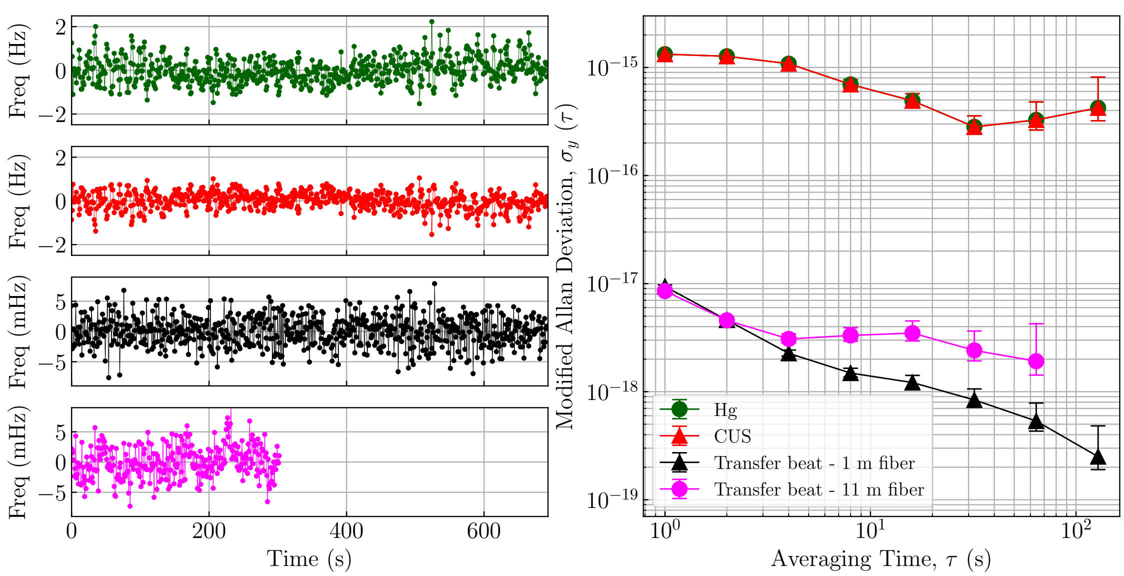

Figure 4.6: The results for the transfer of spectral purity between the Hg laser (1062 nm) and the CUS (1542 nm). The fiber length for bringing the comb's light to the transfer of spectral purity setup was changed to 11 m instead of 1 m for the pink measurement. All the measurements have been measured with a frequency counter in Λ-mode.

We got a fractional stability of the transfer of spectral purity between Hg and the CUS to be $9 \cdot 10^{-18}$ at 1 s. This result is by far better than any laser has shown, which is of $4 \cdot 10^{-17}$ at 1 s.

We wanted to test, if the dispersion effects in the optical fiber bringing the comb's light to the optical setup could have an impact on the stability. The frequency of Hg is at 1062 nm, and the optical fiber bringing the comb is optimized for 1542 nm, we could therefore lack SNR when extending the fiber due to loses. It turns out that neither the SNR nor the stability at 1 s were affected when extending the fiber with 10 m, which is shown as the pink data on figure 4.6.

4.2.2 Single-branch transfer between 698 nm and 1542 nm

A significantly different approach was necessary to transfer from/towards 698 nm. We are using EDFA 2, which is optimized for 1396 nm, so we can frequency double the 1396 nm of the comb to reach the 698 nm of the Sr clock laser. The frequency doubling in the SHG medium depends a lot on the temperature, as it can be seen on figure 4.7, where the spectrum of the SHG for various temperatures is shown. The Sr clock frequency is marked as the dashed yellow line at 698.4 nm, which is the frequency that we want to optimize the temperature of the SHG for.

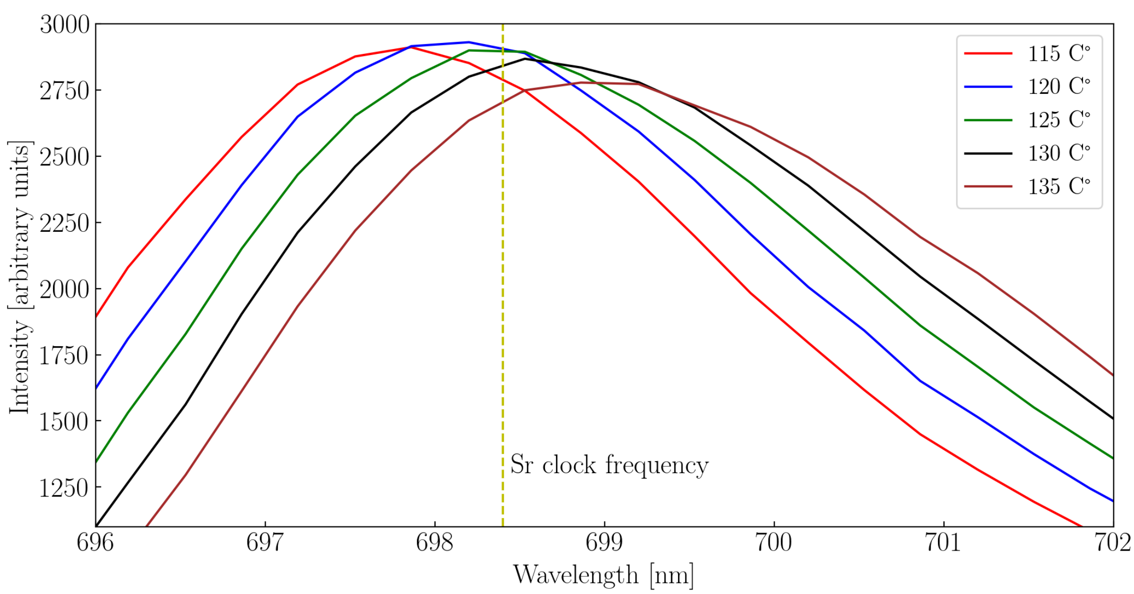

Figure 4.7: The spectrum of the SHG for various temperatures. The Sr clock frequency is marked at 698.4 nm. The data is for the SHG of the assessment comb. The spectrum has been measured with a USB2000 from ocean optics. The wavelength measured has an uncertainty of 1.5 nm.

The optimal temperature is around 125 C° for the SHG medium, since the spectrum for 125 C^o is centered around the clock frequency. The curves of the spectrums are for the SHG of comb in the assessment setup. The temperature can vary for SHG medium, as the SHG in the transfer setup has an optimal temperature of 80 C^o. The SHG was all ready optimized at my arrival for the transfer setup, because it was used for the multi-branch transfer of spectral purity in the past.

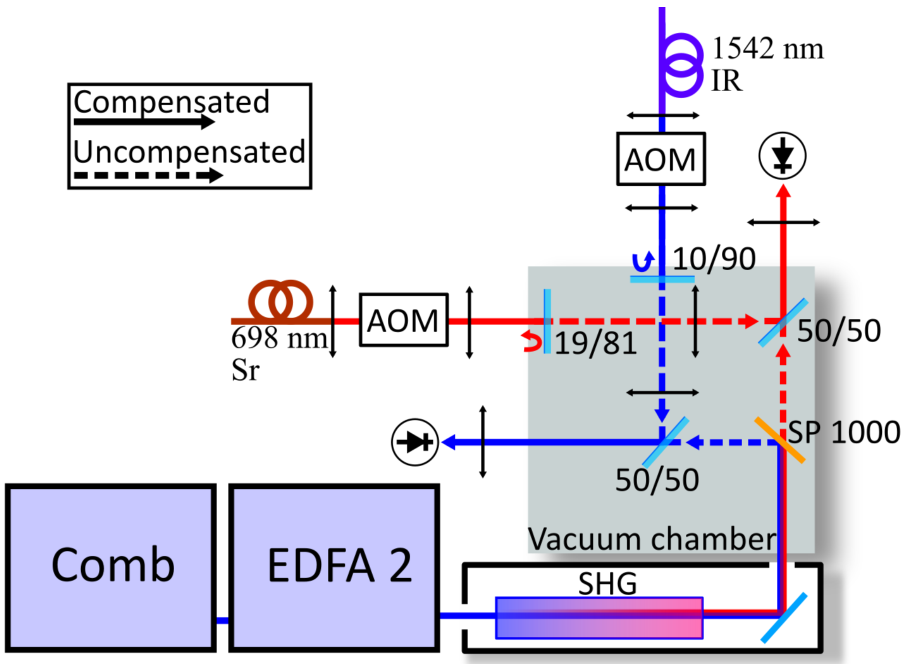

Figure 4.8: Optical setup for transfer of spectral purity from the IR laser (1542 nm) to the Sr laser (698 nm). The light of the comb is split up on a short-pass filter at 1000 nm to be combined with the IR laser and the Sr on different 50/50 beam splitter. The IR laser and the Sr laser have their own retro-reflecting plate for the noise compensation before combined with the comb, where they are detected on different photodiodes.

The optical setup is shown on figure 4.8, where we can see the light of EDFA 2 goes to the SHG. It creates different waist sizes of the 1542 nm light and the generated 698 nm light. This leads to a problem, if we want to do noise compensation of all the lasers on the same retro-reflecting plate, since the beams of the cw lasers must be mode-matched with the comb light. We would also have a problem with the cat's eye, if we were to use it for both Sr and the IR laser, because of the 2 lenses would change accordantly to the wavelengths due to their large frequency separation (dispersion effect). The decision was instead to split up the comb's light after the SHG on a short-pass filter at 1000 nm. The detection of the 698 nm light and the 1542 nm light must be performed by photodiodes of different technologies, so it anyway complicates the setup. The light of the comb can not be seen as compensated when the teeth for the 698 nm and 1542 nm are split up, because the added noise has become uncorrelated when the beams are not in common mode any more. The mode matching is sub-optimal after the SHG because the lenses focusing the comb's light towards the SHG medium can not collimate the beams equally afterwards due to dispersion effects in the collimation lens.

I have designed a vacuum chamber to place the uncompensated paths within. It will be placed just after the SHG, so the noise accumulated due to bad mode matching is as small as possible. The Sr and the IR laser have their own cat's eye and retro-reflecting plate, where they are combined with the comb on independent 50/50 beam splitters. This setup will have a few centimeters of uncompensated paths, and the vacuum chamber around the uncompensated paths are therefore crucial for the design of this setup. The total amount of uncompensated paths are shown as dashed lines in the setup, and the total length is around 20 cm of uncompensated paths, which is a bit more compared to the Hg setup, which can be argued to have 0 cm of uncompensated paths.

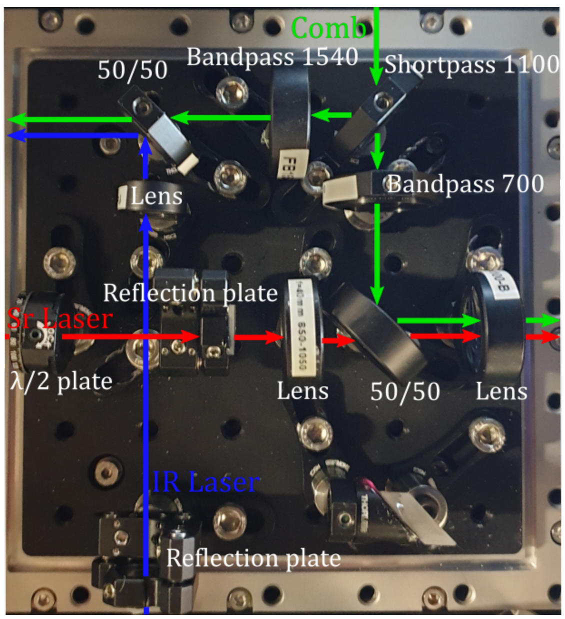

(a)

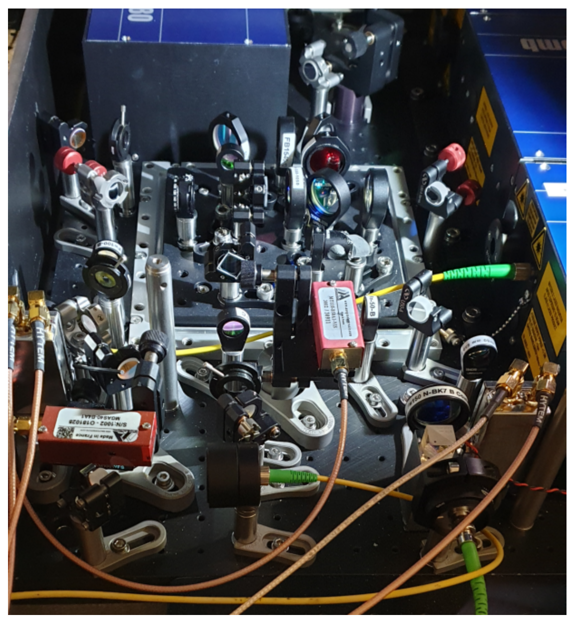

(b)

Figure 4.9: The optical setup for the transfer of spectral purity: In (a) the optical setup and the optical paths within the vacuum chamber. The optical paths are only an illustration and not the exact paths. In (b) the whole optical setup for the transfer of spectral purity is shown to give a better overview of the optical setup.

Pictures of the optical setup for the transfer of spectral purity between Sr and the CUS are shown on figure 4.9. The base of the vacuum chamber is installed underneath the breadboard shown on figure 4.9a, the 3d drawings of the vacuum-lid and the vacuum-base are shown in appendix E. The vacuum-lid is going to be placed on top of the breadboard and vacuum-base. The windows are going to be tilted with a small angle to avoid unwanted reflections. The whole optical setup can also be seen on figure 4.9b to give a better overview of the optical setup.

The transfer signal between the Sr laser and the CUS is locked to the following PLL;

$$\frac{\nu_{\mathrm{Sr}}}{M_{\mathrm{Sr}}} - \frac{\nu_{\mathrm{CUS}}}{M_{\mathrm{CUS}}} = f_{\mathrm{DDS}}, \tag{4.14}$$

where the Sr laser and the CUS will be locked to the synthesizer.

Results

The results for the stability of the transfer of spectral purity from Sr to CUS is shown on figure 4.10. The stability of the Sr laser frequency against the CUS frequency was $2 \cdot 10^{-15}$ at 1 s for this measurement (normalized by Sr frequency), which are shown as the green (Sr) data and the red (CUS). The noise of the green data is much larger than the red data seen on the time trace, but they are rescaled with the frequency of their laser showing that the fractional stability is the same for the transfer.

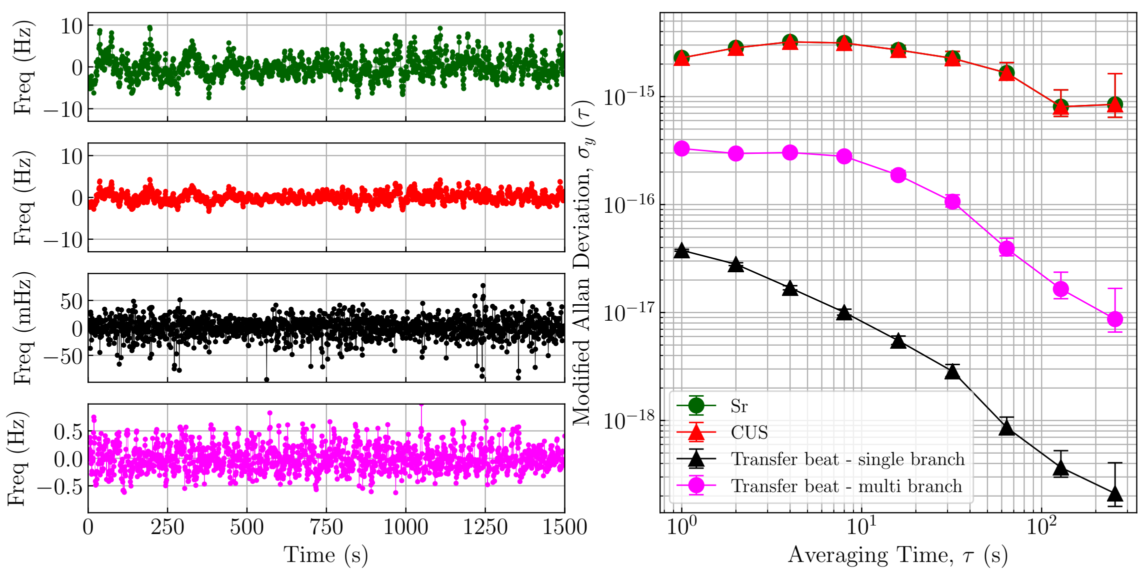

Figure 4.10: The results for the transfer of spectral purity between the Sr laser (698 nm) and the CUS (1542 nm). All the measurements have been measured with a frequency counter in Λ-mode except the multi branch measurement, which was done in Π-mode. This has not affected the stability of the multi-branch transfer, since it only averages faster down for white phase noise, where we are getting the same result in Λ-mode.

The transfer beat is rescaled the same way as Hg, which was done in equation

4.13. The transfer beat for Sr;

$$f'_t/\nu_{\mathrm{Sr}} = (\widetilde{f'}_{\mathrm{CUS}}\frac{N'_{\mathrm{Sr}}}{N'_{\mathrm{CUS}}} - \widetilde{f'}_{\mathrm{Sr}})/\nu_{\mathrm{Sr}}, \tag{4.15}$$

The f_0-free beat note is achieved a bit differently for Sr than the other beat notes. The beat note of Sr after detection on a photodiode; $f_{\mathrm{Sr}} = \nu_{\mathrm{Sr}} - Nf_{\mathrm{rep}} - 2f_0$. The signal contains 2 times f_0 that we have to mix out, which are done by sending the f_0 signal through a multiplier before mixing. This mixes out the $2f_0$ to achieve a f_0-free Sr beat note.

The stability of the transfer of spectral purity from the Sr to the CUS laser achieved a fractional stability of $3.5 \cdot 10^{-17}$ at 1 s, which is seen as the black data on figure 4.10. This is a very good improvement from the multi-branch transfer of spectral purity, which has a fractional stability of $3 \cdot 10^{-16}$ at 1 s. The multi-branch transfer of spectral purity was done directly between Hg and Sr, where EDFA 1 and EDFA 2 were used respectively for the transfer. The assessment was then measured with a Ti:Sapphire comb, which has an operational range of $0.5 - 1.1$ μm, so the assessment measured single-branch, since both the Sr and Hg frequencies are within the operational spectrum.

The design of the distribution of the Sr laser also adds some uncompensated paths to the transfer of spectral purity. The Sr laser is distributed on two different fiber compensations for the transfer setup and the assessment setup. There is approximating 20 cm of uncompensated path between the two distributed paths. We have the option for the future to put these paths under vacuum as well, but the paths was not under vacuum during the recorded data on figure 4.10. The results shown were also measured without any vacuum chamber around the uncompensated path of transfer setup and assessment setup, because the vacuum chamber was finished later than the measured result.

4.3 Dual single-branch transfer of spectral purity

In this section, we transfer the spectral purity directly from the Hg laser to the Sr laser without suffering from the comb's multi-branch noise as described before. To this end, the dual single-branch transfer of spectral purity has the goal of establishing a direct phase relation between Sr and Hg, after elimination of the noise of the different outputs of the comb. This would then lead to common mode Dick noise and therefore to a large rejection of the Dick effect when probing synchronously the Sr and the Hg clocks with their respective lasers now having a phase relation.

The Dick effect can then be rejected by several orders of magnitude when comparing the atomic clocks, if the atoms are experience the same residual noise of their clock lasers. The limitation to how free of the Dick effect the clock comparison can be is decided by the stability of the transfer between Hg and Sr on the one hand, and by the uncompensated phase degrading effects from delivering the lasers to the atoms (propagation noise, thermal noise in doubling crystals for the case of Hg, etc) on the other hand.

We can transfer the spectral purity between the lasers; Sr, Hg or CUS. We can form the two transfer signals, which were described in the previous sections;

$$\frac{\nu_{\mathrm{Sr}}}{M_{\mathrm{Sr}}} - \frac{\nu_{\mathrm{CUS}}}{M_{\mathrm{CUS}}} = f_{\mathrm{DDS1}}. \tag{4.16}$$

$$\frac{\nu_{\mathrm{Hg}}}{M_{\mathrm{Hg}}} - \frac{\nu_{\mathrm{CUS}}}{M_{\mathrm{CUS}}} = f_{\mathrm{DDS2}}. \tag{4.17}$$

The best stability at SYRTE is for the moment the Hg laser. Instead of locking these 2 error signals individually, we mix them to form an unique error signal that is ν_{CUS} free and it can therefore be an advantage to do the transfer from Hg to Sr directly. The transfer signal we would get in this case would then be;

$$\left(\frac{\nu_{\mathrm{Hg}}}{M_{\mathrm{Hg}}} - \frac{\nu_{\mathrm{CUS}}}{M_{\mathrm{CUS}}}\right) - \left(\frac{\nu_{\mathrm{Sr}}}{M_{\mathrm{Sr}}} - \frac{\nu_{\mathrm{CUS}}}{M_{\mathrm{CUS}}}\right) = \frac{\nu_{\mathrm{Hg}}}{M_{\mathrm{Hg}}} - \frac{\nu_{\mathrm{Sr}}}{M_{\mathrm{Sr}}} = f_{\mathrm{DDS}}. \tag{4.18}$$

It is very important for this operation to have ν_{CUS} rescaled by the same value M_{CUS} in the transfer of Sr and Hg. This will make sure that ν_{CUS} will be rejected, when mixing the two transfer signals. The Sr laser can then be locked to the Hg laser, implying a similar stability for both of them if the transfer noise is negligible. The CUS will then have the stability unchanged, since we are not acting on the laser, where it is only used for comparing the noise of EDFA 1 and EDFA 2 to complete a transfer which is immune to the differential noise of the EDFAs.

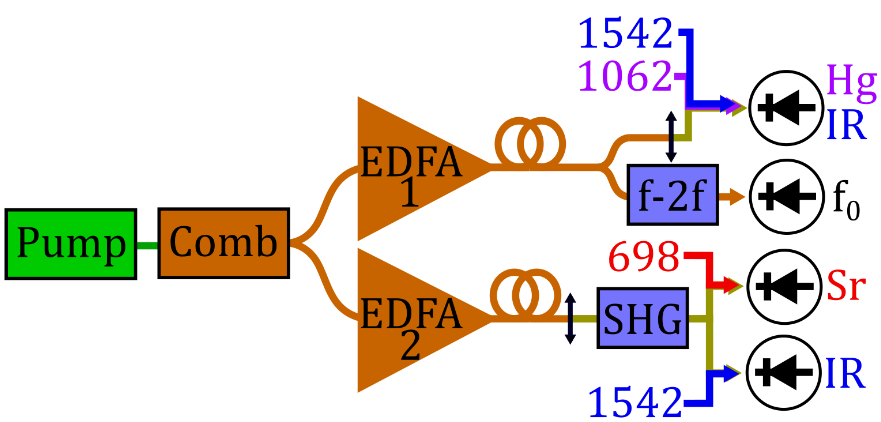

Figure 4.11: Illustration of an optical setup for dual single-branch transfer of spectral purity with Hg (1062 nm), Sr (698 nm) and an IR laser (1542 nm). The transfer oscillator technique is forming the transfer signal between the Hg laser and the IR laser on EDFA 1, and it is forming the transfer signal as well between the Sr laser and the IR laser on EDFA 2.

The illustration of an optical setup for the dual single-branch transfer of spectral purity is shown on figure 4.11, where the transfer of spectral purity uses both the single-branch transfer of spectral purity setups.

A rejection of the Dick effect can also be performed by transferring the spectral purity from the CUS to both the Hg laser and the Sr laser by two PLL (see equation 4.16 and 4.17). This is the intention when the new IR laser is installed, where we can transfer the best stability at SYRTE to the Sr and Hg lasers. The IR laser is expected to have a noise floor in the 10^{-17} level.

Results

The stability between the Hg and Sr clocks are measured by taking the fractional ratio between the measured clock frequencies. The ratio is measured from;

$$y = \frac{\nu_{\mathrm{Hg}}}{\nu_{\mathrm{Sr}}} / \frac{\nu^0_{\mathrm{Hg}}}{\nu^o_{\mathrm{Sr}}}, \tag{4.19}$$

where $\frac{\nu_{\mathrm{Hg}}}{\nu_{\mathrm{Sr}}}$ is the measured ratio, and it being renormalized by the acknowledged frequency ratio; $\frac{\nu^0_{\mathrm{Hg}}}{\nu^o_{\mathrm{Sr}}}$, between the Hg and Sr frequencies.

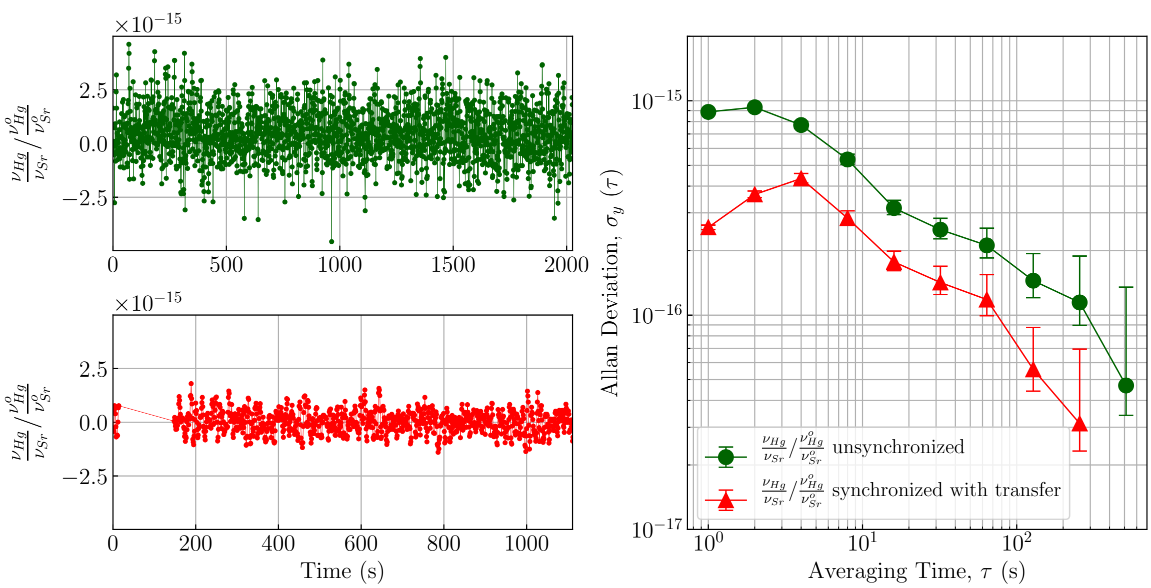

Figure 4.12: Measurement of the renormalized ratio between the frequency of the Hg clock and one of the Sr clocks: The green data is the unsynchronized measurement between the atomic clocks, and the red data is the synchronized interrogations with the dual single-branch transfer of spectral purity from the Hg laser to the Sr laser.

The frequency ratio between the unsynchronized clocks compared to the Hg and Sr synchronized for the clock cycles with transfer of spectral purity gives a stability improvement from $8.9 \cdot 10^{-16}$ to $2.6 \cdot 10^{-16}$ at 1 s, and an improvement with at least a factor of 2 for longer integration times (see figure 4.12). This clearly shows the elimination of the Dick effect through the transfer of spectral purity. This is the first ever result showing single-branch transfer of spectral purity between Hg and Sr clock lasers (to the best of our knowledge).

An investigation of the noise in the paths delivering the clock lasers to the atoms, could further improve the result. This would especially involve an analysis of the noise introduced by twice frequency doubling the Hg laser (1062 nm to 266 nm), but also a compensation or protection of the uncompensated paths for bringing the Hg and Sr clock lasers to the atoms.

Chapter 5

Conclusion

The Dick effect is the limitation to the stability of optical lattice clocks at a few 10^{-16} at 1 s. There is no doubt that we need to make better lasers to probe the atoms. The advancement within the field of ultra stable infra-red cavities gives the short term stabilities that gives an extended coherence time such that the duration of the probing of the clock transition becomes a larger part of the clock cycle time, and reduces the residual noise, all which is needed to reduce significantly the Dick effect. In order to provide optical clocks with an improved stability, the technique of transfer of spectral purity transfers state-of-the-art stabilities obtained in the infra-red domain towards target metrological wavelengths.

5.1 Summary

The stability of clocks at SYRTE is at the $7 \cdot 10^{-16}$ level at 1 s at best. The strategy we follow is on the one hand to build a new long cavity at 1542 nm, and on the other hand to use erbium frequency combs to transfer the stability of the cavity to 698 nm and 1062 nm. In order to evaluate the entire technical noise brought by this process, we had to measure numerous effects that I will now summarize:

The degraded stability due to 10 m of uncompensated paths in optical fibers showed a fractional stability of $7 \cdot 10^{-16}$ at 1 s. This can be compared to the stability due to 75 cm of uncompensated paths in free-space, which showed a fractional stability of $4 \cdot 10^{-18}$ at 1 s. The stability is therefore less degraded in free-space optical setups, with approximating two orders of magnitude. The decision of going to free-space optical setups instead of optical fiber is therefore advantageous.

Among the steps to transfer the spectral purity, the beat notes are all set free of f_0 by mixing out this quantity. We have investigated the following strategy: The new method to detect the offset of the optical frequency comb showed at least a fractional stability of $3 \cdot 10^{-19}$ at 1 s, which was compared to the usual method (detected in a dedicated output just after the EDFA). The accuracy was comparable to the statistical uncertainty within 0.4σ. The results show that this method is compatible with even the best published uncertainty budgets of optical lattice clocks at a few 10^{-18}. The advantages of having more power sent for the detection of optical beat notes (increasing the signal to noise ratio) by removing usual method of detecting the offset is also favorable, especially for the Hg laser (1062 nm) being on the edge of the erbium comb's spectrum.

In order to improve the reliability of the frequency chain to allow long measurement times (days, if not weeks, if necessary), we have focused our efforts on the automatic re-lock of the phase lock loops (e.g: Locking of the frequency comb to the 1542 nm reference cavity), controlling of DDSs and monitoring of optical beat notes as well as automatic re-centering of frequencies, all controllable via the Internet, all paves the way for a completely automatized laboratory without the need of human interaction. We are therefore almost ready for the the PHARAO-ACES mission, which demands an automatized laboratory taking measurements of the clocks multiple times a day all around the year.

The dispatching of an ultra stable cavity can easily put the restrains of the stability. The stability of the new dispatching setup for distributing the ultra stable lasers is crucial for the transfer of spectral purity to optical lattice clocks. This especially comes into play for the installation of a new ultra stable cavity, since the expected stability (down to an order of magnitude better), requires even better performances from the links in order to dispatch the signal without significant degradations. The result for the stability of 75 cm of uncompensated paths has shown that the new dispatching will be restrained to a stability below $4 \cdot 10^{-18}$ at 1 s.

Finally, the core of my work was focused on the transfer of spectral purity: The transfer of spectral purity between the frequencies 1062 nm to 1542 nm reached a stability of $9 \cdot 10^{-18}$ at 1 s, and between the frequencies 698 nm and 1542 nm a stability of $3.5 \cdot 10^{-17}$ at 1 s. The level of performance that is reached by the transfer of spectral purity is compatible with the level of performance for the best lasers in the world that have reached a stability floor at $4 \cdot 10^{-17}$. The stability of our new long cavity will for sure not be limited simply by the transfer itself, having such good stabilities for the transfer of spectral purity.

The dual single-branch transfer allows us to derive a direct relation between the phase of the Sr laser and the phase of the Hg laser, which simplifies the locking procedure (no intermediate lock to the infra-red cavity): The dual single-branch transfer of spectral purity showed an improvement of the stability between the Sr and Hg optical lattice clocks. The stability improved with a factor between 2 and 3.5, because of the rejection of the Dick effect due to synchronized clock cycles with the transfer of spectral purity.

5.2 Prospect

The stability floor of the long cavity will clearly not beat the "worst" transfer at $3.5 \cdot 10^{-17}$ at 1 s, so the transfer will not be the limiting factor.

We are now ready to build the long cavity, we hope a floor somewhere in the

10^{-17} range, which (by calculation) should result in a stability of $10^{-16}/\sqrt{\tau}$. We would still be more than 1 order of magnitude away from the "limit" fixed by the quantum projection noise, but still, we would gain a lot in terms of averaging time.

On top of that, we already saw an improvement when we probed the two clocks synchronously, we will progress further on this technique, that will help to decrease even more the impact of the residual noise. At some point, when the duty cycle becomes $> 80\%$ (possible, hard but possible), then it starts to make sense to use Ramsey spectroscopy instead of Rabi spectroscopy (before that the stability is hardly improved).

We will also be able to generate ultra stable microwave signals with the new cavity. This will be done by locking the frequency comb to the long cavity, which would improve the comb's stability. The detection of the repetition rate would then generate an ultra stable microwave signal, which can be used to probe caesium and rubidium in the atomic fountains. This could replace the cryogenic sapphire oscillator, since it is cumbersome to maintain.

All these things will also help us in the test of fundamental constants, Lorentz invariance and the search for dark matter. We are also going to implement a transportable clock, with an excellent fiber link, which could lead to a clock that would not need a local cavity, which simplifies many things (transportable is not necessarily compatible with having a super well isolated cavity). This would also raise the prospect of using transportable optical clocks for chronometric geodesy.

Chapter 6

Bibliography

[1] https://www.nist.gov/si-redefinition/meter. 7/28/2019.

[2] https://physics.nist.gov/cuu/Units/meter.html. 11/12/2018.

[3] https://physics.nist.gov/cuu/Units/second.html. 11/13/2018.

[4] J. Guena, M. Abgrall, D. Rovera, P. Laurent, B. Chupin, M. Lours, G. Santarelli, P. Rosenbusch, M. E. Tobar, R. Li, K. Gibble, A. Clairon, and S. Bize. Progress in atomic fountains at lne-syrte. *IEEE Transactions on Ultrasonics, Ferroelectrics, and Frequency Control*, 59(3):391–409, March 2012.

[5] A. Al-Masoudi A. Amy-Klein C. Bærentsen C. F. A. Baynham E. Benkler S. Bilicki S. Bize W. Bowden J. Calvert V. Cambier E. Cantin E. A. Curtis S. Dörscher M. Favier F. Frank P. Gill R. M. Godun G. Grosche C. Guo 1 A. Hees I. R. Hill R. Hobson N. Huntemann J. Kronjäger S. Koke A. Kuhl R. Lange T. Legero B. Lipphardt C. Lisdat J. Lodewyck O. Lopez H. S. Margolis H. Álvarez-Martínez F. Meynadier F. Ozimek E. Peik P.-E. Pottie N. Quintin 7 C. Sanner L. De Sarlo 1 M. Schioppo R. Schwarz A. Silva U. Sterr Chr. Tamm R. Le Targat P. Tuckey G. Vallet T. Waterholter D. Xu 1. B. M. Roberts, P. Delva and P. Wolf. Search for transient variations of the fine structure constant and dark matter using fiber-linked optical atomic clocks. Jul 2019, arXiv:1907.02661.

[6] https://www.rp-photonics.com/optical_fiber_communications.html. 2/18/2019.

[7] Malvin Carl Teich Bahaa E. A. Saleh. *Fundamentals of Photonics*, chapter 5. Wiley, 2 edition, 2007.

[8] Peter W. Milonni and Joseph H. Eberly. *Laser physics*, chapter 5. Wiley, 2010.

[9] Jun Ye and Steven T. Cundiff. *Femtosecond Optical Frequency Comb: Principle, Operation, and Appliations.* Kluwer Academic Publisher / Springer Norwell, MA, 2004.

[10] https://www.rp-photonics.com/nonlinear_polarization_rotation.html. 2/27/2019.

[11] https://www.rp-photonics.com/four_wave_mixing.html. 2/27/2019.

[12] William J. Riley. *Handbook of Frequency Stability Analyse*. NIST Special Publication 1065, 2008.

[13] Erik Benkler, Christian Lisdat, and Uwe Sterr. On the relation between uncertainties of weighted frequency averages and the various types of allan deviations. *Metrologia*, 52, 04 2015.

[14] Rudolf Grimm, Matthias Weidemüller, and Yurii B. Ovchinnikov. Optical dipole traps for neutral atoms. volume 42 of *Advances In Atomic, Molecular, and Optical Physics*, pages 95 – 170. Academic Press, 2000.

[15] Rodolphe Le Targat. *Horloge à réseau optique au Strontium : une 2ème génération d'horloges à atomes froids*. PhD thesis, Observatoire de Paris, LNE-SYRTE, 1 2011. Taken from PhD. defence.

[16] Philip G. Westergaard. *Horloge à réseau optique au Strontium : en quête de la performance ultime*. PhD thesis, Observatoire de Paris, LNE-SYRTE, 10 2010.

[17] Maxime FAVIER. *Mercury Optical Lattice Clock: From High-Resolution Spectroscopy to Frequency Ratio Measurements*. Theses, Université Pierre et Marie Curie, October 2017.

[18] Hidetoshi Katori, Masao Takamoto, V. G. Pal'chikov, and V. D. Ovsiannikov. Ultrastable optical clock with neutral atoms in an engineered light shift trap. *Phys. Rev. Lett.*, 91:173005, Oct 2003.

[19] Martin M. Boyd, Tanya Zelevinsky, Andrew D. Ludlow, Sebastian Blatt, Thomas Zanon-Willette, Seth M. Foreman, and Jun Ye. Nuclear spin effects in optical lattice clocks. *Phys. Rev. A*, 76:022510, Aug 2007.

[20] Christopher J. Foot. *Atomic Physics*. Oxford university press, 2014.

[21] Anders Brusch, Rodolphe Le Targat, Xavier Baillard, Mathilde Fouché, and Pierre Lemonde. Hyperpolarizability effects in a sr optical lattice clock. *Phys. Rev. Lett.*, 96:103003, Mar 2006.

[22] G. Santarelli, C. Audoin, A. Makdissi, P. Laurent, G. J. Dick, and A. Clairon. Frequency stability degradation of an oscillator slaved to a periodically interrogated atomic resonator. *IEEE Transactions on Ultrasonics, Ferroelectrics, and Frequency Control*, 45(4):887–894, July 1998.

[23] Pierre Lemonde. *PHARAO: ÉTUDE D'UNE HORLOGE SPATIALE UTILISANT DES ATOMES REFROIDIS PAR LASER; RÉALISATION D'UN PROTOTYPE*. Theses, Université Pierre et Marie Curie - Paris VI, November 1997.

[24] Fabio Stefani, Olivier Lopez, Anthony Bercy, Won-Kyu Lee, Christian Chardonnet, Giorgio Santarelli, Paul-Eric Pottie, and Anne Amy-Klein. Tackling the limits of optical fiber links. *J. Opt. Soc. Am. B*, 32(5):787–797, May 2015.

[25] P. A. Williams, W. C. Swann, and N. R. Newbury. High-stability transfer of an optical frequency over long fiber-optic links. *J. Opt. Soc. Am. B*, 25(8):1284–1293, Aug 2008.

[26] F. Guillou-Camargo, V. Ménoret, E. Cantin, O. Lopez, N. Quintin, E. Camisard, V. Salmon, J.-M. Le Merdy, G. Santarelli, A. Amy-Klein, P.-E. Pottie, B. Desruelle, and C. Chardonnet. First industrial-grade coherent fiber link for optical frequency standard dissemination. *Appl. Opt.*, 57(25):7203–7210, Sep 2018.

[27] http://www.refimeve.fr/index.php/fr. 9/3/2019.

[28] C. Lisdat, G. Grosche, N. Quintin, C. Shi, S.M.F. Raupach, C. Grebing, D. Nicolodi, F. Stefani, A. Al-Masoudi, S. Dörscher, S. Häfner, J.-L. Robyr, N. Chiodo, S. Bilicki, E. Bookjans, A. Koczwara, S. Koke, A. Kuhl, F. Wiotte, F. Meynadier, E. Camisard, M. Abgrall, M. Lours, T. Legero, H. Schnatz, U. Sterr, H. Denker, C. Chardonnet, Y. Le Coq, G. Santarelli, A. Amy-Klein, R. Le Targat, J. Lodewyck, O Lopez, and P.-E. Pottie. A clock network for geodesy and fundamental science. *Nature Communications*, 7:12443, August 2016.

[29] T. Legero, D. G. Matei, S. Häfner, C. Grebing, R. Weyrich, F. Riehle, U. Sterr, W. Zhang, J. Robinson, L. Sonderhouse, E. Oelker, and J. Ye. 1.5 μm lasers with sub 10 mhz linewidth. In *Conference on Lasers and Electro-Optics*, page SW1J.1. Optical Society of America, 2017.

[30] O. Gobron, K. Jung, N. Galland, K. Predehl, R. Le Targat, A. Ferrier, P. Goldner, S. Seidelin, and Y. Le Coq. Dispersive heterodyne probing method for laser frequency stabilization based on spectral hole burning in rare-earth doped crystals. *Opt. Express*, 25(13):15539–15548, Jun 2017.

[31] Philip E. Ciddor. Refractive index of air: new equations for the visible and near infrared. *Appl. Opt.*, 35(9):1566–1573, Mar 1996.

[32] John Liu Murray R. Spiegel. *Schaum's*. Rensselaer Polytechnic Institute, 2 edition, 1968.

Appendix A

Deviation of the transmission through a Fabry–Pérot cavity

We can describe the strength of the reflected field of a cavity to understand how a Fabry–Pérot interferometer works. We can consider U_0 as field of the incident wave hitting the cavity. If the field U_0 is being reflected of the first cavity mirror, the field reflected would be;

$$U_1 = \sqrt{r}e^{i\pi}U_0 = -\sqrt{r}U_0, \tag{A.1}$$

where r is the reflection coefficient. We can also consider the field U_0 entering the cavity and being reflected on the second mirror and transmitted back through the first mirror;

$$U_2 = -\sqrt{r}Te^{i\varphi}U_0, \tag{A.2}$$

where T is the sum of first entering the cavity, and the field later being transmitted back through the first mirror again. The phase $e^{i\varphi}$ comes from the accumulated phase on a round trip. We can describe the coefficient doing an extra round trip in the cavity with $R = re^{i\varphi}$, this is assuming a symmetric cavity. We can describe the N'th reflection from the cavity as;

$$U_{N+2} = R^N U_2 \qquad (N \geq 0). \tag{A.3}$$

We want to sum over all the reflections to see the behavior of the cavities total reflection;

$$\frac{U_R}{U_0} = -\sqrt{r}(1 - [Te^{i\varphi}\sum_{N=0}^{\infty} R^N]). \tag{A.4}$$

We can use this for the infinite series;

$$\sum_{k=0}^{\infty} R^k = \frac{1}{1-R} \qquad (|R| < 1). \tag{A.5}$$

The energy is conserved in the resonator, this implies that the relation between the transmission and the reflection follows from Fresnel formula; $r + t = 1$. We can use equation A.5 to rewrite the equation for the total reflection of a cavity as;

$$\frac{U_R}{U_0} = -\sqrt{r}\Big(1 - \frac{Te^{i\varphi}}{1-R}\Big) = -\sqrt{r}\frac{1-e^{i\varphi}}{1-re^{i\varphi}}. \tag{A.6}$$

The result of the reflection is called the reflection coefficient of a cavity. We can now calculate the intensity as the amplitude of the field squared, $I = |U|^2$:

$$\frac{I_R}{I_0} = \Big|\frac{U_R}{U_0}\Big|^2 = r\Big|\frac{1-e^{i\varphi}}{1-re^{i\varphi}}\Big|^2 = \frac{4R\sin^2(\varphi/2)}{(1-R)^2 + 4R\sin^2(\varphi/2)}. \tag{A.7}$$

The transmission through the cavity can be calculated by using Fresnel formula on equation A.7;

$$\frac{I_T}{I_0} = 1 - \frac{I_R}{I_0} = \frac{1}{1+F\sin^2(\varphi/2)}, \tag{A.8}$$

where $F = \frac{4r}{(1-r)^2} = (2\mathcal{F}/\pi)^2$ [8].

Appendix B

the beat note between a laser and an optical frequency comb

To explain the frequency of a beat note between a laser and an optical frequency comb, an understanding of the interference between light fields has to be explained. The electric field of light at a point can formulated as;

$$E_1(t) = A_1\cos(\omega_1 t), \tag{B.1}$$

where A_1 is the amplitude of the field, and ω_1 is the frequency. The intensity from the interference between two light fields (E_1 and E_2 propagating in the same direction) can then be expressed as;

$$\begin{aligned} I &= |E_1 + E_2|^2 = |A_1\cos(\omega_1 t) + A_2\cos(\omega_2 t)|^2 \\ &= A_1^* A_2\cos(\omega_1 t)\cos(\omega_2 t) + A_1 A_2^*\cos(\omega_1 t)\cos(\omega_2 t) + |A_1|^2 + |A_2|^2 \end{aligned} \tag{B.2}$$

We can now use the cosine relation; $\cos(\omega_1 t)\cos(\omega_2 t) = \frac{\cos([\omega_1+\omega_2]t)+\cos([\omega_1-\omega_2]t)}{2}$ [32], to get the final expression for the beat note between E_1 and E_2;

$$I = \mathrm{Re}\{A_1 A_2\}\cos([\omega_1 - \omega_2]t) + \mathrm{Re}\{A_1 A_2\}\cos([\omega_1 + \omega_2]t) + |A_1|^2 + |A_2|^2. \tag{B.3}$$

There are two oscillating terms in equation B.3. A slow oscillation ($[\omega_1 - \omega_2]t$) and a fast oscillation ($[\omega_1 + \omega_2]t$). The fast oscillation will be several of hundreds of THz when dealing with optical signals, which is extremely far from what we are able to detect. The slow oscillating term will oscillate with the difference in frequency between the optical signals, which we can detect for optical signals on a photodiode.

The optical frequency comb can be written as;

$$f_N = N f_{\mathrm{rep}} + f_0. \tag{B.4}$$

We will only detect the frequency of the beat note for the optical comb frequency vs the laser when their frequencies have opposite signs, following the logic of equation

B.3. This gives us the frequency $f_N - \nu_L$. The final beat note between the laser and an optical frequency comb will then become;

$$f_L = N f_{\text{rep}} + f_0 - \nu_L. \tag{B.5}$$

Appendix C

Gaussian beams in a cavity

The cavity curved mirrors results in a gaussian shaped phase front, this is illustrated on figure C.1.

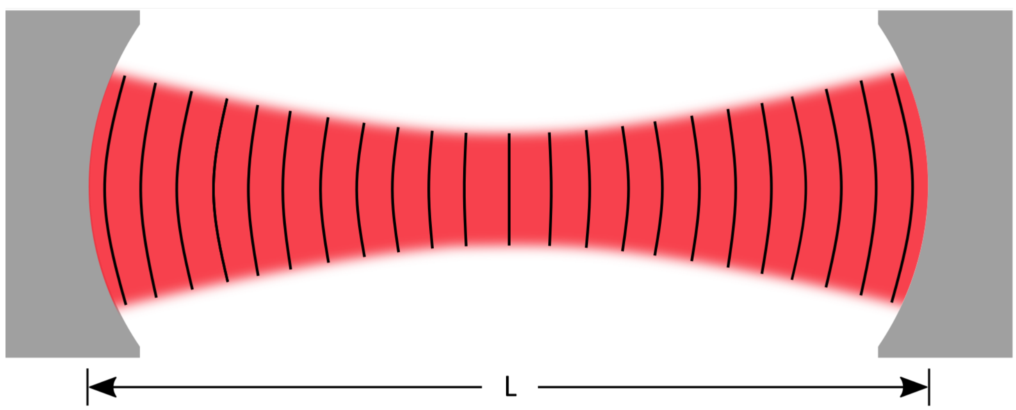

Figure C.1: Illustration of a cavity. The black lines is the phase front of the light inside the cavity. The red is the spatial distribution of the wave, disregarding the standing wave. L is the length of the cavity.

The phase of a gaussian beam propagating along the z direction is $\zeta(z) = tan^{-1}(z/z_0)$, where z_0 is the Rayleigh length. We only need to look at the phase change within the optical axis of the cavity, because the phase front is the same at each point hitting the mirror illustrated on figure C.1. This means that we can calculate the phase change between each mirror and not consider the transverse axis putting it equal to zero for x, y=0;

$$\Delta\varphi = kL - \Delta\zeta, \tag{C.1}$$

where $\Delta\zeta = \Delta\zeta(z_2) - \Delta\zeta(z_1)$ is the accumulated phase for a round trip in the cavity, because of the gaussian properties. L is the length of cavity as seen on figure C.1 and k is the wavenumber. The phase change must be a multiple of π for the standing wave to have the minimal intensity at the surface of the mirrors. Taking equation C.1 into account to calculate the allowed frequencies;

$$\nu_m = m\nu_{\mathrm{FSR}} + \frac{\Delta\zeta}{\pi}\nu_{\mathrm{FSR}}. \tag{C.2}$$

We can see from equation C.2, that we have an offset from having spherical mirrors [7]. $\Delta\zeta$ can be calculated from the Rayleigh length knowing the geometry of the cavity.

Appendix D

Vacuum chamber for the dispatching of the ultra stable cavity

Mechanical drawing made (in Solid Works) for the vacuum chamber used for the dispatching of the ultra stable cavity;

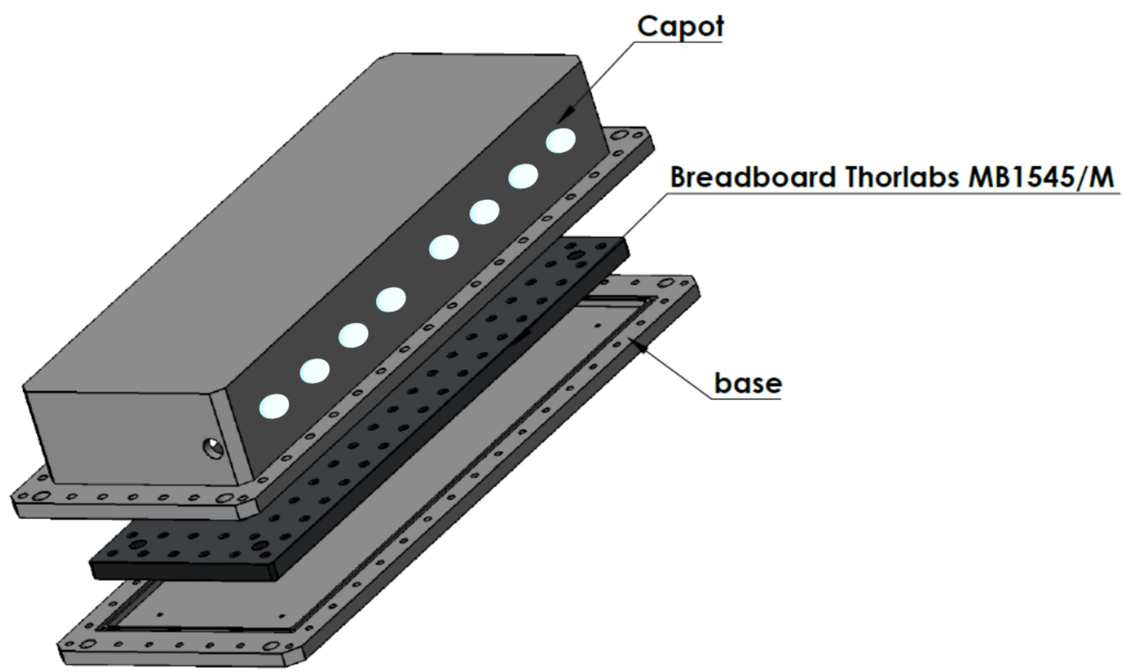

Appendix E

Vacuum chamber for the transfer of spectral purity

Mechanical drawing made (in Solid Works) for the vacuum chamber used for the transfer of spectral purity;